General Disclaimer

One or more of the Following Statements may affect this Document

- This document has been reproduced from the best copy furnished by the organizational source. It is being released in the interest of making available as much information as possible.

- This document may contain data, which exceeds the sheet parameters. It was furnished in this condition by the organizational source and is the best copy available.

- This document may contain tone-on-tone or color graphs, charts and/or pictures, which have been reproduced in black and white.

- This document is paginated as submitted by the original source.

- Portions of this document are not fully legible due to the historical nature of some of the material. However, it is the best reproduction available from the original submission.

Technical Report No. AE-76-1

University of Maryland, College Park
Department of Aerospace Engineering

MEASUREMENTS IN THE NEAR-WALL REGION OF A RELAXING THREE-DIMENSIONAL LOW SPEED TURBULENT AIR BOUNDARY LAYER

K. S. HEBBAR and W. L. MELNIK

Department of Aerospace Engineering

Office of Naval Research
Fluid Dynamics Program
Arlington, Virginia 22217

Contract N00014-75-C-0613
NR 061-212

July, 1976

Abstract

An experimental investigation was conducted at selected loclations of the near-wall region of a three-dimensional turbulent air boundary layer relaxing in a nominally zero external pressure gradient behind a transverse hump (in the form of a 30° swept, 5-foot chord wing-type model) faired into the side wall of a low speed wind tunnel. Wall shear stresses measured with a flush-mounted hot-film gage and a sublayer fence were in very good agreement with experimental data obtained with two Preston probes. With the upstream unit Reynolds number held constant at 3.25×10^5 ft^{-1} approximately one-fourth of the boundary layer thickness adjacent to the wall was surveyed with a single rotated hot-wire probe mounted on a specially designed minimum interference traverse mechanism. The boundary layer (approximately 3.5" thick near the first survey station where the length Reynolds number was 5.5×10^6) had a maximum crossflow velocity ratio of 0.145 and a maximum crossflow angle of 21.875° close to the wall.

The hot-wire data indicated, in agreement with the findings elsewhere, that the apparent dimensionless velocity profiles in the viscous sublayer region are universal and that the wall influence is negligible beyond $y^+ = 5$. The existence of wall similarity in the relaxing flow field was confirmed in the form of a log law based on the resultant mean velocity and resultant friction velocity (obtained from measured skin friction).

This experimental investigation addressed the question of the existence of near-wall collateral flow field, a question that is of some relevance in the context of defining a suitable inner boundary condition in some presently available prediction methods (using rate equations for Reynolds

stress). The experimental mean direction profiles indicated a relatively smaller collateral region adjacent to the wall. The smallest collateral region extended from the nearest point to the wall ($y^+ \approx 1$) up to $y^+ = 9.7$, corresponding to a resultant mean velocity ratio (local to freestream) of 0.187. The unusual feature about these profiles was the presence of a narrow region of slightly decreasing crossflow angle (1° or less) that extended from the point of maximum crossflow angle down to the outer limit of the collateral region. This behavior was caused by small local transverse pressure gradients close to the wall which opposed the crossflow. A sublayer analysis of the flow field slightly overestimated the decrease of crossflow angle. It is concluded that in the absence of these gradients, the skewing of the flow could have been much more pronounced practically down to the wall (limited only by the resolution of the sensor), implying a near-wall non-collateral flow field consistent with the equations of motion in the neighborhood of wall.

The streamwise relaxation of the mean-flow field based on the decay of crossflow angle was found to be much faster in the inner layer than in in the outer layer. Although the data was not sufficiently complete to define the beginning of flow relaxation, the present investigation led to two significant observations based on the streamwise distance covered by the measurements (34"):

(i) the relaxation of the mean flow in the inner layer and the wall shear stress vector was practically complete in approximately 10 boundary layer thicknesses and,

(ii) the relaxation of the turbulence was relatively slower and was not complete over the same distance.

Acknowledgments

This work was performed at the University of Maryland while the first author was a graduate research assistant and later a Minta Martin fellow on leave from the National Aeronautical Laboratory, Bangalore - 560017, India. The authors gratefully acknowledge the unstinting efforts of Dr. Allen E. Winkelmann which were instrumental to the accomplishment of these experiments.

This research was funded partially by the Minta Martin Fund for Aeronautical Research, by NASA under Grant NGR-21-002-303 and by the Office of Naval Research under Contracts N00014-67-A-0239-0029 and N00014-75-C-0613. Computer time for this investigation was supported in full through the facilities of the Computer Science Center of the University of Maryland.

Table of Contents

List of Tables

List of Figures

List of Symbols

A,B	Log law constants (equation (2))
c_f	Skin friction coefficient
c_p	Pressure coefficient
C	Constant in linearized response equation for hot wire (equation (4))
C_1	Constant related to C (equation (4b))
d	Outside diameter of Preston probe, also diameter of hot wire sensor
D	Pipe diameter, also constant in equation (14)
e	Instantaneous a.c. voltage (of hot wire output) from linearizer
E	d.c. voltage (of hot wire/hot film output) from linearizer
h	Sublayer fence height
k	Constant in angular response equation for hot wire (equations (4) and (4a)), also thermal conductivity
K	Non-dimensional velocity at the apex of a polar plot (equation (12))
l	Length of hot wire sensor
L	Effective streamwise length of hot-film, also length of pipe between exit plane of inlet nozzle and test section
n	Exponent in generalized King's formula
p	Pressure
Δp	Output of sublayer fence/Preston probe, also pressure drop along pipe
Q	Dynamic head

P_f	Power dissipated by flush-mounted hot-film gage
Pr	Prandtl number
R	Resistance
ΔR	Resistance elevation
Re	Reynolds number
R_L	Reynolds number based on L
T	Temperature
u,v,w	Turbulence fluctuations in x,y,z directions, respectively (Figs. 1 and 3)
u_1,v_1,w_1	Turbulence fluctuations in x_1,y_1,z_1 directions, respectively (Figs. 1 and 3)
U,V,W	Mean velocity components in x,y,z directions, respectively (Figs. 1 and 3)
$\overline{U}$	Resultant mean velocity (=U in 2-dimensional flows)
$\overline{U}^*$	Resultant friction velocity based on resultant mean wall shear stress (=U* in 2-dimensional flows)
$\overline{U}^+$	Dimensionless velocity = $\overline{U}/\overline{U}^*$
$\overline{U}_\infty$	Local freestream velocity
$U_{\infty r}$	Freestream velocity at the upstream reference station
x,y,z	Cartesian coordinates in reference axes system with x parallel to tunnel centerline (Figs. 1 and 3)
x_1,y_1,z_1	Cartesian coordinates in local axes system with x_1 parallel to $\overline{U}$ (Figs. 1 and 3)
x^+	Dimensionless distance = $x\overline{U}^*/\nu$

x^*	Nondimensionalized output of sublayer fence/Preston probe (Figs. 16 and 17)
y	Distance from test wall
y^+	Dimensionless distance = $y\bar{U}^*/\nu$ (friction distance parameter)
y^*	Nondimensionalized wall shear stress (Figs. 16 and 17)

Greek Symbols

α	Crossflow angle, (yaw) angle between flow direction and normal of sensor
α_w	Limiting streamline angle (wall corssflow angle)
γ	Angle in polar plot (see the sketch and equation (12) in subsection 6.3.4)
μ	Absolute (dynamic) viscosity of air
ν	Kinematic viscosity of air
ρ	Density of air
σ	Freestream velocity ratio = $U_\infty/U_{\infty r}$
τ	Shear Stress
$\bar{\tau}_w$	Resultant mean wall shear stress
ψ	Yaw angle (equation (4b))

Subscripts

int	Intersection
max	Maximum
r,ref	Reference
w	Wall
∞	Freestream

Superscripts

$\bar{}$ (overbar)	Time mean

Chapter 1

Introduction

The notable feature of a three-dimensional boundary layer that distinguishes it from two-dimensional flows is the so-called 'secondary flow' or 'crossflow' (Fig. 1.). Whenever there is a turning of the streamline in the main flow (as in a curving channel or as in front of an obstacle in an otherwise two -dimensional boundary layer), a radial or lateral pressure gradient is imposed on the boundary layer by the turning flow. The resulting crossflow skews the boundary layer velocity vectors toward the center of curvature of the main flow. At any location in the flow field, because of continuously decreasing velocity in the boundary layer the skewing continuously increases as the wall is approached. Consequently, the velocity profile does not lie in a single plane. The limited number of experiments available to date seem to indicate that the streamwise profiles are close to two-dimensional forms, particularly so when the crossflow is small. However, there is no single model which can satisfactorily describe even a simple crossflow profile.

Despite the fact that three-dimensional turbulent boundary layers are of great practical interest because of their wide occurrence in nature, their study has been, until recently, almost neglected in comparison to the attention given to two-dimensional flows. The analysis of three-dimensional turbulent boundary layers is in a state of flux as compared with the analysis of two-dimensional problems [1, (2, p. 4), 3]. On the experimental side, very few detailed studies of the three-dimensional problem have been published. This is not surprising when one considers the relatively great complexities involved in measuring the pertinent time-mean and fluctuating quantities in a three-dimensional turbulent boundary layer. In regard to

the phenomenon of separation in three-dimensional flows, very little is known both experimentally and theoretically [4]. As a result of the recent advances in the development of computational techniques, the success of two-dimensional prediction methods as shown by the 1968 Stanford conference [5] and the recent advances in experimental techniques and data processing, the interest in three -dimensional flows is growing steadily [(2, p. 4), 6].

1.1 Previous investigations

Two-dimensional turbulent boundary layers have been understood fairly well [2, pp. 115 and 163]. Most theoretical approaches to the solution of a two-dimensional turbulent boundary layer depend on experimental data to model the shear stress distribution (i.e., to model the closure equation). With three-dimensional flows, the data must in addition provide information on the directional characteristics of the flow, i.e., the distributions of the shear stress vector and the mean velocity vector across the boundary layer. The prediction methods [7-12] presently available show some success in treating the incompressible three-dimensional turublent boundary layer. A critical assessment of some of these methods may be found in references [(2, chapter 8), 6]. The prediction method of Mellor [7] using a simple eddy viscosity model is adequate to calculate the mean velocity field in many cases of engineering interest. Nash's model [8] assumes that the turbulent shear stress vector acts in the same direction as the mean velocity gradient vector (as would be required by the scalar eddy viscosity assumption) whereas the Bradshaw model [9] allows for a misalignment between these two vectors. Both these models use essentially the same shear stress closure assumption that is based on the two-dimensional form of the empirically determined turbulent kinetic energy equation of Bradshaw, et al. [13] suitably modified for three-dimensional flows. Common to all of these calculation techniques is

the need for complete and detailed experimental data to evaluate existing theoretical models and to develop more adequate models for the fluctuation terms in the time-averaged equations for the mean motion (Reynolds equations) [1].

A number of experimental investigations on three-dimensional turbulent boundary layers have been reported to date [14-36]. Many of these have focused attention on the so-called rapidly yawing or suddenly skewed boundary layers [14, 19, 21, 24, 29]. In many of these flow configurations the presence of a bluff body standing in an oncoming, nominally two-dimensional turbulent boundary layer caused the skewing of the boundary layer. These boundary layers are capable of producing a wide range of crossflows and pressure gradients and, therefore, the experimental data from them is quite valuable in looking for correlations (of mean velocity profile) based on local parameters [29]. However, because the pressure gradients dominate the mean flow field, they cannot be considered as adequate test cases to provide meaningful data for studying and improving the assumptions made in turbulence models (such as those of Nash and Bradshaw) for the distribution of shear stress.

The finite swept-step experimental data of Johnston [14] refutes the assumption in the Nash model regarding the direction of shear stress. Even the Bradshaw model fails to predict the direction of shear stress correctly. However, in the absence of more experimental data of this kind, this test cannot be taken as a conclusive one. Moreover, as pointed out above, Johnston's experimental data cannot be considered as a good test case for the Nash and Bradshaw models. In his flow configuration, the meanflow development was influenced primarily by the pressure gradients (induced by a swept forward-facing step mounted on the floor of a wind tunnel) and only

to a minor extent by the shear stress gradients. In the experimental study of Bradshaw and Terrell [15], a 45° swept wing as used to develop a three-dimensional flow wherein the mean flow was influenced primarily by the shear stress gradients. The boundary layer which was nominally 1.1 inches thick had a crossflow of about 7.5° at the trailing edge and relaxed over a flat plate (under nominally zero pressure gradient) attached to the trailing edge of the wing. This data is better suited for comparison with the Nash and Bradshaw models. Although these measurements, which are also partially reported in reference [9], tend to support the Bradshaw model, both experiment and theory seem to confirm the Nash model in the inner third of the boundary layer [14]. The question of the correlation between the directions of the shear stress vector and the man-velocity gradient vector, therefore, still remains unresolved.

Another unresolved question concerns the nature of the mean-flow field very close to the wall. Only a small number of (reliable) experimental data close to the wall is available. Most of the existing data in the inner region of the boundary layer seems to have been somewhat restricted by the size and/or response of the probes used, resulting in inadequate spatial resolution [37-39]. In fact, most of the existing data indicates near-wall collateral flow, i.e., in the inner region very close to the wall (sometimes extending up to local-to-freestream velocity ratios of as high as 0.5) the mean velocity vector does not change its direction. Only the recent work by Rogers and Head [25] using a specially designed hot-wire anemometer device showed a velocity profile with a skewed flow almost right down to the wall, the data point closest to the wall corresponding to the resultant velocity ratio (local to freestream) ob about 0.2. This is much closer to the wall than other experimenters have been able to probe. Similar trends are also observed in the later data of Vermeulen [28]. It is, therefore, clear that more

(reliable) data is still needed to resolve experimentally the existence (or nonexistence) of near-wall collateral flow field in a three-dimensional turbulent boundary layer. This is all the more important because the existence of such a collateral flow field is not predicted either by numerical calculations or by a sublayer analysis of the flow field. In fact, numerical calculations by East and Pierce [37] indicate that the assumptions of near-wall collateral flow, as suggested by many experimentalists, may not be correct [38]*. The boundary layer equations in the neighborhood of the wall indicate a continuous skewing of the velocity vector all the way down to the wall (just as in the case of three-dimensional laminar boundary layers) as long as the pressure gradient is not codirectional with the wall shear stress [2, p. 102].

1.2 Present investigation

This investigation was undertaken to provide answers to the two basic unresolved questions concerning the existence (or nonexistence) of near-wall collateral flow and the angle between the shear stress vector and the mean-velocity gradient vector in a three-dimensional turbulent boundary layer. Although the objective of the original investigation was to obtain and analyze such experimental data, for reasons that will become clear soon, the nature of the data obtained severely restricted the scope of the investigation to the form presented here. The experimental data was analyzed with particular emphasis on the nature of the mean flow field very close to the wall and the streamwise relaxation characteristics of the mean flow and some turbulence

*The question of the existence of a near-wall collateral flow field is of relevance to numerical difference solutions, such as those of Nash and Bradshaw, where the question of inferring and defining a limiting wall streamline direction is of some interest [38].

quantities in the inner layer region.

The final selection of the experimental arrangement for this investigation was based on a careful examination of the previous investigations and the practical problems associated with different geometries. As strongly advocated by Bradshaw [1], a satisfactory test case is the flow past an infinite swept wing [15], where the mean-flow development is primarily influenced by the shear stress gradients. The experimental configuration of flow geometry and flow conditions sutdied in this investigation was selected to approximate this test case on a larger scale (but with a low aspect ratio wing).

To facilitate the spatial resolution of the measurements, a relatively thick two-dimensional turbulent boundary layer was first developed on the side wall of the University of Maryland Boundary Layer Research Tunnel (essentially a low speed wind tunnel) over a run length of about 12 feet and then allowed to flow over a transverse hump faired into the side wall. The hump was in the form of a 30° swept, approximately 8% thick (symmetric) 5-foot chord wing-type model that spanned the tunnel height. Near the trailing edge, the boundary layer was approximately 3.5" thick with a wall crossflow of 21°. It relaxed downstream of the hump under nominally zero external pressure gradient and eventually returned to a two-dimensional state. The measurements reported in this study were made downstream of the hump. The flow configuration downstream of the hump was similar to the flow field in the experimental study of Bradshaw and Terrell [15], the boundary layer being about three times as thick with nearly three times the induced wall crossflow.

In order to hold the scale effect constant throughout, all the measurements reported in this investigation were made at a constant upstream reference Reynolds number of 3.25×10^5 per foot corresponding to a local freestream velocity of 53-57 feet per second in the relaxing region. A traverse

mechanism specially designed for near-surface anemometer studies (to insure minimal probe interference) enabled an investigation of the near-wall region of the relaxing boundary layer at selected locations. The experiments included near-wall measurements of time-mean and fluctuating velocity in planes parallel to the wall with a single rotated hot-wire probe and wall shear stress measurements with various shear stress devices (a flush-mounted hot-film gage, a sublayer fence and two Preston probes). Two-dimensional experiments (conducted in the absence of the hump) provided the necessary data to estimate the wall proximity correction for hot-wire readings very close to the wall and also some data on the initial state of the turbulent boundary layer toward which the relaxing flow was expected to return asymptotically. The shear stress devices were calibrated in a pipe flow and the hot-wire in a free jet.

Because of the traverse limitation imposed by the hot-wire probe and the traverse mechanism, the hot-wire could only be traversed over a distance of approximately one-fourth of the boundary layer thickness from the wall, i.e., the inner layer and a little protion of the adjacent outer layer. With a conventional traverse mechanism and a conventional hot-wire probe, these hot-wire surveys could have been extended into the outer layer as well to complete the boundary layer traverse at each location and thus enhance the userfulness of the data; but the available time was rather, unfortunately, too short to permit such an extension. For the same reason, the most important measurement, namely of Reynolds stresses, that is very crucial to test the prediction methods could not be undertaken. In these respects, the hot-wire surveys reported in this study are incomplete and, therefore, could not be used to assess prediction methods.

Although some spanwise variations were expected in the flow field downstream of the hump (because of its low aspect ratio), the nominal two-dimensional boundary layer upstream of the hump was contaminated by transverse nonuniformities, which would be even amplified in flowing over the hump [40]; the nonuniformities would require a much finer spatial resolution of the initial data (for prediction methods) than was possible in this investigation. Consequently, the experimental data (even if it were complete!) would be somewhat less satisfactory as a test case for assessing prediction methods [1]. Nevertheless, considered over a restricted spanwise region, the observed spanwise variations did not preclude the interpretation of the data obtained from the near-wall hot-wire measurements and the wall shear stress measurements. This report is, therefore, restricted in its scope to the presentation and analysis of the experimental data with particular emphasis on the nature of the mean-flow field very close to the wall and the streamwise relaxation of the flow field in the inner layer region.

The presentation in subsequent chapters is as follows. After describing the wind tunnel facility and the selection of flow geometry in Chapter 2, the details of instrumentation, and the calibation are given in Chapter 3. Chapter 4 deals with the actual experiments and Chapter 5 with the reduction of the experimental data. A detailed discussion of the experimental results is presented in Chapter 6. Finally, some conclusions and recommendations based on the present investigation follow in Chapter 7.

Some preliminary results of this investigation were presented at the 28th annual meeting of the Fluid Dynamics Division of the American Physical Society [41]. This report is based in part on the Ph.D. dissertation of Hebbar [42].

Chapter 2

Wind Tunnel Facility and Flow Geometry

A brief description of the wind tunnel is given in the following section. Several modifications were incorporated into the wind tunnel to improve the quality of the flow in the test section. Some features of these modifications are described in Appendix A. After briefly commenting on the quality of the two-dimensional flow in section 2.2, the configuration of the wing-like model and the test wall is described in section 2.3. The details of prototype model studies that led to the selection of the flow geometry for the present investigation are given in reference [40].

2.1 Wind tunnel

A schematic diagram of the boundary layer research tunnel (the modified wind tunnel) used in the present investigation is shown in Fig. 2. It is a low-speed indraft-type open-circuit tunnel with a 20-foot long closed test section of nominal cross-section 18" wide x 46.5" high. Air is sucked through an air-filter enclosure by means of a Westinghouse centrifugal all-purpose fan driven by a 3-phase delta-wound, 50 HP General Electric induction motor. The inlet section consists of a bell-mouth entry section followed by a honeycomb-screen assembly. The honeycomb structure is made up of plastic drinking straws (0.236" o.d., 0.007" wall and 8.25" long) stacked against a stainless steel screen (20 mesh, 0.010 inch wire and 64% open area ratio). Six inches behind this screen are four polyester screens spaced 3 inches apart and held in a wooden frame. Each polyester screen is 16.5 mesh, 0.0138" dia monofilament with 59% open area ratio. A 5 ½ -foot long three-dimensional contraction made of masonite and of area ratio 6.9 connects the inlet section to the test section. Tripping elements located on all four walls just at the beginning of the test section insure early transition of the boundary layer. Each trip is made of 1/16"

thick x 1/4" wide aluminum strip glued to the surface. A 26 ½ - foot long diffuser section made of steel joins the rectangular test section to the circular inlet of the fan by a gradual area transition. The mass flow through the fan and, therefore, the flow through the test section is remote-controlled by means of a motor driven actuator which varies the opening of the inlet guide vanes of the fan. Flow velocities up to about 80 feet per second in the test section are possible. The random fluctuations in the freestream velocity in the test section are within ± 0.3% (as observed on a micromanometer).

The test section consists of three sections of 1-inch thick plywood sheet, the upstream section being 4 feet long (Fig. 2). The rear side wall of the test section is heavily braced to minimize vibration. A 1/4-inch thick 8-foot long aluminum plate epoxied to the rear side wall of the downstream section provides a smooth working surface (test wall).

2.2 Quality of two-dimensional flow in the test section

The side walls of the test section were adjustable so that a nominally zero pressure gradient could be maintained over the entire length of the test section. The longitudinal static pressure distribution measured on the aluminum plate showed a very small favorable pressure gradient which was less than 0.3% of the upstream reference dynamic head per foot, i.e., $\frac{\partial c_p}{\partial x} < 0.3 \times 10^{-2}$/foot [40].

The longitudinal intensity of freestream turbulence in the test section, $(\sqrt{\overline{u^2}}/U_\infty)$, was 0.2% at a freestream velocity of 50 ft/sec [40] .

As reported in reference [40], the turbulent boundary layer developed on the aluminum plate (in the absence of the wing-like model) was not truly two-dimensional; boundary layer surveys in a transverse direction revealed the existence of nonuniformities even in regions sufficiently away from the corners.

Reference [40] describes in detail several attempts aimed at improving the quality of the boundary layer flow, these attempts finally culminating in certain modifications to the original (unmodified) wind tunnel. Some of these modifications and some results of a preliminary study of the nonuniformities are summarized in Appendix A. Unfortunately, very little improvement was accomplished with these modifications.

2.3 Configuration of wing-like model and test wall

The selection of the wing-like model and the number and spacing of instrumentation ports (each 3/4" diameter) and static taps on the test wall was based on a quantitative investigation of the flow region behind a prototype wing-like model. The results of the above investigation (reported in reference [40]) showed that the prototype wing-like model was generally satisfactory from considerations of separation, steadiness, crossflow and boundary layer growth. It induced a relatively storng crossflow in the thick boundary layer developed on the wall of the test section.

In order to provide a smooth working surface and to facilitate accurate location and machining of static pressure taps and instrumentation ports in the relaxing region, it was decided to use a 1/4-inch thick well polished aluminum plate behind the hump. The ports served as predetermined stations for hot-wire surveys and wall shear stress measurements. As indicated by Conrad probe surveys and static pressure surveys [40,42], most of the relaxation occurred over a distance of the first 16 inches from the trailing edge of the prototype model, the relaxation further downstream being asymptotic. This suggested closer location of static taps and instrumentation ports in this region (particularly close to the trailing edge). Considered over a limited spanwise region extending on either side of the tunnel center line, the transverse traverse survey data indicated only slight variations in the spanwise direction. To investigate

these variations, several instrumentation ports were located in the spanwise direction.

Figures 2 and 3 show the design of the wing-like model and the test wall with instrumentation ports and static taps, respectively. The final model was constructed of contoured plywood ribs covered by masonite which provided a smooth hump surface for the flow. The details of construction and installation in the wind tunnel may be found in reference [40]. The streamwise distance between the trailing edge and the first spanwise row of static taps was 1/8 inch and that between the trailing edge and the spanwise row of instrumentation ports was 3/4 inch. The trailing edge thickness was estimated to be 0.0002". In all, the test wall contained 10 instrumentation ports (numbered 1 to 7 in the streamwise direction and 8, 1, 1a and 9 in the spanwise direction) and 77 static taps. When not in use, each port was closed with a custom -fitted plug having a static tap at its center.

Chapter 3

Instrumentation and Calibration

The experimental investigation envisaged the following measurements at predetermined locations (Fig. 3) in the flow field of the relaxing three-dimensional turbulent boundary layer:

(i) time-mean and fluctuation measurements of velocity vector in the near-wall region with a single rotated hot wire,

(ii) time-mean measurements of wall shear stress vector with a flush-mounted hot-film gage, a sublayer fence and two Preston probes and,

(iii) local freestream velocity measurements with a conventional Pitot-static probe.

In addition, the wall static pressure distribution was measured.

Special care to minimize flow disturbances was required in the design of various probes and the traverse mechanism used in the present investigation. The traverse mechanism was externally mounted on the test wall so that a probe could be introduced through the working surface (Fig. 2). This arrangement facilitated hot-wire measurements as close as 0.0005" from the wall with minimum interference. The hot wire calibration was accomplished in a small free jet facility and the calibration of wall shear stress devices in a pipe flow facility. The details of the instrumentation and some aspects related to the calibration are given in the following sections. Appendix B describes the design of the flush-mounted hot-film gage. A more detailed description and performance of the calibration facilities may be found in [42].

3.1 Traverse mechanism for near-wall studies

For accurate measurment of time-mean velocity and direction profiles a traverse mechanism with precise linear as well as angular movement is

required. To minimize flow interference the traverse mechanism should be mounted externally right behind the test wall at the point of measurement with the probe protruding through the test wall (Fig. 2). A traverse mechanism was designed and developed to meet the afore-mentioned requirements and at the same time be capable of receiving differenct probes. Essentially, it is a development of the Wills hot-wire probe [43] and is similar to that of Rogers and Head [25] in principle and in operation but differs in constructional details. A sectional drawing of the traverse mechanism is shown in Figure 4. Figure 4a shows two photographs of the traverse mechanism mounted externally on the rear side wall of the tunnel at port 7. A detailed description of the traverse mechanism, its mounting and initial orientation may be found in [42].

A Starrett micrometer head (1) serving as both a driving mechanism and an indicating mechanism for the linear motion is held fixed at the center of an outer top plate (2). It has a travel of 1" with a resolution of 0.0001". The rotating spindle of the micrometer head is secured to a short stainless steel connecting rod (22) in such a way that only its translational motion is transferred to the connecting rod without any backlash. Near the other end, the connecting rod is secured tightly to a yoke (6) that guides along two well lubricated and accurately machined stainless steel guide rods (5) held between two inner plates (4 and 9). These guide rods, the inner plates and the yoke together furnish a driving mechanism for the angular motion. A rotation of 140^{0} with a resolution of one minute is possible with this arrangement. Thus a probe may be rotated if secured to the inner bottom plate or translated if secured to the free end of the connecting rod or both translated and rotated by a proper design of the probe assembly as described below.

The hot wire probe assembly consists of a stainless steel probe holder (21) that slides freely inside an inner brass cylinder (16) which rotates inside an outer brass cylinder (15). The design of the traverse mechanism is such that when it is rotated, both the probe holder and the inner brass cylinder rotate together as a single unit. This feature is very important and critical in the case of a hot-wire probe since any relative motion between them will distort the alignment of the hot wire support needles (19) leading to buckling or breaking of the hot wire (18). The linear and the angular motions of the probe can be controlled independently. If desired, the linear motion can be locked at any position by turning the lock nut on the micrometer head. Likewise, the angular motion can be locked at any orientation by tightening a locking screw in the vernier arrangement (see Fig. 4a).

After mounting the traverse mechanism, the probe is aligned with respect to the normal to the local horizon by means of a small home-made probe alignment sighting device consisting of a 50X pocket microscope (Fig. 5). This microscope is preset so that one of its cross-hairs aligns with the local horizon* when the bubble of the spirit level is in the center. The mouth of the Preston probe, the hot-wire sensor, the hot-film sensor or the sublayer fence is aligned perpendicular to the local horizon. In the case of the hot-wire probe, it is the sensitive portion of the wire that is aligned. The traverse mechanism is rotated until the probe is aligned and the corresponding angle reading taken as the reference direction for all subsequent angular measurements.

*Operationally, this reference direction was convenient. In this investigation the difference between the directions of the local freestream line and the local horizon was small (see subsection 4.2.2).

The distance of the probe from the surface is measured in terms of the micrometer readings. To obtain the absolute distance from the micrometer reading. it is necessary to know the exact distance of the probe from the surface at some reference position. For the hot-wire probe used in the present investigation the closest distance permissible was very nearly 0.0005", the limit being imposed by the thickness of the copper coating at the two ends of the hot wire. The approximate reference distance estimated from an optical sighting before the beginning of a hot wire survey served as a starting point for an electrical method of determining the reference distance that was accomplished toward the end of the survey when the hot wire was very close to the surface. After the hot wire has been traversed down to the optically determined reference distance (which was 0.001" from the wall in the present investigation), the electrical method consists of further traversing the hot wire toward the surface in small steps of 0.0001" and very carefully observing its mean electrical output on the sensitive range of a digital voltmeter. The output increases until the copper coated ends just begin to touch the wall. Thereafter the output begins to decrease because further traversing of the hot wire tends to lift the central sensitive portion of the hot wire away from the wall. Once the output just begins to decrease, the hot wire is traversed away from the surface to avoid any possible damage to the hot wire. The micrometer reading just before the hot wire output begins to decrease gives the reference value corresponding to the distance that is half the diameter of the copper coated portion. The method is quite satisfactory but requires extreme care in its execution.

3.2 Hot-wire probe

The design features of the single rotated hot-wire probe used in the present investigation are shown in Fig. 6. Figure 6a shows a photograph of

the probe assembly and photomacrographs of the needles and the hot wire soldered to the needle tips. The sensor itself consists of a central sensitive section of 3.8 μm (0.00015") diameter and 1.25 mm (0.050") long platinum coated tungsten wire with approximately 0.001" dia. copper plated end sections* soldered to the tips of two sewing needles mounted 1/8 inch apart in a probe holder. The needles were specially ground down [40] to taper from 0.021" diameter at the root to 0.012" diameter at the tip. Details of probe holder construction and hot wire soldering are given in [42].

Each of the hot wires used in the present investigation had a length-to-diameter ratio of 333.33 and a nominal sensor resistance of 6 ohms (at 25°C). The combined resistance of the needles and the electrical leads was nominally 0.47 Ω (at 25°C). The hot wires were operated from a DISA 55D01 constant temperature anemometer unit at a resistance of usually 1.8 times the cold resistance.

3.3 Flush-mounted hot-film gage

The design features of the flush-mounted hot-film gage are shown in Fig. 7. Figure 7a shows a photograph of the hot-film gage assembly and a photomacrograph of the hot-film sensor. The design considerations for hot-film gages are described in Appendix B.

The hot-film gage consists of a thin platinum film deposited at the center of a pyrex disk mounted flush at one end of an inner brass cylinder** which rotates freely inside an outer brass cylinder. The sensitive portion of the film is 0.004" wide, 0.130" long and about 2000°A thick. It is coated with alumina (about 9500°A thick). Its two ends are connected to two short gold pins (positioned in the pyrex disk) by gold paste. Insulated electrical leads (#26 gage PVC wire) soldered to the gold pins are taken out through the open end of the inner brass cylinder. The inner and outer brass cylinders

---

*Obtainable as a replacement sensor in cards of 12 wires from: Thermo-Systems, Inc., 2500 North Cleveland Avenue, St. Paul, Minnesota 55113.

** The machined inner brass cylinder was sent, for subsequent deposition of the hot film, to: Thermo Systems Inc., 2500 N. Cleveland Ave., St. Paul, MN 55113.

are machined so that their ends are flush and they fit to the traverse mechanism.

The hot-film used in the present investigation had an aspect ratio of 32.5 and a nominal film resistance of 14.025 ohms at 25°C. The leads, each about 2 feet long, had a resistance of nearly 0.21 ohms. The usual operating resistance as set on the DISA 55D01 constant temperature anemometer was 19.00 ohms corresponding to a film temperature of 250°C.

3.4 Sublayer fence

A sublayer fence was used in the present investigation to duplicate the measurements of the hot-film gage so as to provide an independent check on the performance of the latter and also to serve as a stand-by in case the hot-film gage malfunctioned or got damaged (burnt out) during its operation*. It was also the intention to study in some detail the directional characteristics and the calibration of the fence and to assess its suitability as a vector meter for surface stress measurements in a three-dimensional turbulent boundary layer [42].

The constructional details of the sublayer fence used in the present investigation are shown in Fig. 8. Figure 8a shows a photograph of the sublayer fence assembly and two photomacrographs of the fence. The sublayer fence unit consists of an inner brass cylinder that can rotate freely inside an outer brass cylinder. These two cylinders are machined so that they fit to the traverse mechanism. The inner cylinder serves as a probe holder for the fence which is located at the center of the working (ground) face of the

*Only one spare hot-film gage was available. But this had developed some problem apparently associated with contact resistance. The hot-film gages were quite expensive.

inner cylinder. The fence is ground flush with the working surface except for the center section of 0.125" length where it is stoned to a height of 0.003" above the surface. The aspect ratio of the fence is 41.67. The static pressure drop across the fence is sensed by two slots (each 0.003" wide and 0.125" long) on either side of the fence. Manometer connections are made at the rear end of the inner cylinder.

3.5 Preston probes

These probes were intended to serve as standards to check out the hot-film gage and the sublayer fence in two-dimensional measurements. In three-dimensional measurements, they essentilly served as overall checks on the performance of the hot-film gage and the sublayer fence. Because of their poor angular resolution, they were originally not intended for measuring the direction of the wall shear stress; however, subsequently they were used in the present investigation for measuring the direction of the wall shear stress as well.

Figure 9 shows the constructional details of two Preston probes used in this investigation. Figure 9a shows the photographs of the Preston probe assemblies and some photomacrographs of the probe tips. Each probe assembly consists of an inner brass cylinder rotating freely inside an outer brass cylinder. These two cylinders are machined so that their ends are flush and they fit to the traverse mechanism. The inner cylinder serves as a probe holder. Manometer connection is made at the rear end of the inner cylinder to monitor the total head indicated by the probe. In actual use, the wall static tap nearest to the Preston probe is chosen for monitoring the wall static pressure.

The Preston probes were constructed from hypodermic stainless steel tubing. The large probe with an outside diameter of 0.032" had an inside-to-outside diameter ratio of 0.625 and a length-to-outside diameter ratio of 4, the corresponding figures for the small probe with an outside diamter of 0.018" being 0.555 and 7, respectively. The bent tip was carefully positioned in the inner cylinder so that the mouth of the probe rested squarely at the center of the working surface of the inner cylinder and then glued to it with epoxy.

3.6 Hot-wire calibration

The near-surface anemometer studies planned in the present investigation called for a calibration facility that could provide known flow velocities for calibrating hot wires. A small free jet facility (nozzle exit diameter = 2") was specially designed and constructed for a speed range of 1 to 55 ft/sec. Figure 10 shows a photograph of the free jet facility with the hot-wire probe mounted for calibration. The details of this facility and its performance are given in [42].

The low speed calibration of the free jet facility (performed with a smaller nozzle) facilitated the direct verification of the validity of the extrapolated linearized hot-wire calibration curve in the low speed range (<10 ft/sec). Figure 11 shows a low speed calibration of the hot wire in the free jet facility. A discussion of the extrapolation of hot-wire calibration to low speeds, related measurements and their implications also appears in [42].

3.7 Calibration of wall shear stress devices

The wall shear stress studies planned in the present investigation necessitated a reliable facility that could provide known wall shear stresses

for calibration of measurement devices. A knowledge of the static pressure gradient, $(\frac{dp}{dx})$, and the diameter of the pipe, D, is all that is needed to determine the wall shear stress in a fully developed pipe flow, where a momentum balance yields the following simple relation [44, p. 503]:

$$\tau_w = -(\frac{dp}{dx})(\frac{D}{4}) \qquad (1)$$

A pipe flow facility can, therefore, serve as a primary standard for calibration of wall shear stress measurement devices. The pipe flow facility used in the present investigation is a modification of the set-up originally used in reference [45] and is described in detail in [42].

Figure 12 shows a portion of the pipe flow facility with the traverse mechanism mounted at the test section. The inside diameter of the pipe was 8.25" and the length of the pipe between the exit plane of the inlet nozzle and the test section was 46' 9.25", giving an (L/D) = 68. The blower was located about 8 feet downstream of the test section and the nearest joint to the test section was 20 feet upstream. A 3/4" diameter instrumentation port and a mounting flange provided at the test section were specially designed to mount the wall shear stress devices and the traverse mechanism. Seven, 0.042" diameter static pressure taps located 12" apart along the pipe furnished data to evaluate the static pressure gradient in the test section. The static tap (0.021" diameter) used for monitoring the reference static pressure during calibration of the Preston probes was located in the test section plane but was displaced 2.3" from the instrumentation port. A mount was provided in the plexiglas observation section downstream of the test section for installing a Pitot-static probe to monitor the pipe centerline velocity.

Chapter 4

Experiments

In order to hold the scale effect constant throughout, all the measurements reported in this investigation were carried out at a constant upstream Reynolds number of 3.25×10^5/foot corresponding to a freestream velocity of 53-57 feet per second in the relaxing region. The upstream reference station was located at a distance of 5 feet from the beginning of the test section and port 1 nearly 12 feet downstream of the reference station. A standard Pitot-static probe permanently installed at this station was used to monitor the tunnel speed on a micromanometer. Before setting up the speed, the tunnel was allowed to run for sometime to attain steady state conditions. In the case of hot wire surveys, this time was restricted to about 20 minutes to minimize the calibration drift due to temperature change. With the hot-film measurements large times amounting to 2-4 hours were necessary depending on the ambient conditions inside and outside the tunnel area. With the sublayer fence and the Preston probe measurements, about 30 minutes were satisfactory.

Before starting with the three-dimensional wall and near-wall measurements, some two-dimensional measurements were made in the turbulent boundary layer (in the absence of the hump). Earlier measurements [40] had indicated a thickness of nearly 3.5" for the two-dimensional boundary layer. The near wall measurements made in this investigation were limited by the traverse mechanism to 0.95" so that each hot wire survey covered the entire inner layer region and a little portion beyond it. The survey points (i.e., y values) in the boundary layer excluding a distance of 0.010" of the viscous sublayer region adjacent to the wall were distributed in such a way that when plotted

on a log scale the wall coordinates y^+ were very nearly equally spaced. Although the traverse mechanism was designed to minimize backlash, the actual traversing was always done in one direction only, from the outermost position of the hot wire toward the test wall.

Details of measurements in two- and three-dimensional boundary layers are given in the following sections. The data obtained from two- and three-dimensional experiments was reduced from calibration curves. Some typical calibration curves are shown in Figs. 13-17. The details of the calibration experiments and a brief discussion of the calibration data are given in [42].

4.1 Two-dimensional experiments

These experiments were performed to (i) check out various probes, the instrumentation and the traverse mechanism and (ii) determine the angular response of the flush-mounted hot-film gage and the sublayer fence. Those experiments relating to the angular response are described in [42]. More importantly, the two-dimensional measurements provided the necessary data from which to estimate the wall proximity correction for hot wire readings very close to the wall. These corrections were later utilized in the three-dimensional hot-wire data very close to the wall (see subsections 5.3.1 and 6.3.2). These measurements also provided information on the initial state of the boundary layer in the absence of the wing-like model. The two-dimensional experiments described below were made at only two locations (ports 1 and 7, Fig. 3). In the three-dimensional flow field port 1 corresponded to the first streamwise measuring station in the relaxing region and port 7 to the last station. They were 34" apart, port 1 being 0.75" behind the trailing edge.

4.1.1 Hot wire surveys

After calibration the hot wire the probe was positioned in the instrumentation port and secured to the traverse mechanism. The hot wire sensor

was aligned to ± 0.125° with the normal to the local horizon and its distance from the wall when closest to it was estimated optically with a slanted mirror -microscope sighting device. The hot wire was repositioned at its outermost position before commencing the hot wire survey. At each survey point both the d.c. compnent* of the linearized anemometer output voltage and the mean square of the a. c. component of the filtered output voltage were recorded with the hot wire oriented in its normal position, +45° position and -45° position, in succession. The linearized anemometer output signal was usually filtered at 20 KHz. Toward the end of the traverse the micrometer reading corresponding to the reference distance was determined by the electrical method (see section 3.1). The hot wire was then repositioned again at its outermost position and its output checked for any drift during the actual traverse. The hot wire probe was then taken out of the wind tunnel and calibrated again in the free jet. When the drift was small (<3%), the calibration curve interpolated from the initial and final calibration curves was used for reducing the hot wire survey data; otherwise the experiment was usually repeated in its entirety.

No directional profile survey with the hot wire was necessary in the two-dimensional boundary layer. However, sample directional measurements were made during the hot wire survey to check the collateral nature of the boundary layer.

4.1.2 Wall shear stress measurements

The hot-film gage and the sublayer fence used in the present investigation were checked against the Preston probes by making two-dimensional wall shear stress measurements at ports 1 and 7.** Because of the two-dimensional nature

---

*The d. c. component was not required in +45° and -45° positions of the hot wire.

**The applicability of a Preston probe in a two-dimensional turbulent boundary layer with zero pressure gradient has been well established [46].

of the boundary layer no direction measurement was necessary. In the case of the hot-film gage, after the tunnel attained steady state conditions, the readings of the two thermometers (one at the inlet to the tunnel and the other mounted to the base plate of the traverse mechanism) were noted down and the cold resistance of the hot-film gage measured on the CTA.* The film operating resistance was set at 19.00 Ω (as indicated on the CTA), the anemometer output voltage passed through a zero-suppressor circuit and the d. c. component of the suppressed signal recorded after 5 minutes. As a check on the measurement, it was the usual practice to measure the output at other values of the film operating resistance (18.90 Ω and 18.80 Ω as indicated on the CTA). In the case of the sublayer fence and the Preston probes, the output was monitored on a micromanometer after the tunnel attained steady state conditions. The usual response time allowed was 4-5 minutes for the sublayer fence and the larger Preston probe and 10 minutes for the smaller one.

4.2 Three-dimensional experiments

Unlike the two-dimensional case additional direction measurements were required in the three-dimensional experiments. Consequently, the three-dimensional experiments extended over much longer periods compared to the two-dimensional experiments. The direction of the mean velocity vector was required to align the hot-wire probe for measuring the velocity. Therefore, during the hot wire surveys of the mean velocity vector, the direction measurement preceded the magnitude measurement. During the wall shear stress measurements, the direction measurement did not always have to precede the magnitude measurement

---

*Constant temperature aneomometer

as the direction of the mean wall shear stress vector was often known* from a previous hot wire survey (by extrapolation) or wall shear stress measurement.

All direction measurements were accomplished by the bisector method. It was the usual practice to check the direction by repeating the experiment with the probe oriented at a different angle between the sensor and the normal to the local mean direction of flow.

The following subsections describe the three-dimensional measurements in some detail.

4.2.1 Wall static pressure measurements

It was pointed out in section 2.4 that the static taps (77 in all) in the aluminum flat plate were intended to map out the wall static pressure field in the region behind the trailing edge of the hump. The wall static pressure measurements were carried out with a micromanometer with tap #22 serving as the reference tap (Fig. 3). The static pressure difference between the static tap at each port location and the corresponding reference static tap for the Prestor probe measurement was measured directly. To avoid unduly long response time damping tubes were not used in the pressure leads. Because of fluctuations about 3 minutes were still needed to take a good average reading. The initial reading of the micromanometer was checked for every tap reading before changing taps.

4.2.2 Pitot-static probe measurements

A separate run was made to measure the local freestream velocity at each port location with a conventional Pitot-static probe. The total-head tube of the Pitot-static probe was 0.125 inches in diameter and had an opening of

---

*It is not essential that this should be known exactly for the error involved in the magnitude measurement is small for small misalignments of the sensors with the local normal to the shear stress vector (see [42]).

0.043 inches. A dummy plug was used to position the probe at a port location. The probe tip was located at a distance of approximately 8 inches from the wall and 1.75 inches ahead of the center of the port. The probe was aligned with the local horizon* using a spirit level. The output of the probe was measured on the micromanometer. No damping was used in the pressure leads.

4.2.3 Hot wire surveys

Because of the direction measurements, the procedure followed in a three-dimensional hot wire survey differed in certain respects from that for a two-dimensional hot wire survey described earlier and is briefly described below highlighting the essential differences.

First the procedure outlined for a two-dimensional survey was followed up to and including the setting of the tunnel speed. At each survey point the mean direction of the flow was determined by the bisector method. The direction survey was continued until the last survey point closest to the wall as predetermined optically was reached. After completing the direction survey there, the hot wire was repositioned at its outermost position and the usual hot wire velocity traverse of the boundary layer commenced. At each survey point, the hot wire was first oriented with the normal to the local mean direction of the flow which was known from the the preceding direction survey. The d. c. component of the linearized anemometer output voltage and the mean square of the a. c. component of the filtered output voltage were recorded. The hot wire was then rotated in succession through +45° and -45° from its orientation and the corresponding mean squares of the a. c. component of the filtered output voltage were recorded. Towared the end of the traverse the micrometer reading corresponding to the reference distance was determined

---

*The misalignment between the streamline at the edge of the boundary layer and the local horizon is estimated to be at the most 1° in the three-dimensional field and 0.5° in the two-dimensional field in the absence of the hump [40].

by the electrical method (see section 3.1). The hot wire was then repositioned again at its outermost position and its output checked for any drift during the actual traverse. The hot wire probe was then taken out of the wind tunnel and calibrated again in the free jet facility.

4.2.4 Wall shear stress measurements

The primary objective of these measurements was to make independent wall measurements (direction* and magnitude of the wall shear stress vector) at the port locations and to compare these with the extrapolated/estimated results of the hot wire data. If the direction of the limiting streamline was already known from an extrapolation of the hot wire data or from a wall shear stress measurement, the shear stress device was oriented with the local normal to this direction and the procedure outlined in subsection 4.1.2 followed for magnitude measurement.

The direction measurement was accomplished next.** When the direction of the limiting streamline was not known, the direction measurement preceded the magnitude measurement. In either case, the direction was accurately determined by the bisector method.

---

* The Preston Probes were originally not intended for direction measurement.

** Whenever a prior knowledge of the limiting streamline was available, the magnitude measurement was made first to keep the drift in the initial conditions to the bare minimum, particularly with hot-film measurements.

Chapter 5

Reduction of Experimental Data

The procedure followed in reducing various raw data is briefly described in sections 5.1 to 5.4 and an estimate of possible experimental errors associated with various measurements is given in section 5.5. The reduced data is presented in the form of tables and/or graphs. The results are discussed in the next chapter.

5.1 Wall static pressure data

The reduction of the data from the wall static pressure measurements was straightforward. The pressure difference (between any tap and the reference tap #22) was nondimensionalized by the dynamic head of the upstream reference station.

5.2 Pitot-static probe data

The local freestream velocities prevailing during hot wire surveys and wall shear stress measurements are required for nondimensionalization of the measured flow variables.

The freestream velocity ratio (local to upstream reference velocity), σ, can be determined for each port location from the Pitot-static probe data. Since the upstream reference Reynolds number was held constant for all tests, the reference velocity $U_{\infty r}$ would be slightly different because of different atmospheric conditions; but the area of the effective potential flow geometry at any port location remained the same because, all other things unchanged, constant Reynolds number implies constant displacement thickness. Therefore, the prevailing local freestream velocity during a test run may be determined simply by multiplying the measured velocity at the upstream reference station

with local freestream velocity ratio σ obtained from the Pitot-static probe data.

5.3 Hot wire data

For hot wire surveys at each port location, a mean calibration curve was used to obtain the resultant mean velocities from the d. c. components of the linearized output voltages. The mean calibration curve was interpolated from the initial and final calibration curves to correspond to the actual hot wire survey time. Figure 13 shows the initial and final calibration curves for a typical three-dimensional hot wire survey. The resultant friction velocity, $\bar{U}^*$, used to evaluate the wall coordinates was based on the resultant mean skin-friction coefficient determined from the 0.032" dia Preston probe measurement[†] at the respective port location. A wall proximity correction curve obtained from the two-dimensional data was used to correct the mean velocity data from hot wire surveys close to the wall ($y^+ < 5$). The resultant mean skin-friction coefficient was estimated from the measured velocity profile using Bradshaw's simplified version [47] of Clauser's technique [48]. The limiting streamline angles were extraplated from the mean direction profiles.

The turbulence data was first reduced in the local axes system x_l y_l z_l and then transformed to the reference axes system xyz. Using $-\overline{u_l w_l}$ correlation the mean of flow direction determined from the hot wire measurement was corrected to estimate the mean-flow direction. Details pertaining to the reduction of hot wire data are given in the following subsections.

5.3.1 Wall proximity corrections for hot-wire readings

A hot wire indicates an increased output as a solid wall is approached

---

[†]The choice is discussed later in subsection 6.4.1

and, therefore, the indicated (or apparent) velocity is larger than the true value. Although the effect is usually attributed to the increased cooling of the hot wire near a colder solid boundary [49-52], the actual mechanism of the wall influence on the hot wire is not fully understood [53]. Recent measurements [54, 55] show the importance of the inclination of the probe needles to the wall. In general the wall influence depends on the distance between the hot wire and the wall, the overheat ratio, the flow velocity, the wall material and the probe geometry. All hot wire readings close to the wall have to be corrected for wall proximity effects.

There is no simple unique correction curve valid for all cases*; the wall influence is best estimated on an individual basis for any given flow configuration and probe geometry. It is based on the observation made by Oka and Kostić [56] that the apparent dimensionless velocity profiles in the viscous sublayer are universal too and that the wall influence ceases at the same wall coordinate $y^+ = 5$. From the two-dimensional law of the wall plots shown in Fig. 18, an estimate of the wall proximity corrections could be made for the observed readings close to the wall. Noting that $U^+ = y^+$ in the linear sublayer region, it is seen that the apparent or indicated velocities U^+ are higher than the true values for $y^+ < 5$ and the wall proximity effects cease beyond $y^+ = 5$. Therefore, the correction ΔU^+ is given by the difference between U^+ and true U^+ $(=y^+)$ at any $y^+ < 5$. These corrections for hot wire readings taken close to the wall at ports 1 and 7 are shown in Fig. 19. The

---

*The method of correction based on extending Wills' laminar correction [50] to the turbulent case failed to yield satisfactory results even for the two-dimensional data (Fig. 20) and, therefore, it was not tried in the case of the three-dimensional hot wire surveys [42].

wall proximity correction curve shown in the figure was obtained by drawing a mean curve to pass through these corrections. It represents the dimensionless difference between apparent and true velocity in the two-dimensional flow versus nondimensional wall coordinates. It is similar to the correction curve of Oka and Kostic obtained from measurements in a fully developed turbulent channel flow but plotted on a log-log scale. Figure 20 shows the corrected mean velocity data close to the wall at port 7. The agreement between the corrected velocity data and the wall velocity gradient line is quite satisfactoyr over the entire sublayer range. All the three-dimensional hot wire data close to the wall, $y^+ < 5$, was, therefore, corrected using the wall proximity correction curve.

5.3.2 Skin friction from measured velocity profiles

The Prantdl law of the smooth wall [44, p. 540] in the logarithmic region of pipe flows and two-dimensional zero pressure gradient turbulent boundary layers is

$$\frac{U}{U^*} = A + B \log \left(\frac{U^* y}{\nu}\right) \qquad (2)$$

where A and B are assumed to be universal constants. The Clauser technique of determining skin friction from a measured velocity profile using equation (2) is well known [48]. An equally accurate but much simpler technique in which the velocity profile is plotted in the usual coordinates has been suggested by Bradshaw [47]. This technique consists in choosing one suitable reference point (U^*y/ν) on log law, equation (2), and then plotting it on the usual axes y, (U/U_∞) for different values of (U_∞/U^*). The resulting curve intersects the measured velocity profile at a well-defined point whose value of (U/U_∞) determines the skin friction from the relation

$$c_f = 2\left(\frac{U^*}{U_\infty}\right)^2 = 2\left[\frac{(U/U_\infty)_{int}}{(U/U^*)_{ref}}\right]^2 \qquad (3)$$

With Patel's values for A and B [46], namely A = 5.45 and B = 5.5, and $(U^*y/\nu)_{ref} = 100$, equation (3) simplifies to

$$c_f = \left(\frac{1}{135.301}\right)\left(\frac{U}{U_\infty}\right)^2_{int} \qquad (3a)$$

The Bradshaw technique was used (with Patel's values for log law constants A and B) to estimate the skin friction from the measured mean velocity profile with the log law based on the resultant mean velocity profile.

5.3.3 Turbulence data

The equations necessary for reducing the mean square turbulence signals from hot wire surveys into longitudinal turbulence $\overline{u_1^2}$, lateral turbulence $\overline{w_1^2}$ and their crosscorrelation $-\overline{u_1 w_1}$ are given below in a local axes system $x_1 y_1 z_1$ [42, 57]. In the case of two-dimensional surveys the local axes system coincides with the reference axes system xyz and there is no need for a coordinate transformation of the reduced turbulence data. However, in the case of three-dimensional surveys these two axes systems do not usually coincide because of the presence of crossflow and, therefore, a coordinate transformation is required if the turbulence data is desired in the reference axes system.

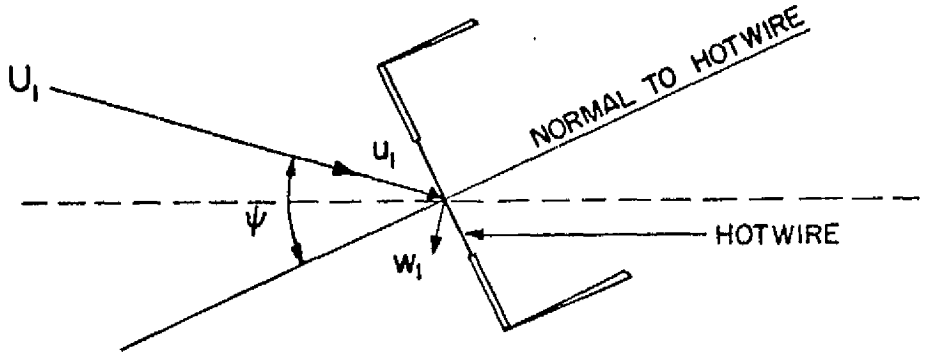

For a linearized single hot wire held normal to the direction of mean flow U_1 (which is $\bar{U}$ in the three-dimensional surveys and U in the two-dimensional surveys)

$$E = C\, U_1 \tag{4}$$

where C is a constant of proportionality. When the hot wire is yawed through an angle ψ (see sketch), it can be shown that

$$E = C_1\, U_1 \tag{4a}$$

$$C_1 = C(\cos^2 \psi + k^2 \sin^2 \psi)^{1/2} \tag{4b}$$

$$\overline{w_1^2} = \left[\frac{\overline{e_1^2} + \overline{e_2^2}}{2\, C_1^2 \tan^2 \psi} - \frac{\overline{u_1^2}}{\tan^2 \psi} \right] \left[\frac{1 + k^2 \tan^2 \psi}{1 - k^2} \right]^2 \tag{5}$$

and

$$-\overline{u_1 w_1} = \left[\frac{\overline{e_1^2} - \overline{e_2^2}}{4\, C_1^2 \tan^2 \psi} \right] \left[\frac{1 + k^2 \tan^2 \psi}{1 - k^2} \right] \tag{6}$$

where $\overline{e_1^2}$ and $\overline{e_2^2}$ denote the mean square output for the $+\psi$ and $-\psi$ orientations, respectively. If $\overline{e^2}$ is the mean square output corresponding to the normal position of the hot wire (i.e., $\psi = 0°$), then

$$\overline{u_1^2} = \frac{\overline{e^2}}{C_1^2} \tag{7}$$

Note that for $\psi = 0°$, $C_1 = C$. Once $\overline{u_1^2}$ is determined from the normal position, $\overline{w_1^2}$ follows from equation (5) and $-\overline{u_1 w_1}$ from equation (6). The second factor in equations (5) and (6) represents the correction factor due to tangetial cooling. The correction factor is quite substantial and increases

with ψ as shown in the following table:

Yaw angle ψ	Correction factors for k = 0.2	
	$\left[\frac{1 + k^2 \tan^2 \psi}{1 - k^2}\right]^2$	$\left[\frac{1 + k^2 \tan^2 \psi}{1 - k^2}\right]$
30°	1.1141	1.0555
45°	1.1736	1.0833
60°	1.3611	1.1667

During the hot wire surveys of the present investigation, the mean square voltages were recorded for three positions of the hot wire: $\psi = 0°$, $\psi = +45°$ and $\psi = -45°$. Constant C was estimated from the respective mean calibration curve. k was determined from the angular response of the hot wire in the free jet (Fig. 14).For a truly two-dimensional flow the correlation of u_1 and w_1 is zero, by definition, i.e. $\overline{u_1 w_1} = 0$. With two-dimensional surveys no coordinate transformation was necessary, i.e., $\overline{u^2} = \overline{u_1^2}$, $\overline{w^2} = \overline{w_1^2}$ and $\overline{uw} = \overline{u_1 w_1}$. In the case of the three-dimensional hot-wire surveys, the reduced turbulence data in the local axes system $x_1 y_1 z_1$ was transformed to the reference axes system using equations (8), (9), and (10) derived below.

In the sketch shown below, α denotes the local flow angle with respect to the reference axes system xyz.

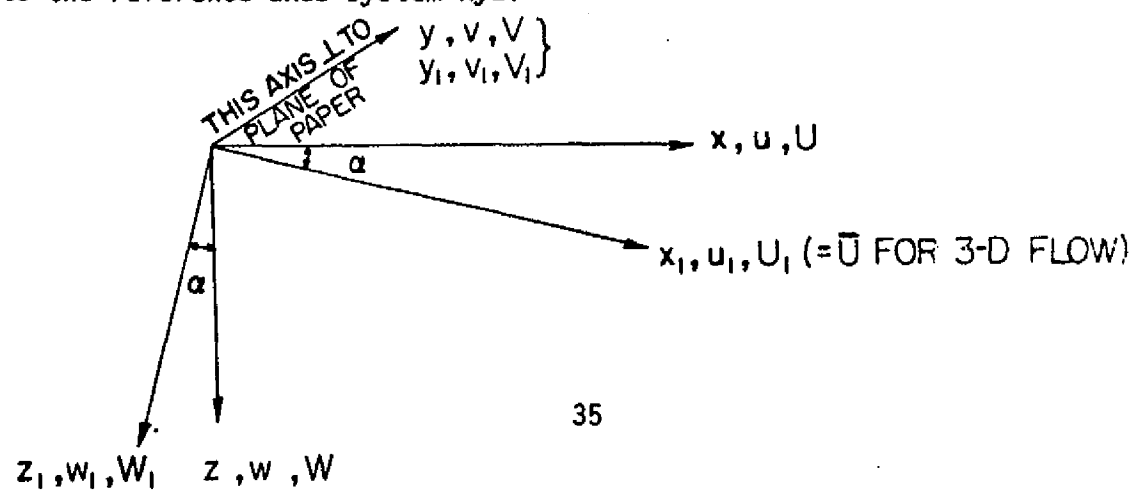

From the sketch it follows that

$$u = u_1 \cos \alpha - w_1 \sin \alpha$$

and

$$w = w_1 \cos \alpha + u_1 \sin \alpha$$

Squaring and taking time averages of these equations, we obtain

$$\overline{u^2} = \overline{u_1^2} \cos^2 \alpha - \overline{u_1 w_1} \sin 2\alpha + \overline{w_1^2} \sin^2 \alpha \qquad (8)$$

and

$$\overline{w^2} = \overline{w_1^2} \cos^2 \alpha + \overline{u_1 w_1} \sin 2\alpha + \overline{u_1^2} \sin^2 \alpha \qquad (9)$$

Multiplying u and w and taking the time average of the resulting equation, we get

$$-\overline{uw} = -\overline{u_1 w_1} \cos 2\alpha - \frac{1}{2} (\overline{u_1^2} - \overline{w_1^2}) \sin 2\alpha \qquad (10)$$

Note that equations (8) and (9) give $\overline{u^2} + \overline{w^2} = \overline{u_1^2} + \overline{w_1^2}$.

5.3.4 Mean direction of flow and mean-flow direction

A direction sensitive instrument such as a hot wire is sensitive to fluctuations in flow direction. Therefore, its mean response will determine a "mean direction of flow" and not the "mean-flow direction" (using the terminology of Rose [58]). The mean direction of flow in any plane is the time-averaged direction of the instantaneous compoent of the velocity vector in that plane whereas the mean-flow direction is defined by mean-velocity components. These two directions are distinct in unsteady flows, the difference being small for small crosscorrelations. As pointed out in reference [59], it is important to distinguish between these two directions when a direction measurement is accomplished by the rotated hot-wire technique as in the present investigation.

In the sketch shown below $\bar{U}$ is the resultant mean velocity and α is the measured flow angle. u_1, w_1 are turbulent fluctuations referred to the local axes system. α_m is the angle of mean-flow direction.

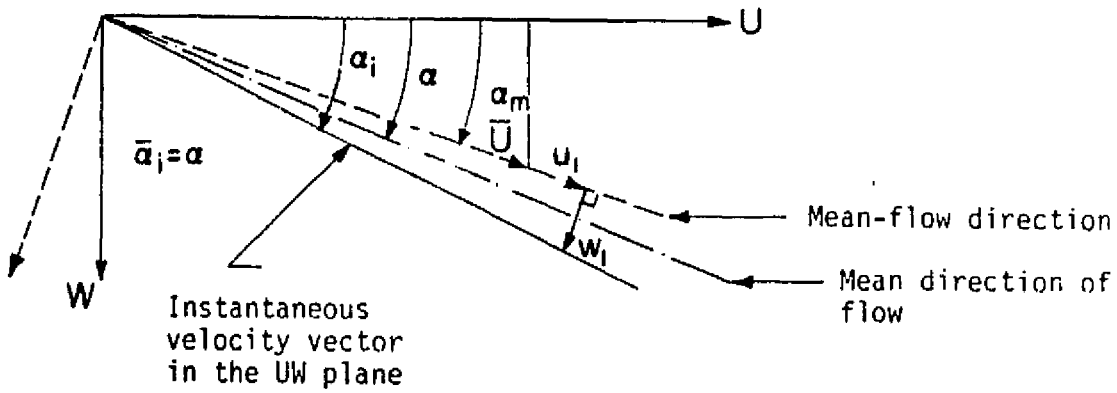

Rose has derived a relationship for the difference between the mean direction of flow and the mean-flow direction. The difference is proportional to the velocity crosscorrelation and is correct to second order in the velocity fluctuations. The same relationship is derived in [42] in a simpler way:

$$(\alpha - \alpha_m) = - \frac{\overline{u_1 w_1}}{\bar{U}^2} \text{, correct to second order} \qquad (11)$$

The cross-correlations obtained from the turbulence data of hot wire surveys were utilized to evaluate the difference between the mean direction of flow and the mean-flow direction.

5.4 Wall shear stress data

The use of the bisector method yielded the direction without any further processing of the data and, consequently, eliminated the need for yaw calibration curves. Wall shear stresses were calculated from the magnitude measurements using appropriate calibration curves (Figs. 15, 16 and 17). The power dissipated by the hot-film gage was calculated from the voltage output and the anemometer

bridge constants. The appropriate data from the wall static pressure measurement at the port location was utilized to correct the measured Preston probe output to refer to the local static pressure. In reducing the sublayer fence/Preston probe data, the output was non-dimensionalized to obtain x* and the corresponding non-dimensionalized wall shear stress y* was read off the respective calibration curves (Figs.16,17) The resultant mean skin-friction coefficients were obtained by non-dimensionalizing the wall shear stress data by the local freestream dynamic head.

5.5 Error estimation

A detailed error analysis will depend on the particular type of probe used and will involve the following considerations:

(i) probe parameters such as sensitivity, response time

(ii) accuracy of calibration

(iii) probe positioning (both linear and angular)

(iv) ambient parameters (such as temperature) influencing calibration

(v) reading accuracies of electronic meters, etc., and

(vi) aerodynamic effects such as flow interference, turbulence, velocity gradients, presence of solid boundary, etc.

Although some idea of obtainable accuracy can be estimated from calibration experiments, aerodynamic effects are very difficult to estimate. A complete analysis of errors is quite complex. However, a reasonable estimate of the overall accuracy of the measurements is possible from a careful analysis of the data itself. Such an analysis has been made for the present data, bearing in mind that:

(i) the flow was unsteady (turbulent)

(ii) all the data was recorded by hand after allowing sufficient response time/integration time

(iii) the probe sensitivity was considerably lower close to the wall and /or in regions of low shear stress close to the trailing edge.

The estimated overall errors in various measurements are summarized below. The values in parentheses refer to the regions close to the wall and/or in regions of low shear stress typified by ports 1 and 9.

(a) Hot wire data

Data		Overall experimental error
Mean flow, $\bar{U}$	angle	$\pm$ 0.125° ($\pm$ 0.5°)
	magnitude	$\pm$ 0.5% ($\pm$ 1%)
Turbulence	$\overline{u_1^2}$	$\pm$ 3% ($\pm$ 4%)
	$\sqrt{\overline{u_1^2}}$	$\pm$ 1.75% ($\pm$ 2%)
	Others	Higher for w_1 fluctuation and much higher for $-\overline{u_1 w_1}$ correlation

(b) Wall shear stress data

Type of device	Overall experimental error in	
	angle	magnitude
Hot-film gage	$\pm$ 0.25° ($\pm$ 0.5°)	$\approx \pm$ 5%
Sublayer fence	$\pm$ 0.5° ($\pm$ 1°)	$\pm$ 1% ($\pm$ 2%)
0.032" dia Preston probe	$\pm$ 0.25° ($\pm$ 0.75°)	$\pm$ 0.5% ($\pm$ 1%)
0.018" dia Preston probe	$\pm$ 0.25° ($\pm$ 1°)	$\pm$ 1% ($\pm$ 2%)

Chapter 6

Discussion of Experimental Results

Before discussing the results, some comments on the nature and limitations of the experimental data are in order. The extension of the hot wire surveys to cover the entire boundary layer region and the measurement of shear stress vector cound not be undertaken for want of time. In this sense the hot wire surveys are imcomplete. Finally, the nominal two-dimensional boundary layer upstream of the hump was contaminated by transverse non-uniformities which would be amplified in flowing over the hump* (see reference [40]). The non-uniformities would require a much finer spatial resolution of the initial data (for prediction methods) than was possible in this investigation. Therefore, The experimental data (even if it were complete!) would be somewhat less satisfactory as a test case [1] for assessing prediction methods. In any case, the interpretation of the local three-dimensional flow phenomenon based on local measurements will not be influenced by spanwise variations.

The hot-wire measurements and the wall shear stress measurements have provided experimental data pertaining to the relaxation characteristics of the mean-flow and the longitudinal and lateral fluctuating quantities in the inner layer region. The data also allowed an evaluation of an overall correlation (of crossflow profile in polar form) between wall shear stress vector and local free stream conditions. The near-wall measurements have provided experimental data bearing on the question of the existence (or nonexistence)

---

* Some spanwise variations were expected because of the low aspect ratio of the hump.

of near-wall collateral flow field. The experimental data is, therefore, discussed with particular emphasis on (i) the nature of mean-flow field very close to the wall and (ii) the streamwise relaxation characteristics of the flow field in the inner layer region.

After discussing the experimental data* in detail, a study is made of the streamwise relaxation of the three-dimensional flow field to the two -dimensional state. An assessment of the effect of small, measured wall static pressure gradient on the flow field close to the wall is made by means of a sublayer analysis in subsection 6.3.5 and the experimental data compared with the resulting predictions.

6.1 Wall static pressure distribution in the relaxing region

The wall static pressure measured in the region behind the trailing edge of the hump (Table 4) indicates a small (less than 3% of the upstream reference dynamic head per foot) favorable pressure gradient in the streamwise direction (Fig. 21). Close to the trailing edge, the streamwise static pressure field above the tunnel centerline relaxes a little faster than that below the tunnel centerline. At a distance of 1 inch below the tunnel centerline corresponding to the streamwise location of instrumentation ports, the estimated streamwise pressure gradient in the neighborhood of port 1 is -2.508% of the upstream reference dynamic head per foot, i.e., $\frac{\partial C_p}{\partial x} = -2.508 \times 10^{-2}$/foot. The curves in Fig. 21a indicate a small (less than 3.5% of the upstream reference dynamic head per foot) adverse pressure gradient in the spanwise direction parallel to the trailing edge. The spanwise pressure gradient in the neighborhood of the tunnel centerline is decreading with the distance from the trailing

*Wherever applicable, the two-dimensional data is briefly commented upon as a representative asympototic state for the relaxing flow field. Appendix C, discusses the two-dimensional data on wall shear stress in more detail.

edge and is practically aero at x = 26.125" and 36.125" . At a distance of 0.75 inches from the trailing edge corresponding to the spanwise location of instrumentation ports, the measured spanwise pressure gradient is within 2% of the upstream reference dynamic head per foot. The transverse pressure gradient in the direction of crossflow (z is positive downwards) can be estimated from the curves in Fig. 21a by suitable interpolation. In the neighborhood of port 1 the estimated transverse pressure gradient is 2.098% of the upstream reference dynamic head per foot, i.e., $\frac{\partial C_p}{\partial z} = 2.098 \times 10^{-2}$/foot.

Taking the boundary layer thickness* at port 1 as approximately 3.5 inches and considering only the streamwise line of instrumentation ports, it is seen that the pressure gradients amount to less than one percent of the upstream reference dynamic head over a distance of one boundary layer thickness and, therefore, the relaxing region along the streamwise line of ports may be considered to be nominally in zero pressure gradient for analysis of the flow field not close to the wall. However, the presence of even small lateral pressure gradients will influence the crossflow field very close to the wall. A sublayer analysis of the flow field with the above estimated values of the pressure gradients indicates a decrease in the crossflow angle close to the wall (subsection 6.3.5). In fact small decreases in crossflow angle were measured at all port locations during the hot wire surveys (subsection 6.3.1).

6.2 Variation of freestream velocity in the relaxing region

Figure 22 and Table 5 show the variation of the local freestream velocity along the streamwise line of ports in the relaxing region behind the trailing

---

*In reference [40], the thickness of the two-dimensional boundary layer (in the absence of the hump) is quoted as 3.5" and that of the three-dimensional boundary layer along the tunnel centerline and 1/2" behind the trailing edge as 3.7".

edge of the hump. The freestream velocity is very nearly constant from approximately 2.5 boundary layer thicknesses downstream of the trailing edge, whereas, in the region close to the trailing edge, the measurements imply a freestream adverse pressure gradient of approximately 2% of the upstream reference dynamic head per foot. Therefore, the streamwise static pressure gradients in the freestream and on the wall differ in sign. However, in terms of the magnitude, both are small and the flow may be treated as having a nominally zero, external, streamwise pressure gradient.

6.3 Mean-flow data from hot-wire surveys

Before discussing the three-dimensional mean-flow data, it is appropriate to make a few comments on the nature of the two-dimensional mean-flow data (Figs. 18-20 and Tables 1-2a) as it will be used for comparison with the relaxing three-dimensional mean flow. The two-dimensional law of the wall plots shown in Fig. 18 clearly show the extent of the logarithmic region typical of profiles in a zero pressure gradient flow. The agreement with the two-dimensional log law using Patel's constants (see subsection 5.3.2) is very good. The measured data compared with the linear curve $U^+ = y^+$ indicates that the wall proximity effects cease beyond $y^+ = 5$. A method of obtaining a simple and satisfactory correction curve for hot wire readings close to a wall has already been discussed in subsection 5.3.1 (Figs. 19 and 20).

6.3.1 Direction profiles in the relaxing region

The mean direction profiles (both measured and corrected) from hot wire surveys are shown in Fig. 23 and the pertinent data in Tables 6-8h. The resultant friction velocity, $\bar{U}^*$, used in evaluating the wall coordinates was based on the resultant skin friction, $\bar{c}_f$, determined from the 0.032" dia Preston probe measurement at the respective location. The particular choice of the

data from this Preston probe to estimate $\bar{U}^*$ from among several wall shear stress data is discussed later in subsection 6.4.1.

As described in subsection 5.3.4, the hot-wire turbulence data was used for making angle corrections to the indicated mean direction of flow to obtain the mean-flow direction (shown by flagged symbols). The correction is small in the outer portions of the inner layer, slowly increases as the wall is approached until $(-\overline{u_1 w_1}/\bar{U}^2)$ is a maximum and then begins to decrease with the decrease of $(-\overline{u_1 w_1}/\bar{U}^2)$. In the region close to the wall where the measured crossflow angle is constant, the correction is within the estimated experimental error in angle measurement and, therefore, not shown in Fig. 23. The maximum correction (-0.61°) occurs for the profile at port 9 and is less than 4% of the measured value. The angle correction is included here to show the effect of turbulence fluctuations on the mean angular response of the hot wire [58, 59]. However, in the present hot wire surveys the effect is small and, therefore, in subsequent discussions no distinction will be made between the mean direction of flow and the mean-flow direction.

The direction profiles (Fig. 23) indicate a small region of collateral flow field (i.e., constant crossflow angle) adjacent to the wall, thus confirming the results of the other investigators [38]. With the exception of profiles at the last three survey stations, which are practically two-dimensional, the data indicates the existence of a collateral flow field up to $y^+ = 9.7$ to 17.6, y^+ increasing with $\bar{U}^*$. The most striking feature in these profiles is the fact that the crossflow angle is actually decreasing in a narrow region extending from the point of maximum crossflow down to the outer limit of the collateral region. Although the actual decrease of crossflow angle itself was samll (of the order of 1° or less) it was observed consistently during the hot wire surveys at all port locations. The value of y^+ at which the maximum

crossflow angle occurs in the inner layer varies from 27.1 to 144.8, y^+ increasing with $\bar{U}^*$ as before. Thus the narrow region of decreasing crossflow extends between $y^+ = 9.7$ and 27.1 at port 9 (the lowest value of $\bar{U}^*$) to $y^+ =$ 17.6 and 144.8 at port 4. It should be noted that the value of y^+ corresponding to the maximum crossflow occurs at the apex of Johnston's triangular plot and widely different values have been quoted in the literature for its upper limit. Further discussion of the crossflow profiles in terms of the Johnston crossflow model is deferred until subsection 6.3.4.

In a three-dimensional boundary layer the crossflow results as a consequence of the impressed lateral pressure field and the crossflow angle increases continuously toward the wall. Because of the presence of small transverse wall static pressure gradients (see section 6.1) opposing the crossflow in the relaxing region, it is not unreasonable to expect some decrease in the crossflow angle as the wall is approached. As will be shown in subsection 6.3.5, a sublayer analysis of the flow field with the estimated values of the pressure gradients does indeed predict a decrease in the crossflow angle close to the wall, the predicted decrease being slightly higher than the measured decrease. A discussion of the spanwise variation and the streamwise relaxation of crossflow angle is deferred until subsection 6.3.6.

6.3.2 Mean velocity profiles in the relaxing region

The shapes of the resultant mean velocity profiles in the inner layer (Fig. 24) close to the trailing edge reflect the history of the boundary layer development over the hump. These profile shapes resemble those in adverse pressure gradient flows. The profile at port 9 which shows the maximum effect is practically linear in the inner layer. The mean velocity distribution in the boundary layer relaxes and becomes fuller with distance from the trailing edge and, at the last port location, it almost approaches the two-dimensional

distribution (in the absence of the hump). The relaxation of the inner layer is reflected in the extent of the wall similarity region in the law of the wall plots which are discussed in the next subsection.

The wall influence is brought out strikingly in Fig. 25 where the (uncorrected) resultant mean velocity data close to the wall is plotted in wall coordinates. The resultant friction velocity $\bar{U}^*$ was obtained from the respective resultant skin friction determined from the 0.032" dia Preston probe measurement. Because of the increased heat transfer from the hot wire in the vicinity of the wall, the apparent (measured) velocities are higher than the true values. Consequently, as the wall is approached, the uncorrected data points fall farther away from the linear distribution $\bar{U}^+ = y^+$. The experimental data shown in Fig. 25 indicates, in agreement with the earlier findings of Oka and Kostic [56] and the present findings from the two-dimensional data in subsection 5.3.1, that the apparent (measured) resultant velocity profiles in the viscous sublayer region are universal (local) and that the wall influence is negligible beyond $y^+ = 5$. The scatter in the region $y^+ < 1.5$ is largely due to errors in measuring very small distances from the wall. It should be noted here that (in the physical coordinates) the extent of the wall proximity effects increases with decreasing $\bar{U}^*$; for example the wall influence which is limited to approximately y = 0.005" from the wall at port 7 extends as far as up to y = 0.008" at port 9 where $\bar{U}^*$ is lowest.

This universality of the apparent profiles justifies the use of the wall proximity correction curve shown in Fig. 19 to correct the experimental data close to the wall ($y^+ < 5$). The corrected data is also shown (by flagged symbols) in Fig. 25. The agreement between the corrected data and the linear distribution $\bar{U}^+ = y^+$ is remarkable in the region $1.5 < y^+ < 5$. The scatter of the uncorrected data carrys over in the corrected data. The effect of

correcting hot wire readings for wall incluence is better represented and appreciated in Fig. 26 where the corrected resultant mean velocity profiles close to the wall are shown in the usual coordinates and compared with the respective wall velocity gradient lines. These lines represent the resultant velocity gradients at the wall which are obtained from the respective resultant skin friction determined from the 0.032" dia Preston probe measurement. The corrected data points approach the respective wall velocity gradient line as the wall is approached and indeed tend to fall on the line in the wall influence region that extends up to $y \approx 0.005$" at port 7 and $y \approx 0.008$" at port 9. The agreement between the corrected data and the respective wall velocity gradient line is exceptionally good in the wall influence region excluding points closest to the wall which could not be precisely located because of errors in measuring very small distances from the wall.

Lack of data on the normal component of turublence, $\sqrt{\overline{v^2}}$, did not allow correction of the hot wire readings for turbulence fluctuations. Within the wall influence region, the present method of wall proximity correction will incidentally include the turbulence correction (based on the validity of a linear distribution $\bar{U}^+ = y^+$, for $y^+ < 5$).

6.3.3 Law of the wall in the relaxing region

The resultant mean velocity profiles in the inner layer of the relaxing region are shown in wall coordinates in Figs. 27 and 27a. The resultant friction velocity, $\bar{U}^*$, was obtained from the resultant skin friction determined from the 0.032" dia Preston probe measurement at the respective location. In the region $y^+ < 5$, the corrected data is shown by flagged symbols. The correction was based on the results of Fig. 19. For purposes of comparison, the log-law relation based on the resultant velocity profile and constants suggested by Patel [46], $\bar{U}^+ = 5.5 \log y^+ + 5.45$, and the linear sublayer

relation $\tilde{U}^+ = y^+$ are also shown in Figs. 27 and 27a.

Before discussing wall similarity in the relaxing region, a few comments on the applicability of the law of the wall in three-dimensional turbulent boundary layers are in order. Wall similarity has been the subject of investigation of many research workers in the past several years. Although the experimental studies [21, 24, 28, 29, 31, 60, 61] have supported the existence of a wall similarity region in three-dimensional flows, none of them has shown any overriding support for any particular form of the law of the wall. A brief assessment of these different laws may be found in reference [31], where it is concluded that, in practice, the different laws differ very little from one another particularly for small crossflows and moderate pressure gradients. Etheridge [31] estimates that the difference between values of skin friction obtained from Clauser plots of the streamwise and the resultant velocity profiles will only be about 4% when the wall crossflow angle is as large as 20°.

The existence of wall similarity in the relaxing region of the present investigation is confirmed by the law of the wall plots shown in Figs. 27 and 27a, thus concurring with the findings of the previous investigators. The agreement of the data with the log-law relation based on the resultant mean velocity profile and Patel's constants is quite satisfactory at all but one port location (port 9). It should be noted that a slight vertical shift of the log-law relation will bring it into closer agreement with the data at port 9. The maximum wall crossflow angle measured was 21° (at port 1) and the pressure gradients in the relaxing region were very small (sections 6.1 and 6.2).

It is now appropriate to discuss the applicability of Preston probes* in the present investigation. A more careful examination of the log-law region in the law of the wall plots indicates that, even at port 9 where the effect of adverse pressure gradient is felt most, there exists sufficient log -law region to justify the use of even the larger Preston probe (0.032" diameter). The log-law region at port 9 is seen to extend up to at least $y^+ = 110$ corresponding to $y \simeq 0.175$" which is much larger than the Preston probe diamter. In regard to angular response, a Preston probe is insensitive to small changes in the local flow direction. The measured variation in the mean flow angle across the mouth of the Preston probe was not more than a degree (subsection 6.3.1) and, therefore, it should not influence the performance of the Preston probe. From these considerations it is concluded that the readings of both Preston probes were unaffected bu the pressure gradient or the crosslfow in the relaxing region.

A complete discussion on the relaxation of the mean flow in terms of the decay of crossflow is deferred until subsection 6.3.6. Some features of the relaxation can be identified in the law of the wall plots. It was mentioned in the preceding section that the resultant mean velocity distribution in the boundary layer becomes fuller with distance from the trailing edge. This is very clearly seen in terms of the extent of the log-law region in the law of the wall plots. As the flow field relaxes in the streamwise direction (port 1 to port 7), the log-law region continuously grows and, at port 7, almost approaches the two-dimensional distribution in the absence of the hump (compare

---

*An illuminating discussion on the qualitative effects of pressure gradients on the law of the wall in two-dimensional flows and consequently on the readings of a Preston probe appears in reference [46]. Similar qualitative effects of pressure gradients on the log law region in three-dimensional turbulent boundary layers have been observed in references [31, 28 and 29].

log plots for port 7 in Figs. 18 and 27a). Thus the three-dimensional boundary layer is gradually relaxing toward a two-dimensional state behind the trailing edge. Furthermore, the relaxation is seen to be relatively faster in the region close to the trailing edge.

6.3.4 Polar plots of mean velocity profiles

Johnston's crossflow model [19] is the simplest polar plot often used to represent the crossflow field in three-dimensional studies [2, Chapter 7]. Sketched below is a typical Johnston's model, where the tip of the velocity vector follows the two sides of a triangle (in the hodograph plane).

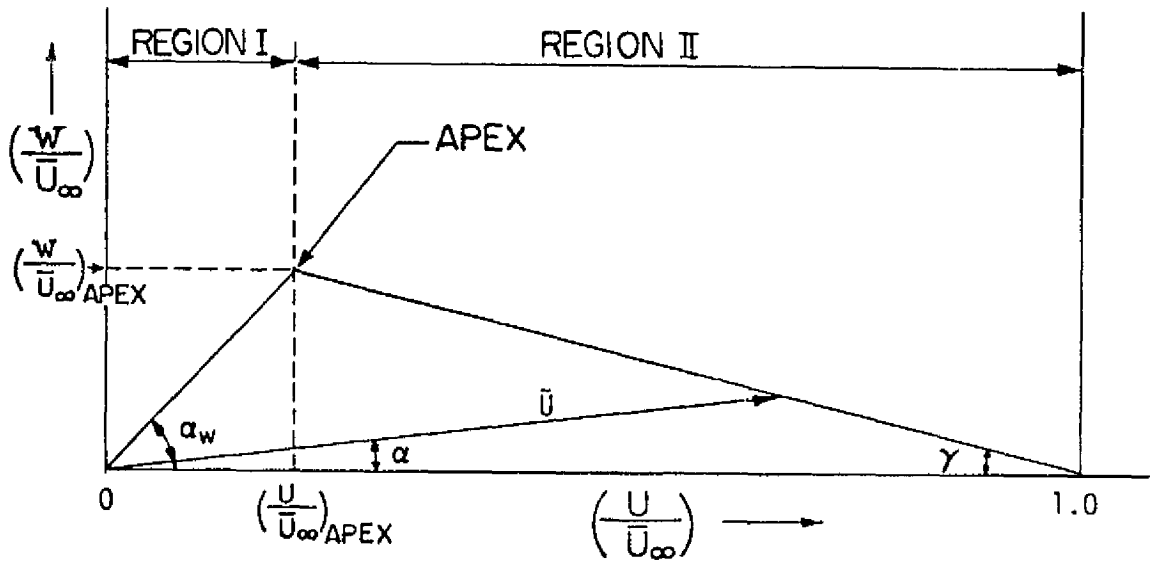

Sketch of Johnston's triangular model

Although the experimental results of several investigators [21, 24, 30, 31, 28] support Johnston's model but with widely different values of the apex location ($15 < y^+_{apex} < 221$), measurements of crossover profiles made by Eichelbrenner and Peube [36], Klinksiek and Pierce [26] and others do not support the model at all. In short, Johnston's Model cannot adequately represent all situations. But, it gives perhaps the simplest and yet fairly accurate representation of the crossflow velocity profile. The representation of the present data in

terms of Johnston's model is discussed below. A detailed discussion of the nature of the flow field close to the wall corresponding to region I of Johnston's model is presented in the following subsection.

The experimental mean velocity profile data at various port locations is presented in polar form in Figs. 28 and 28a. Three vertical arrows labeled on each polar plot identify different locations in the boundary layer. The vast region between the outermost point ($(U/\bar{U}_\infty) = 1$, $(W/\bar{U}_\infty) \approx 0$) and the middle arrow represents the region of increasing crossflow angle. The narrow region between the middle arrow and the leftmost arrow represents the region of decreasing crossflow angle. Finally, the small region between the origin and the leftmost arrow represents the region of collateral flow (constant crossflow angle). Because of the absence of a well-defined apex and the availability of only a few data points in the outer region -- between the rightmost arrow and the outermost point -- the construction of Johnston's triangle was somewhat arbitrary. The triangles were constructed by simply drawing a line that passed through the origin and the data points in the collateral region and a mean line that passed through the outermost point and the few available points in the outer region. The predicted profile shapes close to the wall (shown by dotted lines for ports 1 and 2) were based on a sublayer analysis described in the next subsection. As already mentioned in subsection 6.3.1, y^+ values at which the maximum crossflow angle occurred varied from 27.1 to 144.8 (excluding the profiles at ports 5, 6 and 7). The maximum crossflow velocities occurred at slightly higher values of y^+, which compare with the upper limit of the apex quoted as 16 by Johnston [19], 150 by Hornung and Joubert [21] and 220 by Swamy [30].

The experimental data can now be examined in terms of an overall correlation of Johnston's triangular model proposed and verified by East and Hoxey [24].

The correlation between the magnitude and direction of the wall shear stress vector and the local freestream conditions is readily obtained by applying the sine rule for the triangle (see the sketch):

$$\frac{\sin(\alpha_w + \gamma)}{\sin \gamma} = \frac{1}{K} \cdot \frac{\bar{U}_\infty}{\bar{U}^*} = (1/K) \cdot \sqrt{(2/\bar{c}_f)} \qquad (12)$$

where $K = \bar{U}^+_{apex}$.

Fig. 29 shows the degree of correlation of the experimental data with this equation for different locations of the apex and different values of K. The values of $\bar{c}_f$ were obtained from the 0.032" dia Preston probe data† and γ from appropriate polar plots (Fig. 28 and 28a refer to one particular representation of apex location). In examining this correlation it should be remembered that for $\alpha_w < 5°$ (corresponding to the data at ports 5, 6, and 7), the maximum crossflow is less than 5% of the local freestream velocity and, therefore, the corresponding data points can hardly be considered as satisfactory test cases for three-dimensional profile analysis.

The best agreement between the experimental data and equation (12) is obtained with the apex located at the start of the collateral region (left-most arrow in Figs. 28 and 28a). However, such a model will not be able to adequately represent the data points in the remaining region that is well over 90% of the boundary layer thickness and, therefore, will result in a very bad representation of the complete crossflow profile. Of the remaining three apex representations, the one corresponding to the maximum crossflow angle (middle arrow in Figs. 28 and 28a) gives a poor correlation of the data with equation (12) whereas the other two representations -- one based on maximum crossflow

---

†The choice is disucssed later in section 6.4.1.

W shown by rightmost arrow and the other obtained by drawing lines as in Figs. 28 and 28a -- give reasonable correlation of the data with equation (12) for K = 18.0 and 17.5, respectively. These K-values compare favorably with those quoted in the literature, namely 17.5 by East and Hoxey [24], 16.7 by Swamy [30] and 14 by Johnston [19]. The apex representation as shown in these figures appears to give the best overall representation of the measured cross-flow profiles. To conclude, Johnston's crossflow model correlates the relaxing profile data reasonably well.

6.3.5 Analysis of flow field close to the wall

The very presence of a unusually large number of data points in region I and a relatively few points in region II makes the polar plots (Figs. 28 and 28a) conspicuous when compared with the experimental polar plots of other investigators referred to in the previous subsection. This was of course expected because of the emphasis placed in this investigation on the study of the flow field close to the wall; the traverse mechanism specially designed (to minimize flow disturbances) for surface anemometer studies made it possible to probe the region very close to the wall, $y^+ < 1$ (much closer than has been reported hither to. With wall proximity corrections, the corrected resultant velocity ratios closest to the wall were as low as 0.01. It is, therefore, appropriate to discuss in some detail the nature of the flow field close to the wall corresponding to region I of Johnston's model and to interpret the implications of the present findings in regard to a question that is still open in the literature [38], name the question of the existence (or nonexistence) of near-wall collateral flow field in a three-dimensional turbulent boundary layer.

A careful examination of various experimental polar plots (see, for example, reference [2, Chapter 7]) reveals the fact that region I between the wall and the apex can extend as far as one-tenth of the boundary layer where local-to-freestream velocity ratios may be as high as 0.5. In most of

these plots, region I was constructed by drawing a mean line through the origin and a few available data points (as low as two in some cases) near the apex [37]. Most of the existing data, therefore, indicates collateral flow in this region, i.e., the mean velocity vector does not change its direction. However, recent measurements of Rogers and Head [25] and Vermeulen [28] both using specially designed hot-wire anemometer devices showed skewed flows almost right down to the wall, the data points closest to the wall corresponding to a resultant velocity ratio (local-to-freestream) of about 0.2.

It is important to note that the existence of a collateral flow field is not predicted either by numerical calculations or by a sublayer analysis of the flow field. In fact, numerical calculations by East and Pierce [37] indicate that the assumptions of near-wall collateral flow, as suggested by many experimentalists, may not be correct [38]. A careful study of the boundary layer equations in the neighborhood of the wall leads to the following relation [2, p. 102].

$$\frac{\partial^2 W}{\partial U^2} = \frac{\mu}{\tau_{wx}^2} \cdot \left[\frac{\partial p}{\partial z} - \frac{\tau_{wz}}{\tau_{wx}} \cdot \frac{\partial p}{\partial x} \right] \tag{13}$$

In a collateral flow field $(\partial W/\partial U)$ = constant, i.e., $(\partial^2 W/\partial U^2) = 0$. Thus, equation (13) implies collateral flow field only when either the resultant pressure gradient is zero as in a two-dimensional flow or it is in the direction of the resultant wall shear stress. Therefore, in general, it implies a non-collateral flow field.

In terms of c_p, $\bar{c}_f$, α_w and $\bar{U}_\infty$, equation (13) can be rewritten as

$$\frac{\partial^2 W}{\partial U^2} = D \tag{14}$$

where

$$D = \frac{2\nu}{\bar{U}_\infty^2} \cdot \frac{1}{\bar{c}_f \cdot \cos_w (\bar{U}_\infty/U_{\infty r})^2} \cdot \left[\frac{\partial c_p}{\partial z} - \tan\alpha_w \cdot \frac{\partial c_p}{\partial x} \right] \qquad (15)$$

D has dimensions of sec/ft and may be treated as a local constant (with respect to U) in the neighborhood of the wall for a given velocity profile. Integrating equation (14) using the wall boundary condition on $\frac{\partial W}{\partial U}$ and U, there results

$$(\frac{\partial W}{\partial U} - \tan\alpha_w) = DU \qquad (16)$$

or

$$(\tan\alpha - \tan\alpha_w) = DU \qquad (16a)$$

The change in crossflow angle within the sublayer region, $\Delta\alpha = (\alpha - \alpha_w)$, may therefore be estimated from equation (16a). Integrating equation (16) using the wall boundary condition on W and U and non-dimensionalizing the resulting equation by $\bar{U}_\infty$ we obtain

$$(W/\bar{U}_\infty) = (D/2)\bar{U}_\infty (U/\bar{U}_\infty)^2 + \tan\alpha_W (U/\bar{U}_\infty) \qquad (17)$$

which is a parabolic representation of the polar plot very close to the wall.

The crossflow profiles at ports 1 and 2 which had appreciable wall crossflow angles qualified as suitable test cases for the analysis because the estimates of the wall pressure gradients at these locations were considered to be more accurate and reliable (in view of better spatial distribution of static taps near these ports, see section 6.1, Figs. 3, 21 and 21a). Incidentally, both the hot-wire extrapolation and the hot-film gage data predicted the same wall crossflow angle at either location. The local pressure gradients estimated from the static pressure distribution were: $\partial c_p/\partial z = 2.0979 \times 10^{-2}$/ft and $\partial c_p/\partial x = -2.5080 \times 10^{-2}$/ft at port 1; $\partial c_p/\partial z = 2.7529 \times 10^{-2}$/ft and

$\partial c_p/\partial x$ = -2.5080 x 10^{-2}/ft at port 2. With these values and $\bar{c}_f$ obtained from the 0.032" dia Preston probe data, the estimated D values for hot wire surveys at ports 1 and 2 were 2.4816 x 10^{-3} sec/ft and 1.9836 x 10^{-3} sec/ft, respectively. Some typical values of change of crossflow angle, $\Delta\alpha$, predicted by the analysis are compared with the experimental data in Table 9. The predicted shapes of the polar plots are shown in Figs. 28 and 28a. Although the analysis is strictly valid only very close to the wall, i.e., $y^+ < 5$, the predicted values are shown to higher values of y^+ in order to see the trend and to compare with the maximum decrease of crossflow angle measured during the hot wire survey.

Referring to Table 9 and Figs. 28 and 28a, it is seen that the analysis predicts the observed trend of the flow field close to the wall, i.e., the unusual behavior of decreasing crossflow angle in a narrow region close to the wall. Because the analysis is restricted to the sublayer ($y^+ < 5$), only rough estimates can be expected from the analysis outside this region. The analysis predicts conservative results (overestimates), the overestimation increasing with distance from the wall. This is to be expected as the effect of the wall static pressure field decreases with distance from the wall. The overestimation is seen in the predicted profile shapes which have a slight curvature upwards. With these considerations in mind, it may be concluded that the estimates of decrease of crossflow angle compare qualitatively with the measured values of ports 1 and 2.

With the above considerations of the near-wall flow field in mind, it is concluded here that in the absence of the small local transverse pressure gradients close to the wall, the skewing of the relaxing flow could have been much more pronounced practically down to the wall (limited only by the resolution of the sensor), implying a near-wall <u>non-collateral</u> flow field consistent with the equations of motion in the neighborhood of the wall.

6.3.6 Relaxation of mean flow

A discussion of the streamwise relaxation of the mean flow in terms of the decay of crossflow is more meaningful and pertinent as it is the presence of crossflow that distinguishes a three-dimensional flow from a two-dimensional case. The polar plots of Figs. 28 and 28a show how the three-dimensional flow field returns to a two-dimensional state. In terms of the local free-stream velocity the maximum crossflow velocity is 14.5% at port 1, less than one-half this value downstream of port 4 and less than one-third downstream of port 5. Thus the crossflow decay is relatively faster in the region close to the trailing edge and asymptotic far away from the trailing edge. The polar plot at port 7 is practically a straight line indicative of a two-dimensional state. The polar plots of Fig. 28 give an estimate of spanwise variations in the flow field. The maximum crossflow velocities at ports 8 and 9 are 13.5% and 12.5% respectively, both being lower than the corresponding value at port 1. A better physical picture of the presence of spanwise variations in the resultant mean velocity vector can be obtained by comparing spanwise profiles at ports 8, 1 and 9 in Figs. 23 and 24. Considered over a span of 15 inches between ports 8 and 9, the maximum spanwise variation in the crossflow angle is less than 2.5°. The maximum spanwise variation in the measured resultant mean velocity is approximately 17% or nearly 10% of the local freestream velocity. These variations may be expected to be considerably smaller over a restricted span of, say, 7 inches or approximately 2 boundary-layer thicknesses about the streamwise line of instrumentation ports. Comments regarding the spanwise variations of the wall shear stress vector appear in subsection 6.4.2.

A clearer quantitative picture of the relaxation of the mean flow field is conveyed in Fig. 30 and Table 10 which show the decay of normalized crossflow angle with downstream distance from the trailing edge for various normalized wall

distances. Table 10 was based on values estimated from the direction profiles of Fig. 23. For each normalized wall distance y^+, the crossflow angle has been normalized by the corresponding crossflow angle at port 1. Therefore, all the graphs start with the same ordinate (unity) at port 1. The dash-dot line shown in the figure represents the outer limit of the inner layer, i.e., the locus of the y^+ values denoting the end of the log region in the law of the wall plots of Figs. 27 and 27a. With this line as the boundary, it is safe (conservative) to consider the lower half of the graphs ($y^+ \leq 200$) as completely representing the inner layer region. The upper half of the graphs ($y^+ > 200$) show mixed regions, all of them representing the outer layer region upstream of port 2 but still the inner layer region downstream of port 6.

The slope of each graph represents the local rate of decay of crossflow angle. Thus the rate of decay in the inner layer is much faster in regions close to port 1 and is practically asymptotic in regions close to port 7. At any given location in the region of appreciable crossflow, i.e., upstream of port 4, the local rate of decay decreases away from the wall, being maximum close to the wall. In the region of small crossflow namely downstream of port 4, the opposite trend is apparent. Ports 1 and 7 were located 34 inches apart. For purposes of comparison, the boundary layer thickness at port 1 may be taken as approximately 3.5 inches (see footnote in section 6.1). Considering the relaxation along the limiting y^+ line for the inner layer region (dash-dot line), it is seen that 50% of the measured decay of crossflow takes place in the first 6 inches or nearly 2 boundary-layer thicknesses, 75% in the first 14 inches or nearly 4 boundary-layer thicknesses and 90% in the first 20 inches or nearly 6 boundary-layer thicknesses. Two significant observations can be made from these graphs: (i) the relaxation of the mean-flow field based on the decay of crossflow is much faster in the inner layer than in the outer layer

and (ii) based on the streamwise distance covered, the relaxation is almost complete in approximately 10 boundary-layer thicknesses.

Before closing this section a few comments on the existing experimental data on relaxation studies and the choice of relaxation length scale are in order. These comments equally apply to discussions on the wall shear stress and the turbulence field described in subsections 6.4.2 and 6.5.2, respectively.

Even the two-dimensional data on relaxation studies is limited. Some experiments are described in reference [62] to demonstrate the response of a turbulent boundary layer to disturbances introduced in the layer. A review and comment on some of the experimental investigations (in two-dimensional and pipe flows) on the response of a turbulent boundary layer to sudden changes of surface conditions or of pressure gradients appears in reference [63]. It is concluded there that the response of a turbulent boundary layer is almost instantaneous in the inner part near the wall, but rather slow in the outer part with a relaxation distance of scores of boundary layer thicknesses (for profiles of turbulent intensity and shear stress). The available experimental data on the response of three-dimensional turbulent boundary layers to sudden perturbations is extremely limited. Bradshaw and Terrell [15] studied a relaxing flow field behind a swept wing; the present flow configuration downstream of the hump is similar to that of Bradshaw and Terrell (see section 1.2). Bissonnette [27] studied the response of an axisymmetric turbulent boundary layer to a sudden circumferential strain. Most of the data in [15, 27], unlike the present data, pertains to the outer layer and consequently no attempt has been made to compare the relaxation characteristics of the present study with them. Moreover, the present data (unlike the data in [15, 27]) are not sufficient to define the beginning of flow relaxation and, therefore, any comparison would be very speculative.

In these studies, the boundary layer thickness has been used as a basic relaxation length scale (see also discussion on 'memory' and length scales by Bradshaw [64, pp. 58-59]). Although it may not be an appropriate length scale for the inner layer, it is used in the present study so that the relaxation of the inner layer can be compared with that of the adjacent portion of the outer layer covered by the hot wire surveys. The non-dimensionalized streamwise distance x^+ of each port location, based on the length scale ($\nu/\bar{U}^*$), is also included in Fig. 30.

6.4 Wall shear stress data

In subsection 6.3.3 the applicability of the Preston probes in the present investigation was discussed and justified on the basis of the existence of wall similarity region much larger than the diameter of the Preston probes. In the following subsection the experimental data on wall shear stress obtained from three-dimensional measurements is briefly discussed and compared with the hot wire data. A detailed discussion of the wall shear stress data and an assessment of the relative performance of various shear stress devices may be found in reference [42]. The mean velocity data obtained from the two-dimensional hot wire surveys predicts skin friction values that are in good agreement with direct measurements (see Appendix C).

6.4.1 Wall shear stress vector

Tables 11 and 12 and Fig. 31 show the local limiting streamline angle (measured from the local horizon) and the resultant mean skin friction coefficient $\bar{c}_f$ determined from the wall shear stress measurements in the relaxing region behind the trailing edge of the hump. Also shown for comparison are the wall crossflow angles extrapolated from the hot-wire direction profiles at the respective port locations (subsection 6.3.1) and $\bar{c}_f$ estimated from the resultant mean velocity profile data using Bradshaw's simplified version of Clauser's

technique (subsection 5.3.2). Although the actual direction of the local free-stream could not be determined because of the partial traverse of the hot wire survey, this direction may, for all practical purposes, be assumed to coincide with the local horizon (see the footnote in subsection 4.2.2). The resulting error, if any, would be a very small additive constant and, therefore, would have negligible effect on the analysis of the data.

All direction measurements were accomplished by the bisector method (see section 4.2) and, therefore, independently of the respective yaw calibration curves of various devices. However, yaw calibration experiments established the aerodynamic symmetry of various probes on which the accuracy of the bisector method depends [42]. Estimates of probable overall experimental errors associated with the different types of measurements are given in section 5.5.

The data on limiting streamline angle α_w shows very good agreement between the measurements of the hot film gage and the sublayer fence. As both the devices are based on sublayer similarity such an agreement is not entirely surprising. But what is remarkable is the excellent agreement between the hot film results and the results obtained form extrapolating the hot wire data to the wall. As can be seen in Table 11 and Fig. 31, this agreement is within 0.25°, the hot-film gage predicting slightly higher values in the region of high shear stress. The nature of the agreement attests to the consistency of the experimental data from these probes.

The Preston probes were originally not intended for measuring the direction of the wall shear stress and, therefore, their yaw characteristics were not studied in the two-dimensional boundary layer (in the absence of the hump). However, while measuring the wall shear stress with the Preston probes, the direction also was determined by the bisector method. Surprisingly enough,

as seen in Table 11 and Fig. 31, the values indicated by the 0.032" dia Preston probe agree with those of the hot-film gage to within ± 0.25° except at port 5 where the data of the Preston probe is 0.5° lower. Considering the usually poor directional sensitivity of a Preston probe and the spatial averaging of teh output over its mouth, this remarkable agreement was least expected. In the case of the 0.018" dia Preston probe, the measured angles were apparently consistently lower than those of the hot-film data by about 2° except at port 7 where it was lower than 2.75°. The biased indication of the 0.018" dia Preston probe was traced to its mouth not being well defined and, therefore, to its initial orientation (with the local horizon) which was uncertain* to ± 2°. The data of the 0.018" dia Preston probe shown in Fig. 31 includes a uniform correction of +2° to the measured angles.

Regarding the skin friction, the agreement between the data of two Preston probes and that between the 0.032" dia Preston probe and the hot-film gage is within the estimated precision of the measurements [42, 65]. The hot-film gage generally indicates higher $\bar{c}_f$-values. In regions of higher shear stress (ports 5, 6 and 7), the $\bar{c}_f$-values estimated from the resultant mean velocity profile data are higher than those obtained from the 0.032" dia Preston probe data, whereas in regions of low shear stress they are lower. The data of the 0.032" dia Preston probe (considered more reliable) represents a sort of average of all the data.

Based on the above considerations and the earlier observations that the hot-wire surveys indicated a narrow region of near-wall collateral flow and an appreciable wall similarity region even in low shear stress regions, the

---

*The uncertainty regarding the initial orientation could have been better resolved by making measurements in a known two-dimensional flow field.

skin friction from the 0.032" dia Preston probe measurement and the limiting streamline angle from the hot-film gage measurement are taken as the reference values in the present investigation.

6.4.2 Relaxation of wall shear stress

The ensuing discussion on the relaxation of wall shear stress vector behind the trailing edge of the hump is based on the direction of the limiting streamline indicated by the hot-film gage and the skin-friction coefficient indicated by the 0.032" dia Preston probe, shown in Fig. 31. For comparison the data from the wall shear stress measurements in the two-dimensional boundary layer (in the absence of the hump) is also shown in the figure. It may be noted here that sample directional measurements made during the two-dimensional hot wire surveys confirmed that the boundary layer was collateral, i.e., the limiting streamline angle was zero. A few comments about the measured spanwise variation of the wall shear stress vector are appropriate before considering its streamwise relaxation.

The measured spanwise variation close to the trailing edge is indicated in Fig. 31 by data points corresponding to the spanwise ports 8, 1 and 9. These ports which are 0.75" away from the trailing edge span a total distance of 15", port 1 being a little closer to port 8. The angle of the limiting streamline at port 8 is 2° lower than that at port 1 but that at port 9 is only 1° lower. Compared to the skin friction at port 1, the measured $\bar{c}_f$ at port 8 is 6.6% higher, whereas, at port 9 it is 13.8% lower. Thus, over a span of 15", the overall variation in skin friction is 20.4% of the skin friction at port 1. This may be compared with the results of preliminary studies of the two-dimensional flow field [40] which indicated a skin friction variation of nearly 23% over a span of 15" about the tunnel centerline and nearly 5% over 4". It appears that in regions close to the trailing edge, both the

angle and the skin friction tend to decrease toward the lower end of the span. This tendency is to be expected from the wall static pressure field shown in Fig. 21a, where relatively stronger adverse pressure gradients are seen to prevail below the tunnel centerline.

Because of the low aspect ratio of the hump, some spanwise variations were expected in the flow field downstream of the hump. But the nominal two-dimensional boundary layer upstream of the hump was contaminated by transverse nonuniformities, which would be even amplified in flowing over the hump [40]. With these considerations in mind, it is estimated that, over a restricted span of 7 inches or approximately 2 boundary-layer thicknesses about the streamwise line of ports, the spanwise variation* in the direction and the magnitude of the wall shear stress did not exceed 1° and 10%, respectively, the variations being smaller in regions away from the trailing edge.

Now turning to the streamwise relaxation of the wall shear stress vector, the slope of the curves in Fig. 31 indicates the local rate of change of the wall shear stress with downstream distance. The limiting streamline angle decays rapidly in the region close to the trailing edge, but the rate of decay decreases with downstream distance. The measured angle at the downstream most port is 0.25° which is also the estimated experimental error associated with the hot-film measurement (section 5.5). The skin-friction coefficient increases rapidly in the region close to the trailing edge, the rate of increase decreasing with downstream distance. The measured skin-friction coefficient at the downstreammost port is 2.1% lower than the corresponding two-dimensional value**.

---

*A detailed study of these variations appears in reference [40].

**The three-dimensional $\bar{c}_f$-value will be slightly lower because of the increased boundary layer thickness.

Taking the difference between the measured values at ports 1 and 7 as the total relaxation (decay of α_w and increase $\bar{c}_f$) in a streamwise distance of 34 inches between these ports and the thickness of the boundary layer† at port 1 as approximately 3.5 inches (see footnote in section 6.1), the following observations may be made:

(i) 50% of the relaxation of the direction of the mean wall shear stress vector occurs in the first 4 inches or a little more than a boundary-layer thickness, 75% within the first 10 inches or nearly 3 boundary-layer thicknesses and 90% within the first 19 inches or nearly $5\frac{1}{2}$ boundary-layer thicknesses. The corresponding relaxation of the magnitude of the resultant mean wall shear stress occurs within $2\frac{1}{2}$, 5 and $7\frac{1}{2}$ boundary-layer thicknesses, respectively.

(ii) The mean wall shear stress vector (both direction and magnitude) almost relaxes to a two-dimensional state in approximately 10 boundary-layer thicknesses.

These observations are comparable to those given in subsection 6.3.6 for the relaxation of mean flow in the inner layer region, particularly the region close to the wall.

6.5 Turbulence data from hot-wire surveys

Because of the non-availability of any method to estimate the wall influence on hot-wire turbulence output and lack of time to investigate it, no attempt has been made to correct the turbulence readings for wall proximity effects. Compared to other possible sources of errors, the wall proximity effects on turbulence readings may be expected to be negligible as the turbulence itself decays very rapidly after the peak point. Any small difference arising from

†See comments in subsection 6.3.6 on the choice of relaxation length scale.

the omission of this correction in the turbulence data should have little effect on the interpretation of the relaxation characteristics of the turbulence field. The two-dimensional turbulence data from hot wire surveys, shown in Tables 2-2a and Fig. 32 provided information on the initial state of turbulence in the boundary layer (in the absence of the hump) and, hence, it may be treated as a representative asymptotic state of the relaxing turbulence field. It is, therefore, appropriate to assess it before discussing the turbulence data pertaining to the relaxing field.

A representation of two-dimensional turbulence data* in wall coordinates is more appropriate because, close to the wall, the profile is universal being independent of the Reynolds number [67, 68]. Besides, such a representation reflects the effect of pressure gradient. In Fig. 32, where the two-dimensional turbulence data in wall coordinates is compared with the data from other sources [67 - 69], the indicated maximum values are: 2.52 at $y^+ = 17$ for the longitudinal intensity ($\sqrt{\overline{u^2}}/U^*$) and 1.50 at $y^+ = 40$ for the lateral intensity ($\sqrt{\overline{w^2}}/U^*$). In Laufer's pipe data [68] the corresponding maximum values are approximately 2.625 at $y^+ = 17$ and 1.75 at $y^+ = 55$. Measurements reported by Thinh [54] and Laufer's channel data [67] show a maximum in ($\sqrt{\overline{u^2}}/U^*$) of nearly 2.35 and 2.50, respectively, both at $y^+ = 17$. In Eckelmann's oil channel data ($\sqrt{\overline{u^2}}/U^*$) reaches a maximum value of nearly 2.72 at $y^+ = 13.5$ and decreases to 2.60 at $y^+ = 17$. Thus the two-dimensional profiles of longitudinal and lateral turbulence, particularly the former, are in good agreement with other data available in the literature. The crosscorrelation is practically zero (less than 0.12 U^{*2}), as it should be in a two-dimensional turbulent boundary layer.

6.5.1 Turbulence profiles in the relaxing region

The three-dimensional turbulence data reduced from the hot-wire surveys is shown in Figs. 33-35 and in Tables 8-8h, 13. The profiles in Figs. 33-33b

*For a comparison of the present data with the Klebanoff data [66, (44, P. 467)], see reference [42].

show, in wall coordinates, the turbulence distribution in the inner layer at selected locations of the relaxing region. The root-mean-square values of the longitudinal and lateral turbulence in the local axes system $x_1y_1z_1$, $\sqrt{\overline{u_1^2}}$ and $\sqrt{\overline{w_1^2}}$, have been nondimensionalized by the local skin friction velocity $\bar{U}^*$, and their correlation $\overline{u_1w_1}$ by the square of $\bar{U}^*$. Also shown for comparison in each of these figures is the corresponding two-dimensional profile at port 7. It should be noted that, for the two-dimensional case, both the axes system $x_1y_1z_1$ and xyz coincide.

The point of interest in Fig. 33 is the magnitude and location of peaks of longitudinal turbulence intensity in the relaxing field compared to the two-dimensional data. Although, no quantitative conclusion can be drawn, the increase and shift (away from the wall) in the peaks are clearly seen at all port locations, the effects being more pronounced in the region very close to the trailing edge. This is not surprising in view of the fact that the mean -velocity profiles shown in Fig. 24, particularly those close to the trailing edge, resemble those in two-dimensional flows with adverse pressure gradient where similar effects on turbulent fluctuations have been noticed [70]. Similar trends are noticeable also in the distribution of lateral turbulence intensity in Fig. 33a. Of more significance is the presence of $\overline{u_1w_1}$ correlation* in the relaxing boundary layer particularly close to the trailing edge (Fig. 33b). If the flow field behind the trailing edge were truly an infinite swept flow, the crosscorrelation (in the local coordinate system) would be zero. But, because of the presence of spanwise variations in the relaxing field (caused by the low aspect ratio of the hump), the crosscorrelation is nonzero. An estimate of the spanwise variations in the turbulence field is given in the following subsection.

---

*This correlation was utilized to apply correction to the measured crossflow angles in the boundary layer; see subsections 5.3.4 and 6.3.1.

As regards the location of the peak, more measurements at higher values of y are needed to extend the present range to help in defining the exact location. The outward shift in the peaks in regions close to the trailing edge is very pronounced and appears to extend into the outer layer of the boundary layer. Moreover, in these regions, the maximum values are attained gradually and the peak characteristics of a two-dimensional flow disappears. In the wall coordinates, the maximum values are indicated by the turbulence data at port 9, which is expected from the nature of the mean velocity profile at port 9 (Fig. 24). There does not appear to be any similarity region close to the wall which the Prandtl hypothesis predicts for two-dimensional flows [67]. The indicated maximum values are compared in the following table with the corresponding two-dimensional values at port 7.

Table: Maximum values of turbulence fluctuations in the wall coordinates

	Port 9	Port 7 (two-dimensional)
Longitudinal turbulence, $(\sqrt{\overline{u_1^2}}/\bar{U}^*)$	5.00	2.52
Lateral turbulence, $(\sqrt{\overline{w_1^2}}/\bar{U}^*)$	3.79	1.50
Crosscorrelation $(-\overline{u_1 w_1}/\bar{U}^{*2})$	1.77	<0.12

The hot wire turbulence data transformed into the reference axes system xyz is shown, partially, in Tables 8-8h. This was obtained from the data in the local axes system using equations (8), (9) and (10). Because the crossflow angle α is small (α_{max} = 21.875°), $\overline{u^2}$ and $\overline{w^2}$ do not differ appreciably from $\overline{u_1^2}$ and $\overline{w_1^2}$, respectively. The general trend of variation of $\sqrt{\overline{u^2}}$ and $\sqrt{\overline{w^2}}$ in the inner layer follows that of $\sqrt{\overline{u_1^2}}$ and $\sqrt{\overline{w_1^2}}$, respectively; therefore, they

have not been presented graphically. But, as can be seen in Tables 8-8h, the variation of the crosscorrelation $-\overline{uw}$ in the inner layer is significantly different, both in magnitude and direction, from that of $-\overline{u_1 w_1}$ discussed earlier. Figure 34 shows, in wall coordinates, the variation of $-\overline{uw}$ correlation in the inner layer of the relaxing region. The most striking feature in this figure is the sign reversal of the correlation as the wall is approached. This occurs at all port locations except port 7. The y^+ value corresponding to zero cross-correlation increases with decreasing $\bar{U}^*$, the maximum y^+ value being 40 at port 9. In other words, close to the trailing edge, the sign reversal occurs at greater distances from the wall. It is strongly suspected that the sign reversal is caused by the presence of the slight adverse pressure gradient in the transverse direction that was observed in the spanwise wall static pressure data discussed in section 6.1. Another notable feature is that in the measured range the negative peaks are of the same order of magnitude as the positive ones.

6.5.2 Relaxation of turbulence

Compared to the mean flow field disucssed in subsection 6.3.6, the turbulence field relaxes slower as can be seen by comparing the three-dimensional and two -dimensional turbulence data at the downstreammost port location (port 7) in Fig. 35, where the maximum turbulence flucutations in the boundary layer are plotted against downstream distance. All the fluctuations have been nondimensionalized by the respective fluctuations at port 1. These values are also shown in Table 13. It should be noted that (i) the maximum values occur at different distances from the wall, this distance decreasing with increasing downstream distance fro the trailing edge and (ii) although they correspond to the same upstream reference Reynolds number, the upstream reference velocity in each case is slightly different Nevertheless, the representation in Fig. 35 is considered to be

appropriate for relaxation studies.

The slope of each curve in Fig. 35 indicates the local rate of decrease of maximum turbulence. The decrease is rapid in the region close to the trailing edge, but the rate of decay decreases with downstream distance. The measured maximum values at the downstreammost port are higher than the corresponding two-dimensional values* by 11.16% in $(\sqrt{\overline{u_1^2}})$ and 21.30% in $\sqrt{\overline{w_1^2}}$. Taking the difference between the measured maximum values at ports 1 and 7 as the total relaxation (decay) of turbulence in a streamwise distance of 34 inches between these ports and the thickness of the boundary layer+ at port 1 as approximately 3.5 inches (see footnote in section 6.1), the following observations may be made:

(i) 50% of the relaxation in $(\sqrt{\overline{u_1^2}})_{max}$ $((\sqrt{\overline{w_1^2}})_{max}$, $(-\overline{u_1 w_1})_{max})$ occurs in the first 6.25" (9", 6.75") or nearly 2(2.5,2) boundary-layer thicknesses, 75% in the first 13.25" (18.5", 15.75") or nearly 4 (5.5, 4.5) boundary-layer thicknesses and 90% in the first 22.25" (25", 24.25") or nearly 6.5 (7, 7) boundary-layer thicknesses.

(ii) Compared to the streamwise relaxation of the mean flow discussed in subsection 6.3.6, the relaxation of the turbulence is slower and is not complete in 10 boundary-layer thicknesses.

This relaxation length may be compared with the observations of Bissonnette [27] where the 'history' of turbulence seems to persist for more than 20 boundary layer thicknesses.

Finally, the spanwise variations in the turbulence flow field can

---

*The two-dimensional value of $(\overline{uw})$ correlation is practically zero.

+See comments in subsection 6.3.6 on the choice of relaxation length scale.

be obtained by comparing the maximum values at ports 8, 1 and 9 quoted in Table 13. The lowest values are indicated at port 8 and the highest at port 1, the measured values at port 8 being lower than those at port 1 by 5.42% in $(\sqrt{\overline{u_1^2}})_{max}$, 7.63% in $(\sqrt{\overline{w_1^2}})_{max}$ and 14.78% in $(-\overline{u_1 w_1})_{max}$. The corresponding figures at port 9 are 2.15% and 2.53% and 13.30%. The spanwise variations in the turbulent fluctuations considered over a restricted span of, say, 7" or two boundary-layer thicknesses about the streamwise line of ports may be expected to be not more than: 5% in $(\sqrt{\overline{u_1^2}})_{max}$, 7% in $(\sqrt{\overline{w_1^2}})_{max}$ and 12% in $(-\overline{u_1 w_1})_{max}$.

Chapter 7

Conclusions and Recommendations

The measurements reported in this investigation have provided experimental data pertaining to the characteristics of the flow field in the near-wall region of a three-dimensional incompressible turbulent boundary layer relaxing in a nominally zero external pressure gradient.

The data from the three-dimensional wall and near-wall measurements was analyzed with particular emphasis on:

(i) The nature of the mean-flow field very close to the wall and

(ii) the streamwise relaxation characteristics of the mean flow and some turbulence quantities in the inner layer region.

7.1 Conclusions of the investigation

The findings of the present investigation based on the discussions in the preceding chapter are given below:

(i) Wall proximity corrections: The experimental data indicated, in agreement with the findings of Oka and Kostić [56], that the apparent dimensionless velocity profiles in the viscous sublayer region are universal (local) and that the wall influence is negligible beyond $y^+ = 5$. The agreement between the corrected data and the velocity gradient line at the wall determined from the measured skin friction was exceptionally good in the wall influence region excluding points closest to the wall ($y^+ < 1.5$) which could not be precisely located because of errors in measurement of very small distances from the wall. Wills' correction [50] did not yield satisfactory results even for the two-dimensional data.

(ii) Angle corrections: The maximum angle correction was -0.61° which was less than 4% of the indicated angle. The hot-wire turbulence data ($\overline{u_1 w_1}$ correlation) was used to calculate second order angle corrections to the indicated "mean direction of flow" to obtain the "mean-flow direction".

(iii) Mean direction profiles: The experimental mean direction profiles exhibited the usual features characteristic of a simple crossflow profile but with a relatively smaller collateral region adjacent to the wall (the smallest extending up to $y^+ = 9.7$). The unusual feature about these profiles was the presence of a narrow region of slightly decreasing crossflow angle (one degree or less) that extended from the point of maximum cross-flow angle down to the outer limit of the collateral region. Based on a sublayer analysis of the flow field, it is concluded that in the absence of the small local transverse, adverse pressure gradients close to the wall, the skewing of the flow could have been much more pronounced practically down to the wall (limited only by the resolution of the sensor), implying a near-wall non-collateral flow field consistent with the equations of motion in the neighborhood of the wall.

(iv) Wall similarity region: The existence of wall similarity in the relaxing flow field was confirmed in the form of a log law, thus concurring with the findings of other experimental studies on three-dimensional flows. The experimental data supported the log law based on the resultant mean velocity

and resultant friction velocity (obtained from measured skin friction). Patel's log law constants [46] were adequate. The maximum crossflow angle was 21.875° and the maximum crossflow velocity ratio was 0.145.

(v) Polar representation of crossflow: The experimental polar plots were conspicuous by the presence of an unusually large number of data points in the inner region and relatively few points in the outer region. The closest distance probed was 0.0005" from the wall (much closer than has been reported hitherto); lowest y^+ values were less than 1. The corrected resultant velocity ratios closest to the wall were as low as 0.01. The apex representation shown in Figs. 28 and 28a appears to give the best overall representation of the measured crossflow profiles in terms of an overall correlation between wall shear stress vector and local freestream conditions.

(vi) Wall shear stress data: The consistency of the experimental data was indicated by the excellent agreement of the data (within experimental precision) from different measurement techniques including the velocity profile method. Compared to other devices, the construction and operation of the 0.032" dia Preston probe was much easier and consequently its results were more reliable. The directions of wall shear stress indicated by the hot-film gage were more accurate and reliable. They were in excellent agreement (to within 0.25°) with wall crossflow angles extrapolated from hot wire surveys.

(vii) Turbulence data: The two-dimensional turbulence data (in the absence of the hump) on longitudinal and lateral turbulence, particularly the former, is in good agreement with the well established data available in the literature. The increase and outward shift (away from the wall) in the peaks are clearly seen in the three-dimensional turbulence profiles at all port locations, the effects being more pronounced in the region of low shear stress close to the trailing edge. In these regions the mean velocity profiles resemble those in two-dimensional flows with adverse pressure gradient which exhibit similar effects on turbulent fluctuations. The experimental data does not appear to indicate any similarity region close to the wall which the Prandtl hypothesis predicts for two-dimensional flows. Compared to the two-dimensional peak values, the maximum longitudinal turbulence intensity, $(\sqrt{\overline{u_1^2}}/\overline{U}^*)$, is doubled and the maximum lateral turbulence intensity, $(\sqrt{\overline{w_1^2}}/\overline{U}^*)$, is increased to two and one half times. But the maximum values are attained gradually and the sharp peak characteristic of a two-dimensional flow disappears. Of more significance is the presence of $\overline{u_1 w_1}$ correlation which should be practically zero in the local axes system in a truly infinite swept flow.

(viii) Spanwise variations: Considered over a restricted span of approximately one boundary-layer thickness on either side of the streamwise locations, the spanwise variations are expected to be not more than 10%.

(ix) Streamwise relaxation: The streamwise relaxation of the mean flow field based on the decay of crossflow angle is much faster in the inner layer than in the outer layer. Although the data are not sufficient to define the beginning of flow relaxation, they lead to some significant observations based on the streamwise distance covered by the measurments (34"): The relaxation of the mean flow in the inner layer is almost complete in approximately 10 boundary-layer thicknesses. The wall shear stress vector almost relaxes to a two-dimensional state in approximately the same distance. However, compared to the streamwise relaxation of the mean flow, the relaxation of the turbulence is slower and is not complete in 10 boundary-layer thicknesses.

7.2 Recommendations for further work

The recommendations suggested below follow directly from the limitations of the present data discussed earlier.

(i) Completion of boundary layer surveys: The partial hot wire surveys reported in the present study should be completed by carrying out the measurements (preferably with a hot-wire probe to obtain data on turbulence as well) in the outer layer of the boundary layer at respective locations.

(ii) Measurement of Reynolds shear stress: The distribution of shear stress vector (both magnitude and direction) and of other turbulence quantities in the boundary layer at these locations should be determined (using a single rotated slant hot-wire probe, a conventional X-probe or a triaxial hot-wire probe).

(iii) Test of prediction methods: Measurements should be made at more locations in the spanwise direction close to the trailing edge so as to define an initial data plane (with finer spatial resolution) for use in the presently available prediction methods. The complete experimental data would then be satisfactory as a test case for assessing prediction methods, in particular to experimentally resolve the question of the correlation between the directions of the shear stress vector and the mean-velocity gradient vector.

(iv) Measurements over the hump: To study the upstream history of the relaxing flow field, measurements are required over the transverse hump. In particular, data is required over the rear of the hump to define the beginning of flow relaxation. The complete experimental data with a well defined beginning of flow relaxation will facilitate a detailed study of the dynamics of turbulence field and allow a meaningful comparison of the relaxation characteristics with presently available data on turbulence response to varying mean rate of strain.

(v) Further investigation of mean flow field very close to the wall: It is perhaps worth some effort to consider appropriate modifications to the wind tunnel facility/flow geometry so as to eliminate spanwise variations in the relaxing flow field. Hot wire measurements in such a flow field very close to the wall should provide more definitive information (than was possible to obtain in the present study) to resolve the question of the existence (or nonexistence) of near-wall collateral flow field.

Appendix A

Some Details of Wind Tunnel Modifications

As remarked in Chapter 2, several modifications were incorporated into the wind tunnel to improve the quality of the flow in the test section. Some of these modifications along with some results of a preliminary study of the transverse non-uniformities are given below. Full details concerning these nonuniformities are available in reference [40].

A.1 Air-filter enclosure

The Aerospace Engineering Laboratory area where the tunnel was located formed a part of the general engineering laboratory and as such the surroundings were usually dusty, the situation often aggravating due to soot particles resulting from welding operations in the neighboring Civil Engineering Laboratory. In order to reduce the severity of the dust contamination problem (especially with hot wires and hot films, viz., the problem of dust deposition on hot wires and hot films and the resulting drift in calibration, see reference [71,72]), it was decided to enclose the inlet region with suitable filter media (Fig. 2) supported on a box-like wooden frame against a backing of hexagonal mesh wire netting. The required surface area of filter medi. was arrived at after conducting smoke visualization tests in the inlet region to get a rough estimate of velocity distribution in and around the inlet area. About 550 square feet of filter media were required for which the approximate calculations corresponding to a 50 ft/sec velocity in the test section showed that the maximum velocity through the filter media (based on its frontal area alone) would be less than 130 feet per minute. The pressure drop due to synthetic filter media at this velocity would be negligible. Microtron CA synthetic filter media* was selected for use as

*National Bureau of Standards efficiency = 65-75%. It is obtainable from: Penn Air Company, Pickering Creek Industrial Park, P.O.Box 206, Lionville, Pa. 19353.

a fine filter with Airguard polyester filter media PSF-21* as a prefilter. Throughout the period of this investigation, the filter media performed well and the amount of dust deposition on them was not significant enough to warrant their replacement. A small filter-covered door was provided on the back side of the air-filter enclosure to gain access to the inside of the airfilter enclosure and to the inlet section for periodic inspection. When the tunnel was not in operation, the filter media was covered with a thin plastic sheet to help increase its life span.

A.2 Inlet honeybomb-screen assembly

Although the effects of honeycomb are not quantitatively well defined in the literature, it is known that a honeycomb acts as a flow-straightener and a good suppressor of disturbances due to lateral components of mean velocity. The inlet screens essentially act as (longitudinal) turbulence reducers. It is important to see that the inlet screen wire produces no turbulent wake of its own. According to Bradshaw [73], the inlet screens must have an open area ratio of at least 57% and that the last screen should be of uniform weave and free of wrinkles over its entire cross-sectional area. Some suggestions to improve the tunnel flow are also mentioned in reference [74].

The honeycomb-screen assembly of the original (unmodified) tunnel consisted of $7\frac{1}{2}$-inch long, $1\frac{3}{8}$" dia. and 1/16" thick paper tubes glued together to form a honeycomb structure 60" wide x 88.5" high followed by two screens spaced 1" apart, each with an open area ratio of

*Efficiency (discoloration-atmospheric dust) = 32%. It is obtainable from: National Capital Filter Corporation, 5922 Georgia Avenue, N.W., Washington,D.C. 20011.

43.6%. A preliminary survey [40] of the tunnel wall boundary layer revealed the presence of spanwise non-uniformities even in regions sufficiently away from the corners. A careful qualitative study of the flow field in and around the inlet region by helium bubble tracing technique, smoke visualization and by sprinkling flour on the floor showed that the flow into the inlet over the upper half was quite smooth whereas the flow over the bottom half (bordered by the floor, Fig. 2) was rather unsteady giving rise to regions of intermittent swirl.

In view of Bradshaw's criteria, the screens were too dense and the honeycomb screen assembly was unsatisfactory. In order to improve the flow, it was decided to redesign the honeycomb screen assembly with the available information [73,74]. The old honeycomb structure was replaced by ordinary plastic drinking straws (0.236" o.d., 0.007" wall and 8.25" long) stacked against a stainless steel screen (20 mesh, 0.010 inch wire) with 64% open area ratio. The old screens were replaced by four polyester screens spaced 3 inches apart and mounted on 60" wide x 88.5" high wooden frames, with the first screen positioned 6" behind the stainless steel screen. Each polyester screen was 16.5 mesh, 0.0138" dia monofilament with 59% open area ratio.

Fig. A.1 shows a few results of transverse boundary layer surveys made by Winkelmann [40] on the side wall of the original (unmodified) wind tunnel. At y = 0.5 inch above the wall and over a transverse distance of 15 inches about the tunnel center line, the transverse nonuniformities in speed amounted to nearly 10%. Also shown in the figure is the transverse velocity distribution on the side wall of the modified wind tunnel. As noticed in the figure, very little improvement was accomplished with the new honeycomb-screen assembly which merely changed the locations of peaks and valleys.

Appendix B

Design of Flush-Mounted Hot-Film Gages

The classical analyses of Fage and Falkner [75], Ludwieg [76] and Liepmann and Skinner [77] provided the necessary theoretical background that ultimately led to the development of flush-mounted thin-film gages by Bellhouse and Schultz [65] and Brown [78] that can even detect the fluctuations in the wall shear stress. In turbulent flows, the cube -root relationship between the heat dissipated from a heated element and the local wall shear stress is valid as long as the thermal boundary layer above the element lies entirely within the laminar (or linear) sublayer of the flow field. This restriction imposes an upper limit on the effective streamwise length, L, of the film. The restriction is also essential for equivalence of calibration in laminar and turbulent flows.

Liepmann and Skinner were the first to give an estimate of the upper limit. From an order of magnitude estimate they derived the following criterion:

$$(\rho L U_\infty/\mu) = R_L < (Pr/c_f^2) \tag{B.1}$$

They also give the following lower limit on L so that the boundary-layer type analysis is valid:

$$(c_f Pr R_L^2) >> 1 \tag{B.1a}$$

Combining these two, their analysis leads to the following criterion:

$$(Pr/c_f) > (c_f Pr R_L^2)^{1/3} > > 1$$

or

$$(Pr/c_f) > (Q_w L/k\Delta T) > > 1 \tag{B.1b}$$

where Q_w is the heat flux from the heated element, ΔT is the temperature difference between the heated element and the freestream and k is the thermal conductivity of the medium. Brown's analysis gives the criterion,

$$(U^*L/\nu) < 64\ Pr \qquad (B.2)$$

whereas Pope's criterion [79] further reduces the upper bound for L:

$$(U^*L/\nu) < 32\ Pr \qquad (B.3)$$

It is important to note here that, as deduced from the slope of calibration curve [78], the effective streamwise length has been found to equal approximately three times the geometric streamwise length of the element in turbulent flows. The lowest estimate of the upper bound for the effective streamwise length, L, is obtained from equation (B.3):

$$L < 32\ Pr(\nu/U^*)$$

To satisfy the cube root power relationship throughout the range of operation of the hot film gage, it is necessary to evaluate L based on the maximum value of U* and the minimum value of ν anticipated during the operation. The maximum value of U* occurs in the two-dimensional boundary layer (i.e., in the absence of the hump). The kinematic viscosity, ν, increases with temperature and, therefore, it is safe to base ν on ambient conditions.

Preliminary measurements in the two-dimensional boundary layer at a freestream velocity of $U_\infty \simeq 50$ ft/sec had predicted $c_f \simeq 2.4 \times 10^{-3}$. With these values $U^* = \sqrt{(c_f/2)}U_\infty = 1.732$ ft/sec. Taking $\nu \simeq 1.6 \times 10^{-4} ft^2/sec$ and Pr = 0.72 we obtain

$$L < 0.02554"$$

C.2

Taking geometric streamwise length (i.e., width, w) to be one-third of the effective length, we obtain

$$w < 0.0085"$$

Practical considerations actually dictated the safe minimum width of the film which could be deposited with permissible tolerances on the edges of the film. The minimum width chosen was 0.004"*.

It was desired to have a nominal film resistance in the range of 15-20 ohms. From considerations of angular response of the film [76,80 and 81], a very high aspect ratio film was desirable. However, a high aspect ratio implies a long film and, therefore, poor spatial resolution. As a compromise, the film length was set at 0.125" (which is also the distance between hot wire needles), giving an aspect ratio of 31.25. From these values the required film thickness was estimated to be nearly $2000^{o}A$ for platinum film.

The actual dimensions and characteristics of the hot-film gage used in the present investigation are already given in section 3.3 and Figs. 7 and 7a. It was verified that, within its range of operation in the present investigation, the hot-film gage satisfied the criterion given by equation (B.3).

---

*This figure was arrived at after consultation with the Thermo-Systems Inc., 2500 North Cleveland Avenue, St. Paul, MN 55113, who did the actual deposition of the platinum film.

Appendix C

Two-Dimensional Data on Wall Shear Stress

Table 3 presents the reduced data from the wall shear stress measurements performed with various shear stress devices at ports 1 and 7 in the two-dimensional boundary-layer on the aluminum flat plate (in the absence of the hump). The data is presented in the form of mean skin friction coefficient based on local freestream dynamic head. Table 3 also presents the values of c_f estimated from the mean velocity profile data taken from two-dimensional hot wire surveys at the respective port locations. These c_f values were calculated from Bradshaw's simplified version of Clauser's technique described in subsection 5.3.2. All the data refers to the same upstream reference Reynolds number of 3.25×10^5 per foot. The values within the parentheses were deduced from Patel's calibration curve [46].

First the Preston probe results obtained from the present calibration curves are compared with those from Patel's calibration curve. The present calibration curve for the 0.032" dia Preston probe predicts slightly different values compared to Patel's calibration curve. Since the difference is only less than 0.35% which is well within the experimental error (see section 5.5), the agreement between these two predictions is excellent. This is not surprising because the two calibration curves differ very little at the higher end of the calibration range (Fig. 17). In the case of 0.018" dia Preston probe, the present calibration curve underestimates skin friction compared to Patel's calibration curve. The difference is less than 2% but within the experimental error and, therefore, the agreement between these two predictions is still very good. Because of the good agreement, Patel's calibration curve will not be considered in the subsequent discussion.

The highest values are indicated by the sublayer fence data and

the lowest by the 0.032" dia Preston probe data, the difference being nearly 2%. Surprisingly enough, in spite of the usual calibration problem associated with hot-film gages, the prediction of the hot-film gage agrees well with that of the 0.032" dia Preston probe, particularly at port 7. The c_f-values estimated from the mean velocity profile come very close to the hot-film estimates. It is to be noted that all the measurements predict a slightly higher c_f at port 1, which is expected in a two-dimensional boundary layer developing in a zero pressure gradient.

The Preston probe data was intended to serve as a standard to check out the hot-film gage and the sublayer fence in two-dimensional measurements (see section 3.5). The overall agreement among skin friction values determined by these devices is very good and the performance of the hot-film gage and the sublayer fence is satisfactory in two-dimensional flows. The mean velocity data obtained from the hot wire surveys predicts skin friction values that are in good agreement with direct measurements. The nature of agreement among different measurement techniques points to the consistency of the experimental data. Compared to other devices, the construction and operation of the 0.032" dia Preston probe was much easier and consequently, its results were more dependable. Incidentally, its results were a little conservative, too. Therefore, U* values used in reducing and analyzing two-dimensional hot-wire survey data (subsection 5.3.1 and sections 6.3 and 6.5) were based on the two-dimensional skin friction coefficient obtained from the 0.032" dia Preston probe measurement.

References

1. Bradshaw, P., "Outlook for Three-Dimensional Procedures," Proceedings, Computation of Turbulent Boundary Layers - 1968, AFOSR-IFP-Stanford Conference, Mech. Eng. Department, Stanford University, Vol 1, pp. 427-433, 1969.
2. Nash, J.F. and Patel, V.C., Three-Dimensional Turbulent Boundary Layers, SBC Technical Books, Atlanta, 1972.
3. Smith, A.M.O., "A Decade of Boundary-Layer Research," Applied Mechanics Reviews, pp. 1-9, Jan. 1970.
4. Fernholz, H., "Three-Dimensional Turbulent Boundary Layers: a Report on EUROMECH 33," J. Fluid Mech., Vol. 58, Part 1, pp. 177-186, 1973.
5. Kline, S.J., et al. (Eds.), Proceedings, Computation of Turbulent Boundary Layers - 1968, AFOSR-IFP-Stanford Conference, Mechanical Engineering Department, Stanford University, Vols. 1 and 2, 1969.
6. Wheeler, A.J. and Johnston, J.P., "An Assessment of Three-Dimensional Turbulent Boundary Layer Prediction Methods," Trans. ASME, Series I, J. Fluids Engineering,, Vol. 95 pp. 415-421, 1973.
7. Mellor, G.L., "Incompressible, Turbulent Boundary Layers with Arbitrary Pressure Gradients and Divergent or Convergent Cross Flows," AIAA Journal, Vol. 5, No. 9, pp. 1570-1579, 1967.
8. Nash, J.F., "The Calculation of Three-Dimensional Turbulent Boundary Layers in Incompressible Flow," J. Fluid Mech., Vol. 37, Part 4, pp. 625-642, 1969.
9. Bradshaw, P., "Calculation of Three-Dimensional Turbulent Boundary Layers," J. Fluid Mech., Vol. 46, Part 3, pp. 417-445, 1971.

10. Donaldson, C. duP. and Rosenbaum, H., "Calculation of Turbulent Shear Flows through Closure of the Reynolds Equations by Invariant Modeling," NASA SP-216, 1968.

11. Cebeci, T., "Calculation of Three-Dimensional Boundary Layers I. Swept Infinite Cylinders and Small Cross Flow," AIAA Journal, Vol. 12, No. 6, pp. 779-786, 1974.

12. Cebeci, T., "Calculation of Three-Dimensional Boundary Layers II. Three-Dimensional Flows in Cartesian Coordinates," AIAA Journal, Vol. 13, No. 8, pp. 1056-1064, 1975.

13. Bradshaw, P., Ferriss, D.H., and Atwell, N.P., "Calculation of Boundary-Layer Development Using the Turbulent Energy Equation," J. Fluid Mech., Vol. 28, Part 3, pp. 593-616, 1967.

14. Johnston, J.P., "Measurements in a Three-Dimensional Turbulent Boundary Layer Induced by a Swept, Forward-Facing Step," J. Fluid Mech., Vol. 42, Part 4, pp. 823-844, 1970.

15. Bradshaw, P., and Terrell, M., "The Response of a Turbulent Boundary Layer on an Infinite Swept Wing to the Sudden Removal of Pressure Gradient," NPL Aero. Report 1305, 1969.

16. Gruschwitz, E., "Trubulente Reibungsschichten mit Sekundärströmung," Ing. - Arch., Vol. 6, pp. 355-365, 1935.

17. Kuethe, A.M., McKee, P.B., and Curry, W.H., "Measurements in the Boundary Layer of a Yawed Wing," NACA TN 1946, 1949.

18. Ashkenas, H. and Ridell, F.R., "Investigation of the Turbulent Boundary Layer on a Yawed Flat Plate," NACA TN 3383, 1955.

19. Johnston, J.P., "Three-Dimensional Turbulent Boundary Layer," Gas Turbine Lab. Report No. 39, MIT, May, 1957. Also Trans. ASME, Series D,J. Basic Engineering, Vol. 82, pp. 233-248 and 622-628, 1960.

20. Ashkenas, H., "Turbulent Shearing Stress in the Boundary Layer of Yawed Flat Plates," NACA TN 4140, 1958.

21. Hornung, H.G. and Joubert, P.N., "The Mean Velocity Profile in Three-Dimensional Turbulent Boundary Layers," J. Fluid Mech., Vol. 15, Part 3, pp. 368-384, 1963.

22. Willie, M.G., "An Experimental Study in Three-Dimensional Turbulent Boundary Layer on a Flat Plate with Parallel Flow," Ph.D. Thesis, University of Michigan, 1964.

23. Smith, P.D., "An Investigation into Three-Dimensional Boundary Layers," Ph.D. Thesis, University of London, 1965.

24. East, L.F. and Hoxey, R.P., "Low Speed Three-Dimensional Turbulent Boundary-Layer Data, Parts 1 and 2," A.R.C.R. & M. 3653, 1969.

25. Rogers, B.K. and Head, M.R., "Measurement of Three-Dimensional Boundary Layers," The Aeronautical Journal of the Royal Aeronautical Society, Vol. 73, pp. 796-798, 1969.

26. Klinksiek, W.F. and Pierce, F.J., "Simultaneous Lateral Skewing in a Three-Dimensional Turbulent Boundary-Layer Flow," Trans. ASME, Series D, J. Basic Engineering, Vol. 92, pp. 83-92, 1970.

27. Bissonnette, L.R., "An Experimental Study of the Development of a Three-Dimensional Turbulent Boundary Layer under Rapidly Changing Rate of Strain," Ph.D. Thesis, Princeton University, 1970. Also J. Fluid Mech., Vol. 63, Part 2, pp. 369-413, 1974.

28. Vermeulen, A.J., "Measurements of Three-Dimensional Turbulent Boundary Layers," Ph.D. Dissertation, University of Cambridge, 1971.

29. Prahlad, T.S., "Wall Similarity in Three-Dimensional Turbulent Boundary Layers," AIAA Journal, Vol. 6, No. 9, pp. 1772-1774, 1968. Also AIAA Journal, Vol. 11, No. 3, pp. 359-365, 1973.

30. Swamy, N.V.C., "Turbulent Boundary Layer on a Yawed Flat Plate," Z. Flugwiss., Vol. 19, No. 12, pp. 496-502, 1971.

31. Etheridge, D.W., "Three-Dimensional Turbulent Boundary Layers on 45°Swept Plate and Drag Calculation for a Series of Bodies of Revolution," Ph.D. Thesis, University of London, 1972.

32. Power, J.L., "Wall Shear Stress and Mean-Velocity Measurements in a Three-Dimensional Turbulent Boundary Layer," NSRDC Report 4056, Sept. 1973.

33. Lewkowicz, A., "Two and Three Dimensional Incompressible Turbulent Boundary Layers," Ph.D. Thesis, University of Liverpool, 1965.

34. Van Den Berg, B., et al., "Measurements in a Three-Dimensional Incompressible Turbulent Boundary Layer in an Adverse Pressure Gradient under Infinite Swept Wing Conditions," NLR-TR-72092-U, 1973. Also J.Fluid Mech., Vol.70,Part 1, pp.127-148, 1975.

35. Kehl, A., "Untersuchungen über konvergente und divergente turbulente Reibungsschichten," Ing. - Arch., Vol. 13, pp. 293-329, 1943.

36. Eichelbrenner, E.A., and Peube, J-L., "The Role of S-Shaped Crossflow Profiles in Three-Dimensional Boundary Layer Theory," Laboratoire de Mechanique des Fluides, Poitiers, Final Report, 1966.

37. East, J.L., Jr., and Pierce, F.J., "Explicit Numerical Solution of the Three-Dimensional Incompressible Turbulent Boundary Layer," AIAA Journal, Vol. 10, No. 9, pp. 1216-1223, 1972.

38. Pierce, F.J. and East, J.L., Jr., "Near-Wall Collateral Flow in Three-Dimensional Boundary Layers," AIAA Journal, Vol. 10, No. 3, pp. 334-336, 1972.

39. Pierce, F.J. and Zimmerman, B.B., "Wall Shear Stress Inference From Two and Three-Dimensional Turbulent Boundary Layer Velocity Profiles," Trans. ASME, Series I, J. Fluids Engineering, Vol. 95, pp. 61-67, 1973.

40. Winkelmann, A.E., "Experimental Studies of a Two and a Three-Dimensional Low Speed Turbulent Boundary Layer," Ph.D. Dissertation, University of Maryland, 1976.

41. Hebbar, S.K. and Melnik, W.L., "Experimental Studies of the Near Wall Region of a Three-Dimensional Low Speed Turbulent Boundary Layer," Paper presented at the 28th Annual Meeting of the Fluid Dynamics Division of the American Physical Society, November, 1975.

42. Hebbar, K.S., "An Experimental Investigation of the Near-Wall Region of a Three-Dimensional Incompressible Turbulent Boundary Layer Relaxing in a Zero Pressure Gradient," Ph.D. Dissertation, University of Maryland. 1976.

43. Wills, J.A.B., "Convection Velocities in a Viscous Sublayer," NPL Aero Rept. 1251, 1967.

44. Schlichting, H., Boundary Layer Theory, McGraw Hill Book Company, Fourth Edition, New York, 1960.

45. Stiles, R.K., "A Study of the Correlated Velocity Fluctuations in Turbulent Pipe Flow," M.S. Thesis, University of Maryland, 1969.

46. Patel, V.C., "Calibration of the Preston Tube and Limitations on its Use in Pressure Gradients," J. Fluid Mech., Vol. 23, Part 1, pp. 185-208, 1965.

47. Bradshaw, P., "A Simple Method for Determining Turbulent Skin Friction from Velocity Profiles," J. Aerospace Sci., Vol. 26, p. 841, 1959.

48. Clauser, F.H., "Turbulent Boundary Layers in Adverse Pressure Gradients," J. Aero. Sci., Vol. 21, pp. 91-108, 1954.

49. Comte-Bellot, G., "Hot-Wire Anemometry," In: Annual Review of Fluid Mechanics, Vol. 8, pp. 209-231, 1976.

50. Wills, J.A.B., "The Correction of Hot-Wire Readings for Proximity to a Solid Boundary," J. Fluid Mech., Vol. 12, Part 3, pp. 388-396, 1962.

51. Richardson, E.G., "The Correction of Hot-Wire Readings in a Boundary Layer for Proximity to the Solid Boundary," J. Aero. Sci., Vol. 23, pp. 970-971, 1956.

52. Mak, F.J., "Wall Effects on the Heat Loss from Short Hot-Wire Probes", DISA Conference on Fluid Dynamic Measurements, Vol. 1, pp. 45-52, Leicester University Press, 1972.

53. Vlasov, D.I. and Polyaev, W.M., "Using Hot-Wire Probes for Investigation of Flow in the Boundary Layer along a Permeable Surface," DISA Information, No. 18, pp. 11-14, Sept., 1975.

54. Thinh, N. van, "On Some Measurements Made by Means of a Hot Wire in a Turbulent Flow Near a Wall," DISA Information, No. 7, pp. 13-18, Jan., 1969.

55. Singh, U.K. and Shaw, R., "Hot-Wire Anemometer Measurements in Turbulent Flow Close to a Wall," DISA Conference on Fluid Dynamic Measurements, Vol. 1, pp. 35-38, Leicester University Press, 1972.

56. Oka, S. and Kostić, Ž., "Influence of Wall Proximity on Hot-Wire Velocity Measurements," DISA Information No. 13, pp. 29-33, May, 1972.

57. Patel, R.P., "A Note on Fully Developed Turbulent Flow Down a Circular Pipe," Aeronautical Journal, pp. 93-97, Feb./March, 1974. Also Mechanical Eng. Res. Lab. Report No. 68-7, McGill University, October, 1968.

58. Rose, W.G., "Corrections to Average Measurements in Unsteady Flow," Proceedings, ASME Symposium on Measurement in Unsteady Flow, Worcester, Mass., May 21-23, 1962, pp. 85-89.

59. Mojola, O.O., "A Hot-Wire Method for Three-Dimensional Shear Flows," DISA Information, No. 16, pp. 11-14, July, 1974.

60. Perry, A.E. and Joubert, P.N., "A Three-Dimensional Turbulent Boundary Layer," J. Fluid Mech., Vol. 22, Part 2, pp. 285-304, 1965.

61. Pierce, F.J. and Krommenhock, D.H., "Wall Shear Stress Diagnostics in Three-Dimensional Turbulent Boundary Layers," Virginia Polytechnic Inst., Interium Tech. Rep. No. 2, 1968.

62. Clauser, F.H., "The Turbulent Boundary Layer,"In: Advances in Applied Mechanics, Vol. 4, pp. 1-51, 1956.

63. Tani, I., "Review of Some Experimental Results on the Response of a Turbulent Boundary Layer to Sudden Perturbations," Proceedings, Computation of Turbulent Boundary Layers - 1968, AFOSR-IFP-Stanford Conference, Mechanical Engineering Department, Stanford University, Vol. 1, pp. 483-494, 1969.

64. Bradshaw, P., An Introduction to Turbulence and Its Measurement, Pergamon Press, First Edition, Braunschweig, 1971.

65. Bellhouse, B.J. and Schultz, D.L., "Determination of Mean and Dynamic Skin Friction, Separation and Transition in Low-Speed Flow with a Thin-Film Heated Element," J. Fluid Mech., Vol. 24, Part 2, pp. 379-400, 1966.

66. Klebanoff, P.S. "Characteristics of Turbulence in a Boundary Layer with Zero Pressure Gradient," NACA Report 1247, pp. 1135-1153, 1955.

67. Laufer, J., "Investigation of Turbulent Flow in a Two-Dimensional Channel," NACA TN 2123, 1950.

68. Laufer, J., "The Structure of Turbulence in Fully Developed Pipe Flow," NACA TN 2954, 1953.

69. Reichardt, H. and Reuter, R., "Zur Theorie der Turbulenten Schwankungen in Grenzschichtströmungen," Max-Planck-Inst. für Strömungsforschung, Göttingen, Report 7, August, 1974.

70. Schubauer, G.B. and Klebanoff, P.S., "Investigation of Separation of the Turbulent Boundary Layer," NACA Report 1030, pp. 689-708, 1951.

71. Morrow, T.B., "Effects of Dirt Accumulation on Hot-Wire and Hot -Film Sensors," DISA Conference on Fluid Dynamic Measurements, Vol. 1, pp. 122-124, Leicester University Press, 1972.

72. Collis, D.C., "The Dust Problem in Hot-Wire Anemometry," The Aeronautical Quarterly, Vol. 4, Part 1, pp. 93-102, August, 1952.

73. Bradshaw, P., "Teh Effect of Wind-Tunnel Screens on Nominally Two-Dimensional Boundary Layers," J. Fluid Mech., Vol. 22, Part 4, pp. 679-687, 1965.

74. Loehrke, R.I. and Nagib, H.M., "Experiments on Management of Free-Stream Turbulence," AGARD Report 598,1972.

75. Fage, A. and Falkner, V.M., "Relation Between Heat Transfer and Surface Friction for Laminar Flow," A.R.C.R. & M. 1408, 1931.

76. Ludwieg, H., "Instrument for Measuring the Wall Shearing Stress for Turbulent Boundary Layers," NACA TM 1284, 1950.

77. Liepmann, H.W. and Skinner, G.T., "Shearing-Stress Measurements by Use of a Heated Element," NACA TN 3268, 1954.

78. Brown, G.L., "Theory and Application of Heated Films for Skin Friction Measurement," Paper 18, Proceedings of the 1967 Heat Transfer and Fluid Mechanics Institute (edited by Libby, Olfe and Van Atta), pp. 361-381, Stanford University Press, 1967.

79. Pope, R.J., "Skin Friction Measurements in Laminar and Turbulent Flows Using Heated Thin-Film Gages," AIAA Journal, Vol. 10, No. 6, pp. 729-730, 1972.

80. Drinkuth, R.H. and Pierce, F.J., "Directional Heat Meter for Wall Shear Stress Measurements in Turbulent Boundary Layers," The Review of Scientific Instruments, Vol. 37, No. 6, pp. 740-741, 1966.

81. McCroskey, W.J. and Durbin, E.J., "Flow Angle and Shear Stress Measurements Using Heated Films and Wires," ASME Paper No. 71-WA/FE-17, 1971.

Table 1 Tunnel conditions and wall coordinate parameters for two-dimensional hot wire surveys

Quantity	Port 1 (x=0.75")	Port 7 (x=34.75")
$Re_{\infty r} \times 10^{-5}$/foot	3.26	3.25
$U_{\infty r}$, ft/sec	53.38	53.80
$Q_{\infty r}$, lbf/ft^2	3.326	3.342
Barometric Pressure P, mm Hg	768.7	761.4
Humidity of air W, lb/lb	0.0040	0.0055
T_{air}, °C	23.1	23.3
$(\rho \times 10^3)_{air}$, slugs/ft^3	2.334	2.309
$(\nu \times 10^4)_{air}$, ft^2/sec	1.636	1.655
$c_f \times 10^3$ (from 0.032" dia Preston probe data)	2.496	2.476
U*, ft/sec	1.8859	1.8929
$(dU/dy)_w$, ft/sec/inch	1.8117×10^3	1.8042×10^3

Table 2 Experimental data from two-dimensional hot wire survey at Port 1 (x = 0.75"); Re_{∞_r} = 3.26 x 10^5/foot, U_∞ = 53.38 ft/sec

(refer to Table 1 for tunnel operating conditions)

		Mean flow data				Tubulence data					
y (inches)	y^+	U_{meas} (ft/sec)	U_{corr} (ft/sec)	$\frac{U}{U_\infty}$ corr	U^+_{corr}	$\frac{\sqrt{\overline{u^2}}}{U^*}$	$\frac{\sqrt{\overline{w^2}}}{U^*}$	$\frac{-\overline{uw}}{U^{*2}}$	$\frac{\sqrt{\overline{u^2}}}{U_\infty} \times 100$	$\frac{\sqrt{\overline{w^2}}}{U_\infty} \times 100$	$\frac{-\overline{uw}}{U_\infty^2} \times 100$
0.9385	909.20	41.60	41.60	0.779	21.87	1.74	1.23	0.13	6.20	4.38	0.016
0.8625	835.57	40.90	40.90	0.766	21.50	1.76	1.24	0.13	6.28	4.43	0.016
0.6845	663.13	39.70	39.70	0.744	20.87	1.83	1.27	0.13	6.52	4.54	0.016
0.5435	526.53	38.40	38.40	0.719	20.18	1.89	1.28	0.13	6.75	4.55	0.016
0.4315	418.03	37.30	37.30	0.699	19.61	1.95	1.25	0.10	6.94	4.46	0.013
0.3425	331.81	36.25	36.25	0.679	19.05	1.99	1.25	0.10	7.09	4.45	0.013
0.2725	263.99	35.10	35.10	0.657	18.45	2.01	1.30	0.10	7.16	4.63	0.013
0.2165	209.74	34.20	34.20	0.641	17.98	2.05	1.28	0.08	7.30	4.55	0.011
0.1715	166.14	33.25	33.25	0.623	17.48	2.07	1.31	0.08	7.37	4.67	0.011
0.1365	132.24	32.05	32.05	0.600	16.85	2.08	1.33	0.08	7.41	4.73	0.011
0.1085	105.11	31.15	31.15	0.583	16.37	2.09	1.38	0.08	7.44	4.91	0.011
0.0855	82.83	30.15	30.15	0.565	15.85	2.10	1.38	0.08	7.49	4.93	0.011
0.0675	65.39	29.30	29.30	0.549	15.40	2.12	1.41	0.06	7.54	5.02	0.008
0.0535	51.83	28.25	28.25	0.529	14.85	2.18	1.42	0.06	7.78	5.06	0.008
0.0425	41.17	27.20	27.20	0.509	14.30	2.27	1.35	0.06	8.10	4.80	0.008
0.0335	32.45	26.05	26.05	0.488	13.69	2.34	1.47	0.06	8.35	5.24	0.008
0.0265	25.67	24.60	24.60	0.461	12.93	2.42	1.45	0.06	8.62	5.17	0.008
0.0195	18.89	22.45	22.45	0.420	11.80	2.50	1.36	0.08	8.91	4.86	0.011
0.0145	14.05	20.05	20.05	0.376	10.54	2.48	1.31	0.08	8.83	4.68	0.011
0.0115	11.14	17.40	17.40	0.326	9.15	2.37	1.26	0.08	8.44	4.48	0.011
0.0095	9.20	15.40	15.40	0.288	8.09	2.23	1.15	0.08	7.94	4.12	0.011
0.0085	8.23	13.95	13.95	0.261	7.33	2.10	1.08	0.08	7.51	3.85	0.011
0.0075	7.27	12.85	12.85	0.241	6.75	1.98	0.86	0.06	7.05	3.05	0.008
0.0065	6.30	11.35	11.35	0.213	5.97	1.76	0.93	0.06	6.28	3.31	0.008
0.0055	5.33	10.00	10.00	0.187	5.26	1.57	0.76	0.04	5.59	2.69	0.005
0.0050	4.84	9.15	9.12	0.171	4.79	1.42	0.74	0.04	5.06	2.63	0.005
0.0045	4.36	8.50	8.36	0.157	4.39	1.32	0.50	0.02	4.69	1.78	0.003
0.004	3.87	7.70	7.41	0.139	3.89	1.16	0.52	0.02	4.15	1.84	0.002
0.0035	3.39	7.05	6.50	0.122	3.41	1.03	0.34	0.01	3.68	1.21	0.001
0.003	2.91	6.60	5.70	0.107	2.99	0.89	--	--	3.19	--	--
0.0025	2.42	5.95	4.54	0.085	2.38	0.67	0.31	0.01	2.37	1.12	0.001
0.002	1.94	5.90	3.65	0.068	1.92	0.54	0.12	0.00	1.92	0.42	0.000
0.0015	1.45	6.50	3.08	0.058	1.62	0.36	0.22	0	1.28	0.79	0
0.001	0.97	7.60	2.63	0.049	1.38	0.28	0.18	0	1.01	0.65	0

Table 2a: Experimental data from two-dimensional hot wire survey at Port 7 (x=34.75"); Re_{∞_r} = 3.25 x 10^5/foot, U_∞ = 53.80 ft/sec

(refer to Table 1 for tunnel operating conditions)

		Mean flow data				Tubulence data					
y (inches)	y^+	U_{meas} (ft/sec)	U_{corr} (ft/sec)	$\frac{U}{U_\infty}$ corr	U^+_{corr}	$\frac{\sqrt{\overline{u^2}}}{U^*}$	$\frac{\sqrt{\overline{w^2}}}{U^*}$	$\frac{-\overline{uw}}{U^{*2}}$	$\frac{\sqrt{\overline{u^2}}}{U_\infty}$ x 100	$\frac{\sqrt{\overline{w^2}}}{U_\infty}$ x 100	$\frac{-\overline{uw}}{U_\infty^2}$ x 100
0.939	893.74	41.90	41.90	0.779	22.16	1.75	1.28	0.09	6.16	4.50	0.011
0.863	821.40	41.40	41.40	0.769	21.89	1.78	1.27	0.10	6.27	4.45	0.013
0.685	651.98	39.80	39.80	0.740	21.05	1.88	1.26	0.10	6.60	4.42	0.013
0.544	517.78	38.80	38.80	0.721	20.52	1.93	1.29	0.10	6.78	4.53	0.013
0.432	411.18	37.55	37.55	0.698	19.86	1.96	1.36	0.12	6.90	4.80	0.015
0.343	326.47	36.55	36.55	0.679	19.33	2.03	1.38	0.12	7.15	4.86	0.015
0.273	259.84	35.40	35.40	0.658	18.72	2.06	1.39	0.12	7.23	4.88	0.015
0.217	206.54	34.45	34.45	0.640	18.22	2.10	1.38	0.10	7.37	4.84	0.012
0.172	163.71	33.40	33.40	0.621	17.66	2.12	1.39	0.09	7.43	4.87	0.011
0.137	130.40	32.25	32.25	0.599	17.06	2.12	1.41	0.08	7.47	4.94	0.010
0.109	103.75	31.25	31.25	0.581	16.53	2.13	1.42	0.08	7.50	5.00	0.010
0.086	81.85	30.00	30.00	0.558	15.87	2.14	1.46	0.08	7.53	5.15	0.010
0.068	64.72	29.10	29.10	0.541	15.39	2.16	1.49	0.08	7.60	5.25	0.010
0.054	51.40	28.00	28.00	0.520	14.81	2.21	1.49	0.08	7.77	5.23	0.010
0.043	40.93	27.10	27.10	0.504	14.33	2.30	1.50	0.06	8.07	5.26	0.007
0.034	32.36	25.80	25.80	0.479	13.64	2.37	1.52	0.08	8.33	5.35	0.010
0.027	25.70	24.30	24.30	0.452	12.85	2.46	1.46	0.06	8.63	5.12	0.007
0.020	19.04	22.00	22.00	0.409	11.63	2.54	1.39	0.04	8.92	4.89	0.005
0.015	14.28	19.60	19.60	0.364	10.37	2.53	1.38	0.04	8.90	4.84	0.005
0.012	11.42	17.15	17.15	0.319	9.07	2.43	1.34	0.04	8.55	4.70	0.005
0.010	9.52	15.30	15.30	0.284	8.09	2.30	1.16	0.02	8.10	4.07	0.002
0.009	8.57	14.00	14.00	0.260	7.40	2.19	1.19	0.02	7.71	4.17	0.002
0.008	7.61	12.95	12.95	0.241	6.85	2.06	1.02	0.02	7.24	3.60	0.002
0.007	6.66	11.50	11.50	0.214	6.08	1.88	1.01	0.02	6.60	3.55	0.002
0.006	5.71	10.35	10.35	0.192	5.47	1.71	0.74	0.02	6.00	2.61	0.002
0.0055	5.23	9.80	9.80	0.182	5.18	1.56	0.87	0.02	5.48	3.05	0.002
0.005	4.76	9.05	9.02	0.168	4.77	1.50	0.57	0.02	5.26	2.01	0.002
0.0045	4.28	8.05	7.90	0.147	4.18	1.30	0.77	0.02	4.56	2.70	0.002
0.004	3.81	7.40	7.07	0.131	3.74	1.21	0.56	0.02	4.24	1.96	0.002
0.0035	3.33	6.65	6.07	0.113	3.21	0.99	0.57	0.01	3.49	2.00	0.001
0.003	2.86	6.30	5.35	0.099	2.83	0.88	0.16	0.01	3.09	0.55	0.001
0.0025	2.38	5.80	4.35	0.081	2.30	0.67	0.41	0.01	2.37	1.44	0.001
0.002	1.90	5.75	3.45	0.064	1.82	0.55	0.23	0.01	1.94	0.82	0.001
0.0015	1.43	6.30	2.85	0.053	1.50	0.38	0.28	0.00	1.33	0.99	0.000
0.001	0.95	7.10	2.08	0.039	1.10	0.31	0.14	0	1.10	0.51	0
0.0005	0.48	7.60	0.60	0.011	0.32	-	-	-	-	-	-

Table 3 Two-dimensional data on skin friction

Type of shear stress device	Mean skin friction coefficient, $c_f \times 10^3$ ($Re_{\infty r} = 3.25 \times 10^5$ /foot)	
	Port 1 (x=0.75")	Port 7 (x=34.75")
0.032" dia Preston probe	2.496 (2.500)	2.476 (2.468)
0.018" dia Preston probe	2.517 (2.564)	2.489 (2.535)
Sublayer fence	2.545	2.522
Hot-film gage	2.535	2.484
From mean velocity profile	2.524	2.485

Note: The values within the parentheses are based on Patel's calibration curve [46].

Table 4 Wall static pressure data in the relaxing region

$c_p = [(p - p_{tap\ \#22})/Q_{\infty r}]$, $Re_{\infty r}$: 3.25×10^5 to 3.29×10^5 per foot, $Q_{\infty r}$: 3.539 to 3.557 lbf/ft^2, $U_{\infty r}$: 55.98 to 55.85 ft/sec

Tap #	x, inches from trailing edge	z, inches from centerline	$c_p \times 10^2$
1	0.5	-17.875	-2.066
2	12.125	-17.875	-5.570
3	0.5	-11.875	-1.138
4	12.125	-11.875	-4.596
5	0.125	- 5.875	-0.418
6	0.5	- 5.875	-0.534
7	1.0	- 5.875	-0.696
8	1.75	- 5.875	-0.975
9	2.625	- 5.875	-1.230
10	3.625	- 5.875	-1.602
11	5.125	- 5.875	-2.019
12	7.125	- 5.875	-2.575
13	9.125	- 5.875	-3.017
14	12.125	- 5.875	-3.434
15	16.125	- 5.875	-3.713
16	26.125	- 5.875	-3.945
17	36.125	- 5.875	-4.920
18 (Port 8)	0.75	- 5.0	-0.534
19	0.5	- 3.5	-0.441
20	5.125	- 3.5	-1.625
21	12.125	- 3.5	-2.948
22	0.125	- 1.125	0
23	0.5	- 1.125	-0.069
24	1.0	- 1.125	-0.185
25	1.75	- 1.125	-0.395
26	2.625	- 1.125	-0.580
27	3.625	- 1.125	-0.812
28	5.125	- 1.125	-1.207
29	7.125	- 1.125	-1.741
30	9.125	- 1.125	-2.159
31	12.125	- 1.125	-2.599
32	16.125	- 1.125	-2.946
33	26.125	- 1.125	-3.523
34	36.125	- 1.125	-4.803
35 (Port 1)	0.75	1.0	0.047
36 (Port 2)	2.75	1.0	-0.301
37 (Port 3)	5.75	1.0	-0.998
38 (Port 4)	9.75	1.0	-1.903
39	12.125	1.0	-2.274
40 (Port 5)	15.75	1.0	-2.621

Table 4 Concluded

41 (Port 6)	23.75	1.0	-3.295
42 (Port 7)	34.75	1.0	-4.618
43	0.125	3.125	0.348
44	0.5	3.125	0.279
45	1.0	3.125	0.279
46	1.75	3.125	0.163
47	2.625	3.125	0.047
48	3.625	3.125	-0.163
49	5.125	3.125	-0.441
50	7.125	3.125	-0.975
51	9.125	3.125	-1.393
52	12.125	3.125	-1.857
53	16.125	3.125	-2.322
54	26.125	3.125	-3.436
55	36.125	3.125	-5.038
56 (Port 1a)	0.75	4.5	0.580
57	0.5	5.5	0.928
58	5.125	5.5	0
59	12.125	5.5	-1.647
60	0.125	7.125	1.346
61	0.5	7.125	1.323
62	1.0	7.125	1.277
63	1.75	7.125	1.138
64	2.625	7.125	0.998
65	3.625	7.125	0.743
66	5.125	7.125	0.301
67	7.125	7.125	-0.279
68	9.125	7.125	-0.790
69	12.125	7.125	-1.416
70	16.125	7.125	-1.996
71	26.125	7.125	-3.367
72	36.125	7.125	-6.316
73 (Port 9)	0.75	8.0	1.439
74	0.5	13.125	2.622
75	12.125	13.125	-0.719
76	0.5	19.125	2.205
77	12.125	19.125	-0.951

Table 5 Freestream velocity in the relaxing region (Pitot-static probe data)

Port #	Corresponding x for P-S probe data (inches from trailing edge)	At P - S probe location	
		Measured velocity ratio (local velocity to reference velocity)	% increase in velocity
1	-1	1.0371	3.71
2	1	1.0297	2.97
3	4	1.0256	2.56
4	8	1.0228	2.28
5	14	1.0212	2.12
6	22	1.0216	2.16
7	33	1.0210	2.10
8	-1	1.0443	4.43
9	-1	1.0268	2.68

Table 6 Tunnel conditions for three-dimensional hot wire surveys

Station		Upstream reference values			Local freestream values at port location			Properties of air entering the tunnel				
Port	x, inches	Reynolds Number $Re_{\infty r} \times 10^{-5}$ per ft	Velocity $U_{\infty r}$, ft/sec	Dynamic Head $Q_{\infty r}$, lbf/ft^2	Reynolds Number $\bar{Re}_{\infty} \times 10^{-5}$ per ft	Velocity $\bar{U}_{\infty}$, ft/sec	Dynamic Head $\bar{Q}_{\infty}$, lbf/ft^2	Barometric pressure P mm Hg	Humidity w lb/lb	Temperature T(°C)	Density $\rho \times 10^3$ slugs/ft^3	Viscosity $\nu \times 10^4$ ft^2/sec
1	0.75	3.27	55.74	3.519	3.37	57.47	3.741	757.9	0.0112	26.5	2.265	1.701
2	2.75	3.26	55.83	3.523	3.35	57.37	3.719	760.0	0.0139	27.6	2.260	1.710
3	5.75	3.23	54.41	3.382	3.30	55.66	3.539	761.7	0.0104	25.7	2.284	1.684
4	9.75	3.25	55.79	3.502	3.32	57.05	3.661	756.0	0.0142	27.3	2.250	1.717
5	15.75	3.26	55.93	3.529	3.33	57.16	3.686	760.0	0.0160	27.7	2.256	1.713
6	23.75	3.24	54.44	3.391	3.31	55.61	3.538	763.6	0.0132	25.4	2.288	1.680
7	34.75	3.25	56.01	3.529	3.32	57.19	3.679	757.0	0.0122	28.2	2.249	1.721
8	0.75	3.25	54.16	3.374	3.37	56.22	3.635	764.8	0.0107	24.6	2.301	1.667
9	0.75	3.26	54.85	3.443	3.33	56.00	3.589	764.5	0.0111	26.1	2.289	1.682

Table 7 Wall coordinate parameters for three-dimensional hot wire surveys

Station		$Re_{\infty r} \times 10^{-5}$ per foot	$\bar{U}_\infty$ ft/sec	$\nu \times 10^4$ ft^2/sec	$\bar{c}_f \times 10^3$ (from 0.032" dia. Preston probe data)	$\bar{U}^* = \bar{U}_\infty (\bar{c}_f/2)^{1/2}$ ft/sec	$(\frac{d\bar{U}}{dy})_w = (\frac{\bar{U}^{*2}}{\nu})$ ft/sec/inch
Port	x, inches						
1	0.75	3.27	57.47	1.701	1.171	1.3906	0.9473×10^3
2	2.75	3.26	57.37	1.710	1.364	1.4981	1.0937×10^3
3	5.75	3.23	55.66	1.684	1.614	1.5812	1.2373×10^3
4	9.75	3.25	57.05	1.717	1.827	1.7241	1.4428×10^3
5	15.75	3.26	57.16	1.713	2.071	1.8394	1.6459×10^3
6	23.75	3.24	55.61	1.680	2.277	1.8764	1.7464×10^3
7	34.75	3.25	57.19	1.721	2.425	1.9914	1.9203×10^3
8	0.75	3.25	56.22	1.667	1.248	1.4043	0.9859×10^3
9	0.75	3.26	56.00	1.682	1.010	1.2585	0.7847×10^3

Table 8: Experimental data from three-dimensional hot wire survey at Port 1 (x = 0.75"); $Re_{\infty r}$ = 3.27 x 10^5/foot, $\bar{U}_\infty$ = 57.47 ft/sec

(refer to table 6 for tunnel operating conditions)

		Mean flow data						Tubulence data					
y (ins)	y^+	α_{meas} (degs)	α_{corr} (degs)	$\bar{U}_{meas}$ (ft/sec)	$\bar{U}_{corr}$ (ft/sec)	$\frac{\bar{U}}{U_{\infty corr}}$	U^+_{corr}	$\frac{\sqrt{\overline{u_1^2}}}{U^*}$	$\frac{\sqrt{\overline{w_1^2}}}{U^*}$	$\frac{-\overline{u_1 w_1}}{U^{*2}}$	$\frac{\sqrt{\overline{u^2}}}{U^*}$	$\frac{\sqrt{\overline{w^2}}}{U^*}$	$\frac{-\overline{uw}}{U^{*2}}$
0.940	640.37	8.75	8.49	35.60	35.60	0.619	25.60	4.58	3.60	3.01	4.66	3.50	1.66
0.686	467.33	12.0	11.61	31.30	31.30	0.545	22.51	4.45	3.60	3.45	4.57	3.45	1.76
0.433	294.98	16.5	16.02	27.15	27.15	0.472	19.52	3.93	3.35	3.16	4.10	3.14	1.51
0.274	186.66	19.5	19.07	24.95	24.95	0.434	17.94	3.51	3.19	2.42	3.69	2.98	1.20
0.173	117.85	21.0	20.65	23.25	23.25	0.405	16.72	3.32	2.97	1.71	3.44	2.82	0.54
0.110	74.94	21.625	21.33	21.75	21.75	0.378	15.64	3.19	3.01	1.24	3.29	2.89	0.52
0.069	47.01	21.75	21.5	20.30	20.30	0.353	14.60	3.15	2.97	0.83	3.22	2.90	0.22
0.044	29.97	21.875	21.78	18.75	18.75	0.326	13.48	3.18	2.85	0.29	3.17	2.86	-0.48
0.028	19.07	21.5	21.37	16.35	16.35	0.284	11.76	3.20	2.71	0.32	3.17	2.74	-0.75
0.021	14.31	21.25	21.16	14.75	14.75	0.257	10.61	3.21	2.49	0.17	3.14	2.57	-1.25
0.016	10.90	21.0	21.0	12.70	12.70	0.221	9.13	2.99	2.26	0.13	2.92	2.35	-1.18
0.013	8.86	21.0	21.0	11.10	11.10	0.193	7.98	2.85	2.03	0.13	2.78	2.13	-1.25
0.011	7.49	21.0	21.0	9.70	9.70	0.169	6.98	2.62	1.85	0.19	2.56	1.93	-1.01
0.010	6.81	21.0	21.0	9.15	9.15	0.159	6.58	2.51	1.77	0.08	2.44	1.87	-1.01
0.009	6.13	21.0	21.0	8.30	8.30	0.144	5.97	2.36	1.55	0.11	2.29	1.66	-0.97
0.008	5.45	21.0	21.0	7.60	7.60	0.132	5.46	2.14	1.50	-0.02	2.07	1.60	-0.78
0.0075	5.11	21.0	21.0	7.20	7.20	0.125	5.18	2.04	1.39	0.02	1.97	1.48	-0.74
0.007	4.77	21.0	21.0	6.75	6.72	0.117	4.83	1.99	1.35	0.05	1.93	1.44	-0.68
0.0065	4.43	21.0	21.0	6.35	6.27	0.109	4.51	1.92	1.24	0.02	1.85	1.34	-0.70
0.006	4.09	21.0	21.0	5.90	5.76	0.100	4.14	1.71	1.25	0.04	1.67	1.31	-0.43
0.0055	3.75	21.0	21.0	5.50	5.26	0.091	3.78	1.62	1.11	0.02	1.57	1.18	-0.45
0.005	3.41	21.0	21.0	5.10	4.73	0.082	3.40	1.44	0.96	0.04	1.40	1.02	-0.36
0.0045	3.07	21.0	21.0	4.80	4.24	0.074	3.05	1.29	0.85	-0.02	1.24	0.92	-0.31
0.004	2.72	21.0	21.0	4.45	3.67	0.064	2.64	1.10	0.80	0.01	1.07	0.84	-0.18
0.0035	2.38	21.0	21.0	4.30	3.24	0.056	2.33	0.96	0.64	-0.01	0.92	0.69	-0.17
0.003	2.04	21.0	21.0	4.25	2.78	0.048	2.00	0.74	0.59	0.01	0.73	0.60	-0.06
0.0025	1.70	21.0	21.0	4.40	2.39	0.042	1.72	0.63	0.42	-0.01	0.60	0.45	-0.07
0.002	1.36	21.0	21.0	4.90	2.24	0.039	1.61	0.46	0.39	0.01	0.45	0.40	-0.01
0.0015	1.02	21.0	21.0	5.45	1.99	0.035	1.43	0.38	0.30	-0.01	0.37	0.31	-0.02
0.001	0.68	21.0	21.0	6.45	2.00	0.035	1.44	0.31	--	--	--	--	--
0.0005	0.34	21.0	21.0	7.20	1.62	0.028	1.17	0.29	--	--	--	--	--

Table 8a Experimental data from three-dimensional hot wire survey at Port 2 (x=2.75"); Re_{ft} = 3.26 x 10^5/foot, $\bar{U}_\infty$ = 57.37 ft/sec
(refer to Table 6 for tunnel operating conditions)

		Mean flow data						Turbulence data					
y (ins)	y^+	α_{meas} (degs)	α_{corr} (degs)	$\bar{U}_{meas}$ (ft/sec)	$\bar{U}_{corr}$ (ft/sec)	$\frac{\bar{U}}{\bar{U}_\infty}$ corr	$\bar{U}^+_{corr}$	$\frac{\sqrt{\overline{u_1^2}}}{U^*}$	$\frac{\sqrt{\overline{w_1^2}}}{U^*}$	$\frac{-\overline{u_1 w_1}}{U^{*2}}$	$\frac{\sqrt{\overline{u^2}}}{U^*}$	$\frac{\sqrt{\overline{w^2}}}{U^*}$	$\frac{-\overline{uw}}{U^{*2}}$
0.9405	686.63	7.625	7.42	36.80	36.80	0.641	24.56	4.05	3.08	2.10	4.10	3.01	1.12
0.8265	603.40	8.75	8.52	35.00	35.00	0.610	23.36	4.02	3.09	2.14	4.08	3.01	1.05
0.6865	501.19	10.375	10.10	32.85	32.85	0.573	21.93	3.88	3.15	2.30	3.97	3.05	1.24
0.5515	402.63	11.875	11.55	30.80	30.80	0.537	20.56	3.73	3.04	2.36	3.83	2.91	1.21
0.4335	316.48	13.25	12.94	29.15	29.15	0.508	19.46	3.50	2.94	2.02	3.60	2.81	1.00
0.3515	256.62	14.25	13.93	28.05	28.05	0.489	18.72	3.38	2.83	1.93	3.48	2.70	0.88
0.2745	200.40	14.875	14.59	26.90	26.90	0.469	17.96	3.21	2.74	1.61	3.31	2.63	0.70
0.2265	165.36	15.25	14.98	26.05	26.05	0.454	17.39	3.09	2.78	1.44	3.19	2.67	0.78
0.1735	126.67	15.50	15.27	25.15	25.15	0.438	16.79	3.00	2.71	1.11	3.08	2.63	0.52
0.1105	80.67	15.75	15.57	23.50	23.50	0.410	15.69	2.96	2.65	0.76	3.00	2.60	0.20
0.0695	50.74	15.625	15.47	22.00	22.00	0.383	14.68	2.89	2.70	0.59	2.93	2.66	0.22
0.0445	32.49	15.50	15.38	20.15	20.15	0.351	13.45	2.92	2.63	0.37	2.93	2.62	0.09
0.0285	20.81	15.25	15.19	17.95	17.95	0.313	11.98	2.97	2.42	0.15	2.95	2.44	-0.63
0.0215	15.70	15.00	14.93	16.00	16.00	0.279	10.68	2.96	2.25	0.13	2.92	2.29	-0.80
0.0165	12.05	14.875	14.875	14.00	14.00	0.244	9.34	2.86	2.08	0.11	2.83	2.12	-0.86
0.0135	9.86	14.875	14.875	12.40	12.40	0.216	8.28	2.71	1.82	0.11	2.68	1.87	-0.91
0.0115	8.40	14.875	14.975	11.05	11.05	0.193	7.38	2.57	1.69	0.06	2.53	1.75	-0.88
0.0105	7.67	14.875	14.875	10.15	10.15	0.177	6.77	2.43	1.61	0.02	2.38	1.68	-0.80
0.0095	6.94	14.875	14.875	9.45	9.45	0.165	6.31	2.31	1.55	-0.03	2.27	1.61	-0.73
0.0085	6.21	14.875	14.875	8.90	8.90	0.155	5.94	2.15	1.42	0.03	2.12	1.47	-0.63
0.0080	5.84	14.875	14.875	8.50	8.50	0.148	5.67	2.06	1.34	0.01	2.02	1.40	-0.60
0.0075	5.48	14.875	14.875	8.05	8.05	0.140	5.37	2.01	1.31	0.03	1.97	1.37	-0.55
0.0070	5.11	14.875	14.875	7.65	7.65	0.133	5.11	1.93	1.30	0.06	1.90	1.34	-0.45
0.0065	4.74	14.875	14.875	7.25	7.21	0.126	4.81	1.84	1.04	0.06	1.81	1.10	-0.52
0.0060	4.38	14.875	14.875	6.75	6.67	0.116	4.45	1.72	0.74	0.03	1.67	0.83	-0.57
0.0055	4.01	14.875	14.875	6.30	6.13	0.107	4.09	1.57	0.79	0.03	1.53	0.86	-0.33
0.0050	3.65	14.875	14.875	5.90	5.60	0.098	3.74	1.42	0.75	0.01	1.39	0.81	-0.35
0.0045	3.28	14.875	14.875	5.45	4.97	0.087	3.32	1.30	0.54	0.03	1.27	0.61	-0.32
0.0040	2.92	14.875	14.875	5.20	4.51	0.079	3.01	1.19	0.35	0.03	1.16	0.44	-0.30
0.0035	2.55	14.875	14.875	4.80	3.82	0.067	2.55	1.02	0.34	-0.01	0.99	0.42	-0.23
0.0030	2.19	14.875	14.875	4.55	3.19	0.056	2.13	0.87	0.34	0.01	0.85	0.39	-0.15
0.0025	1.82	14.875	14.875	4.45	2.52	0.043	1.68	0.68	0.23	0.01	0.66	0.27	-0.09
0.0020	1.46	14.875	14.875	4.55	1.93	0.033	1.29	0.57	0.22	0.01	0.56	0.25	-0.06
0.0015	1.09	14.875	14.875	5.05	1.54	0.027	1.03	0.42	--	--	--	--	--
0.0010	0.73	14.875	14.875	5.65	1.05	0.018	0.70	0.35	--	--	--	--	--
0.0005	0.36	14.875	14.875	5.85	-0.03	-0.001	-0.02	0.33	--	--	--	--	--

Table 8b: Experimental data from three-dimensional hot wire survey at Port 3 (x = 5.75"); $Re_{\infty r}$ = 3.23 x 10^5/foot, $\bar{U}_\infty$ = 55.66 ft/sec

(refer to Table 6 for tunnel operating conditions)

		Mean flow data						Tubulence data					
y (ins)	y^+	α_{meas} (degs)	α_{corr} (degs)	$\bar{U}_{meas}$ (ft/sec)	$\bar{U}_{corr}$ (ft/sec)	$\frac{\bar{U}}{\bar{U}_{\infty corr}}$	$\bar{U}^+_{corr}$	$\frac{\sqrt{\overline{u_1^2}}}{U^*}$	$\frac{\sqrt{\overline{w_1^2}}}{U^*}$	$\frac{-\overline{u_1 w_1}}{U^{*2}}$	$\frac{\sqrt{\overline{u^2}}}{U^*}$	$\frac{\sqrt{\overline{w^2}}}{U^*}$	$\frac{-\overline{uw}}{U^{*2}}$
0.939	734.74	6.00	5.82	37.80	37.80	0.679	23.91	3.71	2.80	1.79	3.75	2.75	1.14
0.825	645.54	6.75	6.55	36.20	36.20	0.650	22.89	3.63	2.87	1.84	3.68	2.81	1.22
0.685	535.99	7.50	7.26	34.10	34.10	0.613	21.57	3.55	2.85	1.92	3.60	2.77	1.28
0.550	430.36	8.50	8.25	32.35	32.35	0.581	20.46	3.42	2.81	1.85	3.48	2.73	1.21
0.432	338.03	9.25	9.00	30.80	30.80	0.553	19.48	3.26	2.69	1.67	3.33	2.61	1.04
0.350	273.86	9.75	9.51	29.60	29.60	0.532	18.72	3.15	2.62	1.49	3.22	2.54	0.89
0.273	213.61	10.00	9.76	28.50	28.50	0.512	18.02	3.07	2.52	1.36	3.13	2.45	0.75
0.172	134.58	10.25	10.03	26.80	26.80	0.481	16.95	2.90	2.58	1.09	2.95	2.52	0.71
0.109	85.29	10.00	9.84	25.10	25.10	0.451	15.87	2.82	2.53	0.71	2.86	2.49	0.40
0.068	53.21	9.75	9.61	23.60	23.60	0.424	14.92	2.81	2.51	0.55	2.83	2.48	0.26
0.043	33.65	9.75	9.62	21.75	21.75	0.391	13.75	2.88	2.42	0.41	2.89	2.40	-0.02
0.027	21.13	9.50	9.40	19.20	19.20	0.345	12.14	2.93	2.32	0.25	2.93	2.32	-0.29
0.020	15.65	9.25	9.25	17.05	17.05	0.306	10.78	2.96	2.10	0.21	2.95	2.11	-0.50
0.015	11.74	9.25	9.25	14.75	14.75	0.265	9.33	2.86	1.89	0.11	2.84	1.91	-0.63
0.012	9.39	9.25	9.25	12.95	12.95	0.233	8.19	2.69	1.80	0.08	2.67	1.82	-0.56
0.010	7.82	9.25	9.25	11.40	11.40	0.205	7.21	2.49	1.55	0.01	2.47	1.58	-0.59
0.009	7.04	8.25	9.25	10.60	10.60	0.190	6.70	2.36	1.41	0.03	2.34	1.44	-0.54
0.008	6.26	9.25	9.25	9.60	9.60	0.172	6.07	2.20	1.36	0.01	2.19	1.39	-0.47
0.007	5.48	9.25	9.25	8.45	9.45	0.152	5.34	1.98	1.18	0.04	1.96	1.20	-0.36
0.0065	5.09	9.25	9.25	7.95	7.95	0.143	5.03	1.92	1.13	0.01	1.91	1.16	-0.37
0.006	4.69	9.25	9.25	7.50	7.43	0.133	4.70	1.76	1.06	0.06	1.75	1.07	-0.26
0.0055	4.30	9.25	9.25	7.00	6.89	0.124	4.36	1.68	0.99	-0.06	1.66	1.01	-0.29
0.005	3.91	9.25	9.25	6.50	6.29	0.113	3.98	1.46	0.93	0.04	1.45	0.94	-0.17
0.0045	3.52	9.25	9.25	6.10	5.72	0.103	3.62	1.41	0.78	0	1.39	0.81	-0.22
0.004	3.13	9.25	9.25	5.65	5.06	0.091	3.20	1.21	0.72	0.03	1.20	0.73	-0.12
0.0035	2.74	9.25	9.25	5.25	4.38	0.079	2.77	1.12	0.60	-0.03	1.11	0.61	-0.14
0.003	2.35	9.25	9.25	4.90	3.67	0.066	2.32	0.91	0.53	0.02	0.91	0.54	-0.07
0.0025	1.96	9.25	9.25	4.75	2.94	0.053	1.86	0.83	0.46	-0.04	0.82	0.48	-0.07
0.002	1.56	9.25	9.25	4.60	2.04	0.037	1.29	0.60	0.35	0	0.59	0.36	-0.04
0.0015	1.17	9.25	9.25	4.90	1.42	0.025	0.90	0.44	0.33	0.00	0.44	0.33	-0.01
0.001	0.78	9.25	9.25	5.45	0.77	0.014	0.49	0.40	--	--	--	--	--
0.0005	0.39	9.25	9.25	5.80	-0.30	-0.005	-0.19	0.35	--	--	--	--	--

Table 8c: Experimental data from three-dimensional hot wire survey at Port 4 (x = 9.75"); $Re_{\infty r}$ = 3.25 x 10^5/foot, U_∞ = 57.05 ft/sec

(refer to Table 6 for tunnel operating conditions)

		Mean flow data						Tubulence data					
y (ins)	y^+	α_{meas} (degs)	α_{corr} (degs)	U_{meas} (ft/sec)	U_{corr} (ft/sec)	$\frac{U}{U_{\infty corr}}$	U^+_{corr}	$\frac{\sqrt{\overline{u_1^2}}}{U^*}$	$\frac{\sqrt{\overline{w_1^2}}}{U^*}$	$\frac{-\overline{u_1 w_1}}{U^{*2}}$	$\frac{\sqrt{\overline{u^2}}}{U^*}$	$\frac{\sqrt{\overline{w^2}}}{U^*}$	$\frac{-\overline{uw}}{U^{*2}}$
0.940	786.59	4.5	4.35	39.55	39.55	0.693	22.94	3.25	2.52	1.36	3.28	2.49	1.01
0.686	574.05	5.5	5.33	36.70	36.70	0.643	21.29	3.15	2.49	1.31	3.19	2.45	0.93
0.433	362.33	6.125	5.93	33.60	33.60	0.589	19.49	2.96	2.44	1.27	3.00	2.39	0.94
0.274	229.28	6.25	6.07	31.40	31.40	0.550	18.21	2.80	2.33	1.02	2.84	2.29	0.74
0.173	144.77	6.375	6.21	29.75	29.75	0.521	17.25	2.73	2.31	0.83	2.76	2.27	0.57
0.110	92.05	6.25	6.10	28.00	28.00	0.491	16.24	2.68	2.25	0.69	2.70	2.26	0.46
0.069	57.74	6.00	5.85	26.30	26.30	0.461	15.25	2.69	2.31	0.62	2.71	2.29	0.41
0.044	36.82	5.75	5.62	24.35	24.35	0.427	14.12	2.77	2.24	0.47	2.78	2.22	0.19
0.028	23.43	5.75	5.62	21.50	21.50	0.377	12.47	2.88	2.14	0.22	2.89	2.14	-0.15
0.021	17.57	5.5	5.5	19.55	19.55	0.343	11.34	2.91	1.94	0.20	2.91	1.94	-0.25
0.016	13.39	5.5	5.5	17.05	17.05	0.299	9.89	2.86	1.80	0.16	2.86	1.80	-0.32
0.013	10.88	5.5	5.5	15.30	15.30	0.268	8.87	2.73	1.69	0.16	2.73	1.69	-0.29
0.011	9.20	5.5	5.5	13.60	13.60	0.238	7.89	2.60	1.50	0.13	2.60	1.50	-0.30
0.010	8.37	5.5	5.5	12.85	12.85	0.225	7.45	2.50	1.49	0.02	2.50	1.50	-0.36
0.009	7.53	5.5	5.5	11.60	11.60	0.203	6.73	2.34	1.44	0.13	2.34	1.44	-0.19
0.008	6.69	5.5	5.5	10.80	10.80	0.189	6.26	2.22	1.31	0.07	2.21	1.31	-0.24
0.0075	6.28	5.5	5.5	10.15	10.15	0.178	5.89	2.08	1.24	0.11	2.07	1.24	-0.15
0.007	5.86	5.5	5.5	9.85	9.85	0.173	5.71	2.03	1.16	0.02	2.03	1.17	-0.24
0.0065	5.44	5.5	5.5	9.10	9.10	0.159	5.28	1.89	1.07	0.07	1.89	1.07	-0.17
0.006	5.02	5.5	5.5	8.60	8.60	0.151	4.99	1.82	0.95	-0.04	1.82	0.96	-0.23
0.0055	4.60	5.5	5.5	7.90	7.83	0.137	4.54	1.65	0.97	0.09	1.65	0.97	-0.08
0.005	4.18	5.5	5.5	7.50	7.34	0.129	4.26	1.57	0.78	-0.07	1.57	0.79	-0.18
0.0045	3.77	5.5	5.5	6.75	6.45	0.113	3.74	1.37	0.80	0.07	1.37	0.80	-0.05
0.004	3.35	5.5	5.5	6.30	5.78	0.101	3.35	1.26	0.64	-0.02	1.25	0.65	-0.11
0.0035	2.93	5.5	5.5	5.70	4.91	0.086	2.85	1.07	0.53	0.04	1.07	0.53	-0.04
0.003	2.51	5.5	5.5	5.40	4.22	0.074	2.45	0.93	0.44	-0.04	0.93	0.44	-0.06
0.0025	2.09	5.5	5.5	5.05	3.33	0.058	1.93	0.74	0.37	0.02	0.74	0.37	-0.02
0.002	1.67	5.5	5.5	5.10	2.55	0.045	1.48	0.60	0.33	0.00	0.60	0.33	-0.02
0.0015	1.25	5.5	5.5	5.25	1.66	0.029	0.96	0.48	--	--	--	--	--
0.001	0.84	5.5	5.5	6.00	1.09	0.019	0.63	0.36	--	--	--	--	--
0.0005	0.42	5.5	5.5	7.95	1.34	0.023	0.78	0.26	--	--	--	--	--

Table 8d: Experimental data from three-dimensional hot wire survey at Port 5 (x = 15.75"); $Re_{\infty r} = 3.26 \times 10^5$/foot, $\bar{U}_\infty = 57.16$ ft/sec

(refer to Table 6 for tunnel operating conditions)

		Mean flow data						Tubulence data					
y (ins)	y^+	α_{meas} (degs)	α_{corr} (degs)	$\bar{U}_{meas}$ (ft/sec)	$\bar{U}_{corr}$ (ft/sec)	$\frac{\bar{U}}{\bar{U}_{\infty corr}}$	U^+_{corr}	$\frac{\sqrt{\overline{u_1^2}}}{U^*}$	$\frac{\sqrt{\overline{w_1^2}}}{U^*}$	$\frac{-\overline{u_1 w_1}}{U^{*2}}$	$\frac{\sqrt{\overline{u^2}}}{U^*}$	$\frac{\sqrt{\overline{w^2}}}{U^*}$	$\frac{-\overline{uw}}{U^{*2}}$
0.9395	840.68	3.0	2.90	40.85	40.85	0.715	22.21	2.77	2.17	0.88	2.78	2.15	0.72
0.8545	764.62	3.25	--	--	--	--	--	--	--	--	--	--	--
0.6855	613.39	3.50	3.38	38.40	38.40	0.672	20.88	2.71	2.16	0.87	2.73	2.15	0.70
0.5545	496.17	3.75	--	--	--	--	--	--	--	--	--	--	--
0 4325	387.01	3.75	3.63	35.85	35.85	0.627	19.49	2.60	2.11	0.80	2.61	2.09	0.64
0.3545	317.21	3.75	--	--	--	--	--	--	--	--	--	--	--
0.2735	244.73	3.75	3.63	33.75	33.75	0.590	18.35	2.55	2.07	0.73	2.57	2.04	0.57
0.1725	154.35	3.50	3.38	32.00	32.00	0.560	17.40	2.50	2.05	0.62	2.51	2.04	0.49
0.1095	97.98	3.50	3.39	30.20	30.20	0.528	16.42	2.52	2.00	0.49	2.53	1.98	0.34
0.0685	61.29	3.50	3.40	28.30	28.30	0.495	15.39	2.55	2.02	0.43	2.56	2.01	0.28
0.0435	38.92	3.25	3.15	26.15	26.15	0.457	14.22	2.65	1.99	0.34	2.66	1.98	0.17
0.0275	24.61	3.25	3.15	23.25	23.25	0.407	12.64	2.78	1.88	0.28	2.78	1.88	0.04
0.0205	18.34	3.0	3.0	20.85	20.85	0.365	11.33	2.81	1.79	0.26	2.81	1.78	0.02
0.0155	13.87	3.0	3.0	18.35	18.35	0.321	9.98	2.78	1.62	0.21	2.78	1.62	-0.05
0.0125	11.18	3.0	3.0	16.05	16.05	0.281	8.73	2.66	1.57	0.14	2.66	1.57	-0.10
0.0105	9.40	3.0	3.0	14.40	14.40	0.252	7.83	2.50	1.43	0.07	2.50	1.43	-0.15
0.0095	8.50	3.0	3.0	13.25	13.25	0.232	7.20	2.36	1.43	0.09	2.36	1.43	-0.10
0.0085	7.60	3.0	3.0	12.25	12.25	0.214	6.66	2.26	1.26	0.04	2.26	1.26	-0.14
0.0075	6.71	3.0	3.0	11.00	11.00	0.192	5.98	2.08	1.13	0.11	2.08	1.13	-0.05
0.007	6.26	3.0	3.0	10.40	10.40	0.182	5.65	1.97	1.13	0.09	1.97	1.13	-0.05
0.0065	5.82	3.0	3.0	9.80	9.80	0.171	5.33	1.87	1.01	0	1.86	1.02	-0.13
0.006	5.37	3.0	3.0	9.20	9.20	0.161	5.00	1.77	1.03	0.09	1.77	1.03	-0.01
0.0055	4.92	3.0	3.0	8.62	8.61	0.151	4.68	1.66	0.87	-0.02	1.66	0.87	-0.10
0.005	4.47	3.0	3.0	8.00	7.89	0.138	4.29	1.50	0.82	-0.05	1.50	0.82	-0.08
0.0045	4.03	3.0	3.0	7.60	7.39	0.129	4.02	1.42	0.68	-0.05	1.42	0.68	-0.08
0.004	3.58	3.0	3.0	6.85	6.44	0.113	3.50	1.23	0.65	0.03	1.23	0.65	-0.02
0.0035	3.13	3.0	3.0	6.40	5.72	0.100	3.11	1.12	0.34	0.03	1.12	0.34	-0.03
0.003	2.68	3.0	3.0	6.00	4.93	0.086	2.68	0.99	0.36	-0.03	0.99	0.36	-0.04
0.0025	2.24	3.0	3.0	5.40	3.81	0.067	2.07	0.69	0.30	0.02	0.69	0.30	0.00
0.002	1.79	3.0	3.0	5.35	2.91	0.051	1.58	0.61	0.21	-0.02	0.61	0.21	-0.02
0.0015	1.34	3.0	3.0	6.00	2.43	0.042	1.32	0.41	0.21	0.01	0.41	0.21	0.00
0.001	0.89	3.0	3.9	6.60	1.58	0.028	0.86	0.34	--	--	--	--	--
0.0005	0.45	3.0	3.0	8.50	1.60	0.028	0.87	0.26	--	--	--	--	--

Table 8e: Experimental data from three-dimensional hot wire survey at Port 6 (x = 23.75"); $Re_{\infty r}$ = 3.24 x 10^5/ft, U_∞ = 55.61 ft/sec

(refer to Table 6 for tunnel operating conditions)

		Mean flow data						Tubulence data					
y (ins)	y^+	α_{meas} (degs)	α_{corr} (degs)	$\bar{U}_{meas}$ (ft/sec)	U_{corr} (ft/sec)	$\frac{U}{\bar{U}_{\infty corr}}$	U^+_{corr}	$\frac{\sqrt{u_1^2}}{U^*}$	$\frac{\sqrt{w_1^2}}{U^*}$	$\frac{-\overline{u_1 w_1}}{U^{*2}}$	$\frac{\sqrt{u^2}}{U^*}$	$\frac{\sqrt{w^2}}{U^*}$	$\frac{-\overline{uw}}{U^{*2}}$
0.939	873.97	1.5	1.42	41.80	41.80	0.752	22.28	2.52	2.01	0.72	2.53	2.00	0.66
0.685	637.56	1.625	1.54	39.50	39.50	0.710	21.05	2.45	1.98	0.67	2.47	1.98	0.61
0.432	402.08	1.625	1.54	37.15	37.15	0.668	19.80	2.42	1.89	0.58	2.43	1.88	0.51
0.273	254.09	1.625	1.54	35.05	35.05	0.630	18.68	2.40	1.88	0.51	2.41	1.87	0.45
0.172	160.09	1.5	1.41	33.40	33.40	0.601	17.80	2.39	1.90	0.47	2.39	1.89	0.42
0.109	101.45	1.25	1.18	31.50	31.50	0.566	16.79	2.39	1.90	0.34	2.40	1.90	0.30
0.068	63.29	1.25	1.18	29.40	29.40	0.529	15.67	2.45	1.89	0.31	2.45	1.89	0.26
0.043	40.02	1.25	1.19	27.20	27.20	0.489	14.50	2.57	1.84	0.24	2.57	1.84	0.17
0.027	25.13	1.00	1.00	24.20	24.20	0.435	12.90	2.70	1.80	0.20	2.70	1.80	0.12
0.020	18.61	1.00	1.00	21.90	21.90	0.394	11.67	2.78	1.72	0.22	2.78	1.72	0.13
0.015	13.96	1.00	1.00	19.00	19.00	0.342	10.13	1.72	1.56	0.16	2.73	1.56	0.07
0.012	11.17	1.00	1.00	16.70	16.70	0.300	8.90	2.60	1.54	0.16	2.60	1.54	0.08
0.010	9.31	1.00	1.00	14.95	14.95	0.269	7.97	2.44	1.38	0.02	2.44	1.38	-0.05
0.009	8.38	1.00	1.00	13.85	13.85	0.249	7.38	2.35	1.32	0.02	2.35	1.32	-0.05
0.008	7.45	1.00	1.00	12.70	12.70	0.228	6.77	2.20	1.21	-0.08	2.20	1.21	-0.06
0.007	6.51	1.00	1.00	11.40	11.40	0.205	6.07	2.04	1.10	0.02	2.04	1.10	-0.03
0.0065	6.05	1.00	1.00	10.85	10.85	0.195	5.78	1.96	1.00	-0.02	1.96	1.00	-0.05
0.006	5.58	1.00	1.00	10.10	10.10	0.182	5.38	1.83	0.98	0.06	1.83	0.98	-0.02
0.0055	5.12	1.00	1.00	9.50	9.50	0.171	5.06	1.71	0.82	-0.02	1.71	0.82	-0.04
0.005	4.65	1.00	1.00	8.70	8.63	0.155	4.60	1.55	0.78	0.02	1.55	0.78	-0.01
0.0045	4.19	1.00	1.00	8.10	7.94	0.143	4.23	1.44	0.82	0.02	1.44	0.82	0.00
0.004	3.72	1.00	1.00	7.50	7.17	0.129	3.82	1.32	0.62	-0.02	1.32	0.62	-0.02
0.0035	3.26	1.00	1.00	6.90	6.29	0.113	3.35	1.16	0.47	-0.03	1.16	0.47	-0.02
0.003	2.79	1.00	1.00	6.15	5.18	0.093	2.76	0.98	0.46	0.03	0.97	0.46	-0.02
0.0025	2.33	1.00	1.00	5.80	4.28	0.077	2.28	0.81	0.25	-0.02	0.81	0.25	-0.01
0.002	1.86	1.00	1.00	5.55	3.21	0.058	1.71	0.61	0.32	0.02	0.61	0.32	+0.02
0.0015	1.40	1.00	1.00	5.70	2.25	0.040	1.20	0.49	0.18	-0.01	0.49	0.18	0.00
0.001	0.93	1.00	1.00	6.90	1.90	0.034	1.01	0.34	0.23	0.01	0.34	0.23	+0.01
0.0005	0.46	1.00	1.00	7.45	0.54	0.010	0.29	0.30	--	--	--	--	--

Table 8f: Experimental data from three-dimensional hot wire survey at Port 7 (x = 34.75"), $Re_{\infty r}$ = 3.25 x 10^5/foot, U_∞ = 57.19 ft/sec

(refer to Table 6 for tunnel operating conditions)

		Mean flow data						Tubulence data					
y (ins)	y^+	α_{meas} (degs)	α_{corr} (degs)	$\bar{U}_{meas}$ (ft/sec)	U_{corr} (ft/sec)	$\frac{\bar{U}}{\bar{U}_{\infty corr}}$	U^+_{corr}	$\sqrt{\frac{\overline{u_1^2}}{U^*}}$	$\sqrt{\frac{\overline{w_1^2}}{U^*}}$	$\frac{-\overline{u_1 w_1}}{\bar{U}^{*2}}$	$\sqrt{\frac{\overline{u^2}}{U^*}}$	$\sqrt{\frac{\overline{w^2}}{U^*}}$	$\frac{-\overline{uw}}{\bar{U}^{*2}}$
0.939	905.45	1.0	0.95	43.80	43.80	0.766	21.99	2.25	1.74	0.43	2.26	1.74	0.39
0.685	660.52	1.0	0.94	41.80	41.80	0.731	20.99	2.26	1.75	0.43	2.26	1.75	0.39
0.432	416.56	1.0	0.94	40.10	40.10	0.701	20.13	2.25	1.72	0.43	2.25	1.71	0.39
0.273	263.25	0.75	0.69	37.60	37.60	0.657	18.88	2.26	1.74	0.36	2.26	1.74	0.33
0.172	165.85	0.50	0.45	35.40	35.40	0.619	17.78	2.29	1.73	0.28	2.29	1.73	0.26
0.109	105.10	0.25	0.19	33.35	33.35	0.583	16.75	2.34	1.69	0.28	2.34	1.69	0.27
0.068	65.57	0.125	0.125	31.00	31.00	0.542	15.57	2.36	1.74	0.22	2.36	1.74	0.21
0.043	41.46	0.125	0.125	28.75	28.75	0.503	14.44	2.47	1.71	0.16	2.47	1.71	0.15
0.027	26.03	0.125	0.125	25.80	25.80	0.451	12.96	2.63	1.65	0.10	2.63	1.65	0.09
0.020	19.28	0.125	0.125	23.10	23.10	0.404	11.60	2.68	1.61	0.10	2.68	1.61	0.09
0.015	14.46	0.125	0.125	20.45	20.45	0.358	10.27	2.67	1.53	0.09	2.67	1.53	0.08
0.012	11.57	0.125	0.125	18.05	18.05	0.316	9.06	2.58	1.44	0.02	2.58	1.44	0.01
0.010	9.64	0.125	0.125	16.30	16.30	0.285	8.18	2.46	1.39	0.02	2.46	1.39	0.01
0.009	8.68	0.125	0.125	15.00	15.00	0.262	7.53	2.35	1.30	0.02	2.35	1.30	0.01
0.008	7.71	0.125	0.125	14.15	14.15	0.247	7.11	2.25	1.21	0.02	2.25	1.21	0.01
0.007	6.75	0.125	0.125	12.60	12.60	0.220	6.33	2.08	1.09	0.03	2.08	1.09	0.02
0.0065	6.27	0.125	0.125	12.10	12.10	0.212	6.08	1.99	1.02	0.03	1.99	1.02	0.03
0.006	5.79	0.125	0.125	11.25	11.25	0.197	5.65	1.89	1.02	-0.02	1.89	1.02	0.00
0.0055	5.30	0.125	0.125	10.70	10.70	0.187	5.37	1.81	0.88	0	1.81	0.88	0.00
0.005	4.82	0.125	0.125	9.80	9.76	0.171	4.90	1.68	0.72	0.01	1.68	0.72	0.00
0.0045	4.34	0.125	0.125	9.10	8.96	0.157	4.50	1.53	0.83	-0.02	1.53	0.83	0.00
0.004	3.86	0.125	0.125	8.40	8.10	0.142	4.07	1.43	0.65	-0.02	1.43	0.65	0.00
0.0035	3.37	0.125	0.125	7.55	6.97	0.122	3.50	1.24	0.63	0.02	1.24	0.63	0.02
0.003	2.89	0.125	0.125	6.90	5.91	0.103	2.97	1.12	0.39	0.03	1.12	0.39	0.00
0.0025	2.41	0.125	0.125	6.40	4.92	0.086	2.47	0.89	0.46	0.00	0.89	0.46	0.00
0.002	1.93	0.125	0.125	6.05	3.74	0.065	1.88	0.78	0.00	0.00	0.78	0.00	0.00
0.0015	1.45	0.125	0.125	5.95	2.43	0.042	1.22	0.52	0.27	0	0.52	0.27	0.00
0.001	0.96	0.125	0.125	6.60	1.41	0.025	0.71	0.38	0.24	0	0.38	0.24	0.00
0.0005	0.48	0.125	0.125	7.80	0.54	0.009	0.27	0.32	0.20	0	0.32	0.20	0.00

Table 8g: Experimental data from three-dimensional hot wire survey at Port 8 (x = 0.75:); $Re_{\infty r}$ = 3.25 x 10^5/foot, $\bar{U}_\infty$ = 56.22 ft/sec

(refer to Table 6 for tunnel operating conditions)

		Mean flow data						Tubulence data					
y (ins)	y^+	α_{meas} (degs)	α_{corr} (degs)	$\bar{U}_{meas}$ (ft/sec)	$\bar{U}_{corr}$ (ft/sec)	$\frac{\bar{U}}{\bar{U}_{\infty corr}}$	U^+_{corr}	$\frac{\sqrt{\overline{u_1^2}}}{U^*}$	$\frac{\sqrt{\overline{w_1^2}}}{U^*}$	$\frac{-\overline{u_1 w_1}}{U^{*2}}$	$\frac{\sqrt{\overline{u^2}}}{U^*}$	$\frac{\sqrt{\overline{w^2}}}{U^*}$	$\frac{-\overline{uw}}{U^{*2}}$
0.940	659.90	8.0	7.84	36.80	36.80	0.655	26.20	4.23	3.08	1.87	4.27	3.02	0.63
0.864	606.55	8.875	8.68	35.55	35.55	0.632	25.31	4.26	3.21	2.17	4.32	3.13	0.86
0.686	481.59	11.25	10.95	32.35	32.35	0.575	23.04	4.29	3.30	2.75	4.38	3.18	1.10
0.545	382.60	13.25	12.89	30.00	30.00	0.534	21.36	4.17	3.25	2.88	4.26	3.11	1.06
0.433	303.98	15.0	14.60	28.05	28.05	0.499	19.97	3.96	3.17	2.80	4.09	3.00	1.01
0.344	241.50	16.25	15.84	26.55	26.55	0.472	18.91	3.76	3.12	2.57	3.90	2.95	0.99
0.274	192.35	17.25	16.84	25.50	25.50	0.454	18.16	3.60	3.05	2.38	3.74	2.88	0.92
0.218	153.04	18.125	17.73	24.45	24.45	0.435	17.41	3.47	2.92	2.09	3.60	2.76	0.64
0.173	121.45	18.625	18.27	23.50	23.50	0.418	16.73	3.36	2.90	1.72	3.46	2.77	0.50
0.138	96.88	19.0	18.70	22.80	22.80	0.405	16.24	3.28	2.89	1.39	3.37	2.78	0.35
0.110	77.22	19.25	18.96	22.05	22.05	0.392	15.70	3.22	2.90	1.24	3.30	2.80	0.36
0.069	48.44	19.50	19.27	20.60	20.60	0.366	14.67	3.17	2.90	0.86	3.22	2.84	0.16
0.044	30.89	19.375	19.19	18.95	18.95	0.337	13.49	3.19	2.83	0.58	3.21	2.81	-0.23
0.028	19.66	19.125	18.95	16.85	16.85	0.300	12.00	3.23	2.67	0.44	3.21	2.69	-0.66
0.021	14.74	19.0	18.83	15.00	15.00	0.267	10.68	3.17	2.50	0.34	3.14	2.54	-0.90
0.016	11.23	18.75	18.75	13.15	13.15	0.234	9.36	3.08	2.27	0.30	3.03	2.32	-1.08
0.013	9.13	18.75	18.75	11.60	11.60	0.206	8.26	2.89	2.05	0.27	2.84	2.11	-1.05
0.011	7.72	18.75	18.75	10.30	10.30	0.183	7.33	2.70	1.89	0.17	2.65	1.96	-1.00
0.010	7.02	18.75	18.75	9.60	9.60	0.171	6.84	2.58	1.78	0.17	2.53	1.85	-0.93
0.009	6.32	18.75	18.75	8.80	8.80	0.156	6.27	2.43	1.65	0.07	2.37	1.73	-0.91
0.008	5.62	18.75	18.75	8.00	8.00	0.142	5.70	2.21	1.55	0.10	2.17	1.62	-0.67
0.0075	5.26	18.75	18.75	7.60	7.60	0.135	5.41	2.12	1.47	0.03	2.07	1.54	-0.69
0.007	4.91	18.75	18.75	7.15	7.13	0.127	5.08	2.01	1.37	0.07	1.96	1.43	-0.60
0.0065	4.56	18.75	18.75	6.80	6.73	0.120	4.79	1.91	1.28	0.01	1.86	1.35	-0.60
0.006	4.21	18.75	18.75	6.20	6.08	0.108	4.33	1.70	1.21	0.07	1.67	1.25	-0.38
0.0055	3.86	18.75	18.75	5.95	5.74	0.102	4.09	1.65	1.10	0.00	1.60	1.17	-0.47
0.005	3.51	18.75	18.75	5.45	5.11	0.091	3.64	1.47	0.97	0.03	1.43	1.03	-0.34
0.0045	3.16	18.75	18.75	5.10	4.59	0.082	3.27	1.33	0.85	-0.03	1.28	0.91	-0.32
0.004	2.81	18.75	18.75	4.65	3.93	0.070	2.80	1.11	0.73	0.03	1.09	0.76	-0.19
0.0035	2.46	18.75	18.75	4.45	3.45	0.061	2.46	0.95	0.60	0.02	0.93	0.63	-0.15
0.003	2.11	18.75	18.75	4.30	2.92	0.052	2.08	0.81	0.51	-0.01	0.78	0.55	-0.12
0.0025	1.75	18.75	18.75	4.35	2.43	0.043	1.73	0.59	0.42	0.00	0.58	0.44	-0.05
0.002	1.40	18.75	18.75	4.60	2.02	0.036	1.44	0.51	0.32	-0.01	0.49	0.35	-0.05
0.0015	1.05	18.75	18.75	5.15	1.74	0.031	1.24	0.41	0.19	0.00	0.39	0.22	-0.04
0.001	0.70	18.75	18.75	5.75	1.33	0.024	0.95	0.34	--	--	--	--	--
0.0005	0.35	18.75	18.75	5.95	0.39	0.007	0.28	--	--	--	--	--	--

Table 8h: Experimental data from three-dimensional hot wire survey at Port 9 (x = 0.75"); $Re_{\infty r}$ = 3.26 x 10^5/foot, $\bar{U}_\infty$ = 56 ft/sec

(refer to Table 6 for tunnel operating conditions)

		Mean flow data						Tubulence data					
y (ins)	y^+	α_{meas} (degs)	α_{corr} (degs)	$\bar{U}_{meas}$ (ft/sec)	$\bar{U}_{corr}$ (ft/sec)	$\frac{\bar{U}}{\bar{U}_{\infty corr}}$	U^+_{corr}	$\frac{\sqrt{\overline{u_1^2}}}{U^*}$	$\frac{\sqrt{\overline{w_1^2}}}{U^*}$	$\frac{-\overline{u_1 w_1}}{U^{*2}}$	$\frac{\sqrt{\overline{u^2}}}{U^*}$	$\frac{\sqrt{\overline{w^2}}}{U^*}$	$\frac{-\overline{uw}}{U^{*2}}$
0.9395	585.78	9.25	8.97	30.80	30.80	0.550	24.47	4.95	3.88	2.90	5.02	3.79	1.25
0.8635	538.40	10.25	9.93	29.70	29.70	0.530	23.60	4.93	3.85	3.07	5.00	3.75	1.22
0.6855	427.41	12.75	12.31	27.05	27.05	0.483	21.49	4.78	3.79	3.56	4.89	3.63	1.39
0.5445	339.50	14.75	14.25	25.05	25.05	0.447	19.90	4.47	3.69	3.44	4.61	3.52	1.44
0.4325	269.67	16.75	16.14	23.35	23.35	0.417	18.55	4.22	3.63	3.65	4.41	3.40	1.77
0.3435	214.17	18.0	17.45	22.20	22.20	0.396	17.64	4.03	3.40	2.97	4.19	3.21	1.03
0.2735	170.53	19.25	18.74	21.20	21.20	0.379	16.85	3.83	3.33	2.54	3.98	3.14	0.88
0.2175	135.61	19.75	19.28	20.40	20.40	0.364	16.21	3.68	3.31	2.13	3.82	3.14	0.82
0.1725	107.55	20.25	19.84	19.80	19.80	0.354	15.73	3.59	3.24	1.76	3.71	3.11	0.57
0.1375	85.73	20.50	20.15	19.10	19.10	0.341	15.18	3.49	3.21	1.41	3.59	3.10	0.46
0.1095	68.27	20.75	20.45	18.50	18.50	0.330	14.70	3.43	3.17	1.14	3.51	3.08	0.28
0.0685	42.71	20.875	20.65	17.20	17.20	0.307	13.67	3.38	3.18	0.75	3.43	3.12	0.10
0.0435	27.12	21.0	20.83	15.75	15.75	0.281	12.51	3.40	3.09	0.46	3.40	3.08	-0.33
0.0275	17.15	20.50	20.28	13.75	13.75	0.245	10.93	3.36	2.86	0.46	3.35	2.88	-0.67
0.0205	12.78	20.25	20.02	12.20	12.20	0.218	9.69	3.25	2.67	0.36	3.23	2.70	-0.86
0.0155	9.66	20.0	20.0	10.45	10.45	0.187	8.30	3.09	2.31	0.23	3.03	2.38	-1.18
0.0125	7.79	20.0	20.0	8.95	8.95	0.160	7.11	2.82	2.11	0.15	2.76	2.18	-1.01
0.0105	6.55	20.0	20.0	7.95	7.95	0.142	6.32	2.60	1.89	0.08	2.54	1.97	-0.97
0.0095	5.92	20.0	20.0	7.30	7.30	0.130	5.80	2.45	1.74	0.08	2.39	1.82	-0.89
0.0085	5.30	20.0	20.0	6.75	6.75	0.120	5.36	2.30	1.55	0.00	2.23	1.66	-0.93
0.0075	4.68	20.0	20.0	6.00	5.98	0.107	4.75	2.03	1.48	0.04	1.98	1.55	-0.59
0.007	4.36	20.0	20.0	5.75	5.68	0.101	4.51	1.97	1.32	0.01	1.90	1.40	-0.68
0.0065	4.05	20.0	20.0	5.40	5.27	0.094	4.19	1.82	1.30	0.00	1.77	1.37	-0.52
0.006	3.74	20.0	20.0	5.05	4.82	0.086	3.83	1.68	1.21	0.00	1.63	1.27	-0.44
0.0055	3.43	20.0	20.0	4.70	4.34	0.078	3.45	1.54	1.06	0.02	1.50	1.12	-0.40
0.005	3.12	20.0	20.0	4.45	3.98	0.071	3.16	1.42	0.93	-0.03	1.37	1.00	-0.37
0.0045	2.81	20.0	20.0	4.20	3.56	0.064	2.83	1.26	0.85	0.03	1.23	0.89	-0.25
0.004	2.49	20.0	20.0	4.00	3.12	0.056	2.48	1.11	0.69	0.02	1.08	0.75	-0.23
0.0035	2.18	20.0	20.0	3.80	2.63	0.047	2.09	0.92	0.67	0.00	0.89	0.70	-0.13
0.003	1.87	20.0	20.0	3.77	2.23	0.040	1.77	0.75	0.49	0.00	0.72	0.53	-0.10
0.0025	1.56	20.0	20.0	3.85	1.79	0.032	1.42	0.63	0.50	0.00	0.62	0.52	-0.05
0.002	1.25	20.0	20.0	4.40	1.76	0.031	1.40	0.45	0.37	0.01	0.45	0.37	-0.02
0.0015	0.93	20.0	20.0	5.00	1.64	0.029	1.30	0.38	0.29	0.00	0.37	0.30	-0.02
0.001	0.62	20.0	20.0	5.50	1.31	0.023	1.04	0.33	--	--	--	--	--
0.0005	0.31	20.0	20.0	5.65	0.53	0.009	0.42	--	--	--	--	--	--

Table 9 Comparison of sublayer analysis with measured change of crossflow angle

PORT 1 (x = 0.75")					PORT 2 (x = 2.75")				
			$\Delta\alpha=(\alpha-\alpha_w)$, in degrees					$\Delta\alpha=(\alpha-\alpha_w)$, in degrees	
y (inches)	y^+	$(U/\bar{U}_\infty)$	Analysis Equation (16a)	Measured Value	y (inches)	y^+	$(U/\bar{U}_\infty)$	Analysis Equation (16a)	Measured Value
0.0015	1.02	0.032	0.23	0	0.001	0.73	0.018	0.11	0
0.0045	3.07	0.069	0.49	0	0.004	2.92	0.076	0.45	0
0.0075	5.11	0.117	0.83	0	0.007	5.11	0.129	0.76	0
0.016	10.90	0.206	1.45	0	0.0165	12.05	0.236	1.39	0
0.021	14.31	0.239	1.68	0.25	0.0215	15.70	0.269	1.59	0.125
0.028	19.07	0.265	1.86	0.50	0.0285	20.81	0.302	1.78	0.375
0.044	29.97	0.303	2.12	0.875	0.0445	32.49	0.338	1.99	0.625
					0.0695	50.74	0.369	2.17	0.75
					0.1105	80.67	0.394	2.32	0.875

Table 10 Distribution of crossflow angle in the relaxing boundary layer

y^+	α at Port 1, (x=0.75") in degrees	Normalized crossflow angle ($\alpha/\alpha_{Port\ 1}$) at Port							
		2 (x=2.75")	3 (x=5.75")	4 (x=9.75")	5 (x=15.75")	6 (x=23.75")	7 (x=34.75")	8 (x=0.75")	9 (x=0.75")
$\leq$ 10	21.00	0.708	0.440	0.262	0.143	0.048	0.006	0.893	0.952
20	21.40	0.706	0.437	0.259	0.142	0.047	0.006	0.888	0.958
30	21.60	0.711	0.438	0.262	0.143	0.049	0.006	0.889	0.963
50	21.50	0.721	0.451	0.272	0.153	0.053	0.006	0.898	0.963
100	20.95	0.737	0.477	0.294	0.167	0.064	0.009	0.893	0.955
150	19.90	0.764	0.502	0.312	0.178	0.073	0.020	0.894	0.955
200	18.50	0.795	0.530	0.335	0.195	0.081	0.030	0.903	0.965
300	16.00	0.825	0.584	0.378	0.225	0.097	0.050	0.912	0.959
400	13.50	0.867	0.627	0.433	0.267	0.115	0.067	0.933	0.963
500	11.30	0.903	0.673	0.496	0.305	0.133	0.088	0.956	0.973
600	9.30	0.925	0.737	0.559	0.355	0.156	0.107	0.957	0.968
650	8.40	0.952	0.762	0.595	0.381	0.173	0.119	0.976	0.988

Table 11 Limiting streamline (wall crossflow) angle data in the relaxing boundary layer

Station		Resultant mean wall shear stress direction α_w, in degrees, measured by				
Port	x inches	hot-film gage	sublayer fence	0.032" dia Preston probe	0.018" dia Preston probe	hot wire extrapolation
1	0.75	21.0	21.0	20.75	19.5 (21.5)	21.0
2	2.75	14.875	14.5	15.125	13.25 (15.25)	14.875
3	5.75	9.5	9.5	9.625	7.5 (9.5)	9.25
4	9.75	5.75	5.5	5.5	3.5 (5.5)	5.5
5	15.75	3.25	3.0	2.75	1.0 (3.0)	3.0
6	23.75	1.25	1.5	1.25	-0.5 (1.5)	1.0
7	34.75	0.25	0	0.25	-2.5 (-0.5)	0.125
8	0.75	19.0	18.75	19.0	16.75 (18.75)	18.75
9	0.75	20.0	19.5	20.0	18.0 (20.0)	20.0

Note: The values within the parentheses include a correction of +2°.

Table 12 Resultant mean skin-friction data in the relaxing boundary layer

Station		Resultant mean skin friction, $\bar{c}_f \times 10^3$, predicted by ($Re_{\infty r} = 3.25 \times 10^5$/foot)				
Port	x, inches	hot-film gage	sublayer fence	0.032" dia Preston probe	0.018" dia Preston probe	Mean velocity profile
1	0.75	1.188	1.167	1.171	1.152	1.156
2	2.75	1.403	1.365	1.364	1.369	1.329
3	5.75	1.647	1.644	1.614	1.581	1.588
4	9.75	1.856	1.828	1.827	1.841	1.818
5	15.75	2.099	2.025	2.071	2.011	2.080
6	23.75	2.318	2.224	2.277	2.210	2.334
7	34.75	2.429	2.411	2.425	2.369	2.452
8	0.75	1.314	1.315	1.248	1.257	1.236
9	0.75	1.023	1.046	1.010	1.015	0.921

Table 13 Distribution of maximum turbulence fluctuations in the relaxing boundary layer

Station		$\frac{(\sqrt{\overline{u_1^2}})_{max}}{(\sqrt{\overline{u_1^2}})_{max,\ Port\ 1}}$	$\frac{(\sqrt{\overline{w_1^2}})_{max}}{(\sqrt{\overline{w_1^2}})_{max,\ Port\ 1}}$	$\frac{(-\overline{u_1 w_1})_{max}}{(-\overline{u_1 w_1})_{max,\ Port\ 1}}$
Port	x, inches			
1	0.75	1	1	1
2	2.75	0.952	0.943	0.795
3	5.75	0.922	0.907	0.721
4	9.75	0.879	0.868	0.605
5	15.75	0.812	0.798	0.447
6	23.75	0.819	0.752	0.380
7	34.75	0.838	0.696	0.257
Port 7, x = 34.75" (2-D result)		0.754	0.574	0.064
8	0.75	0.946	0.924	0.852
9	0.75	0.978	0.975	0.867

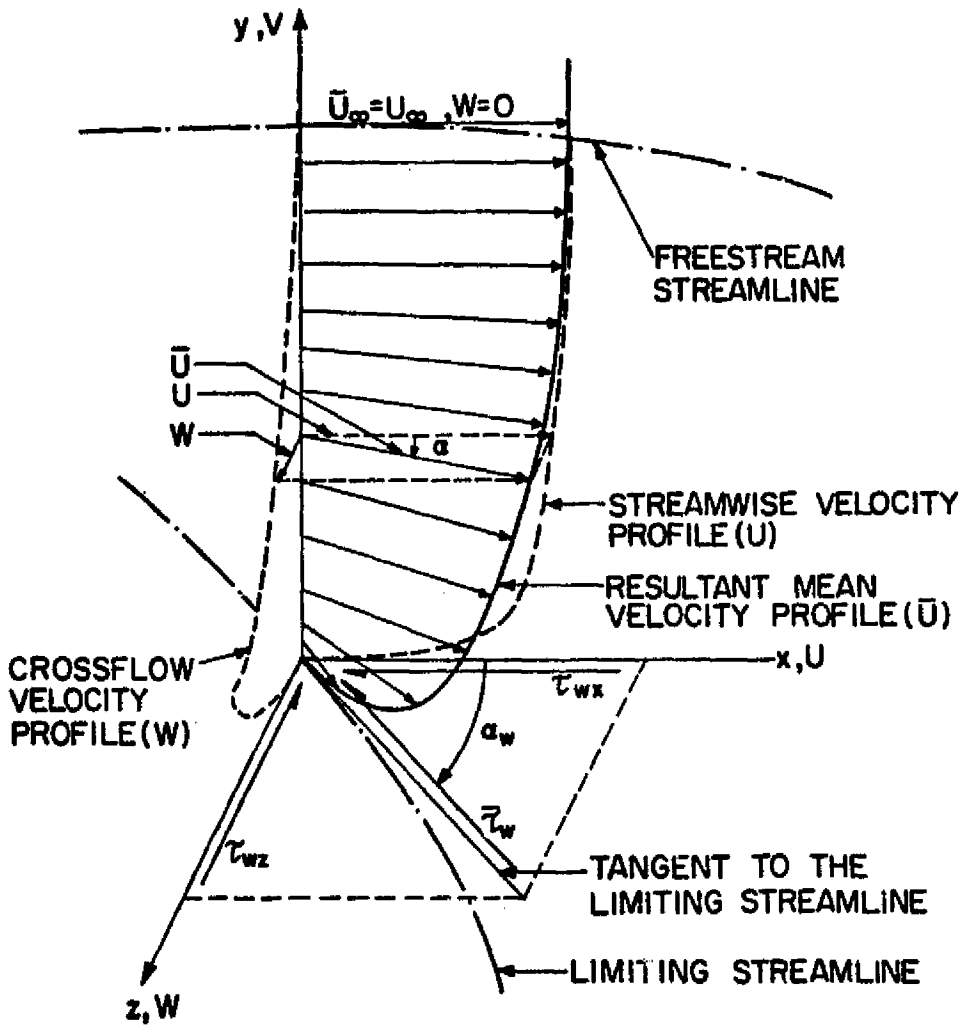

FIGURE 1: SKETCH OF A 3-DIMENSIONAL (SKEWED) MEAN VELOCITY PROFILE IN STREAMLINE COORDINATES

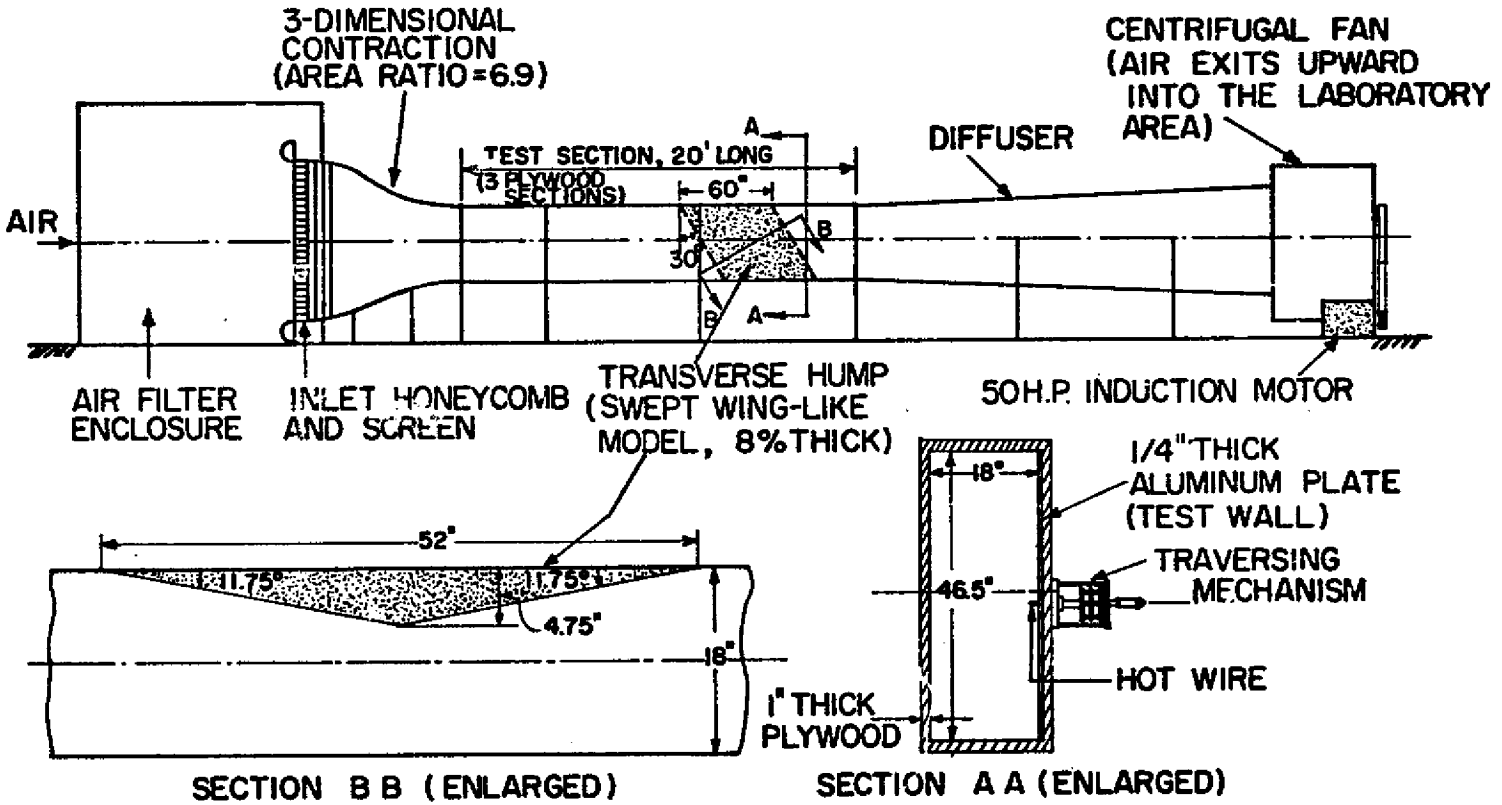

FIG. 2: BOUNDARY LAYER RESEARCH TUNNEL

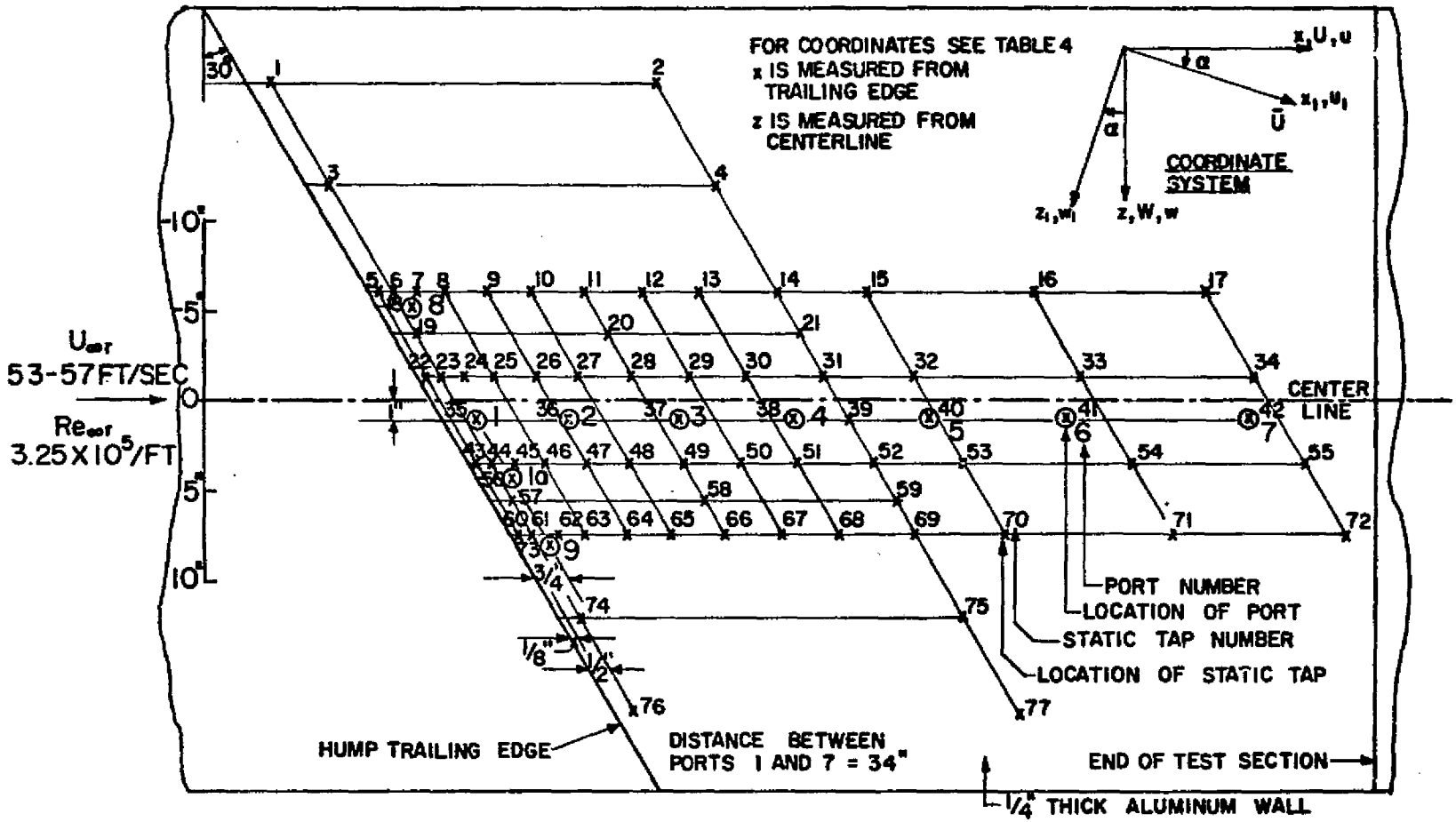

FIG. 3: LOCATION OF INSTRUMENTATION PORTS AND STATIC TAPS

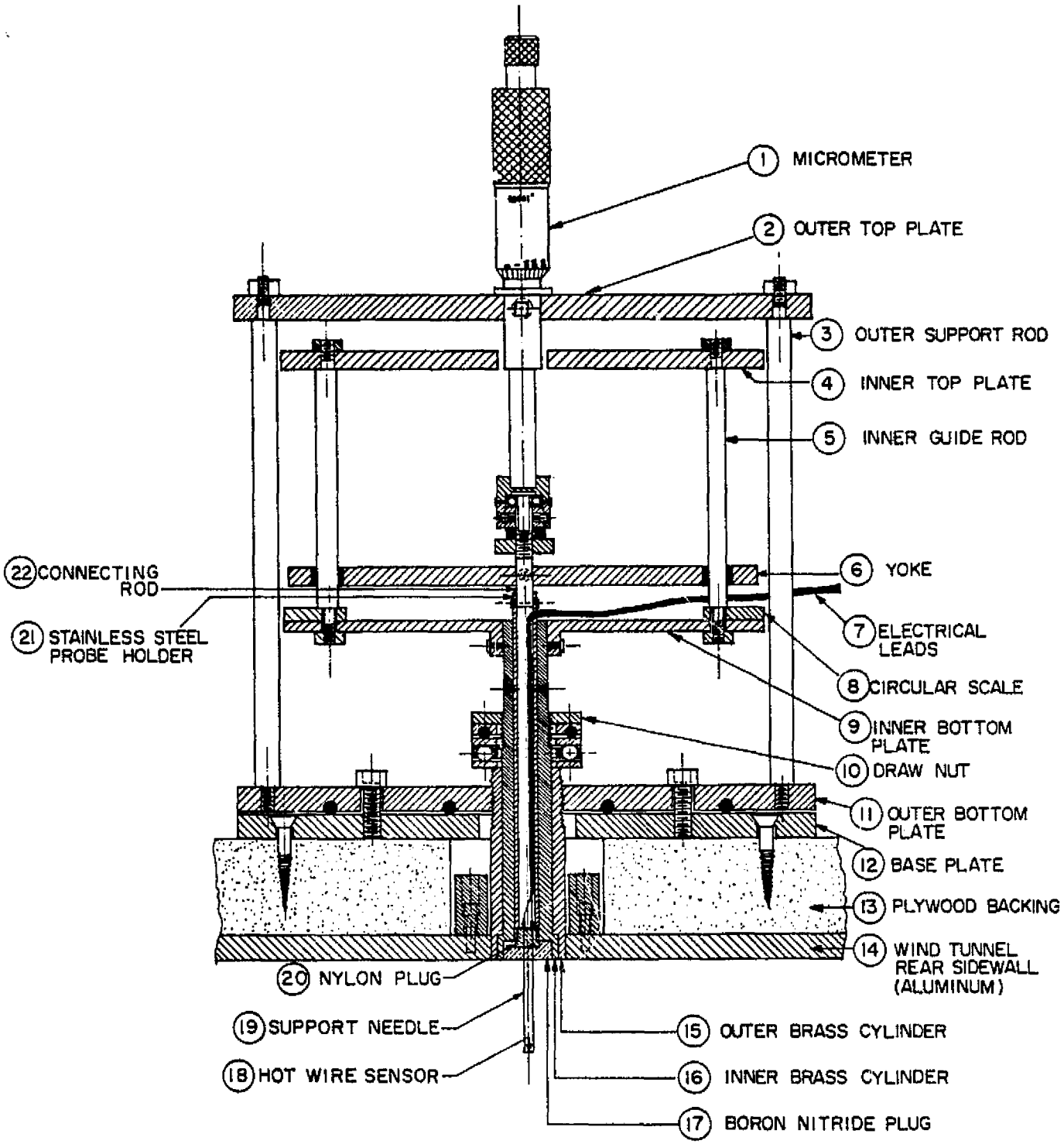

FIG. 4: SECTIONAL DRAWING OF THE TRAVERSE MECHANISM FOR NEAR-WALL STUDIES

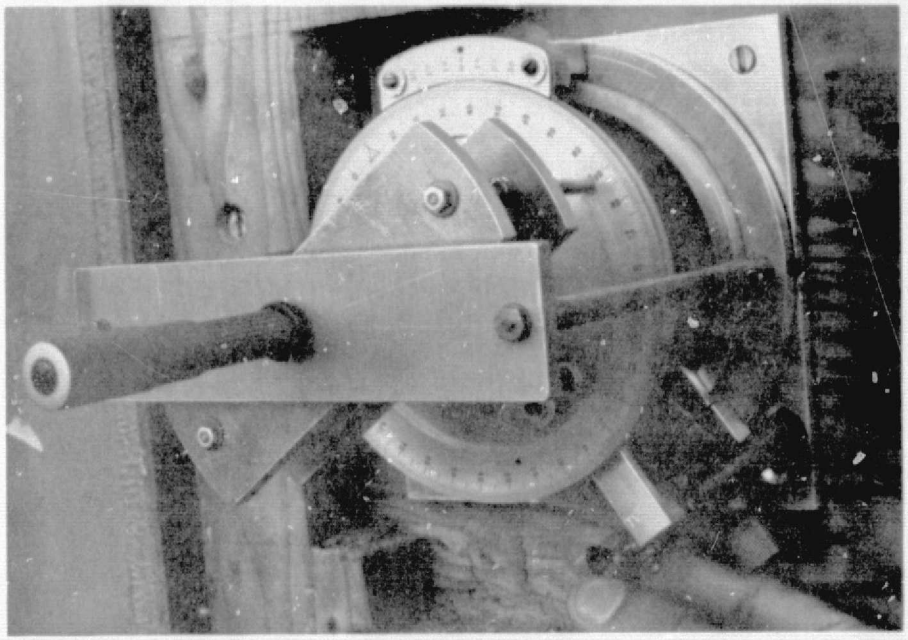

Traverse mechanism mounted on the tunnel side wall
(Fingers are operating the vernier control mechanism)

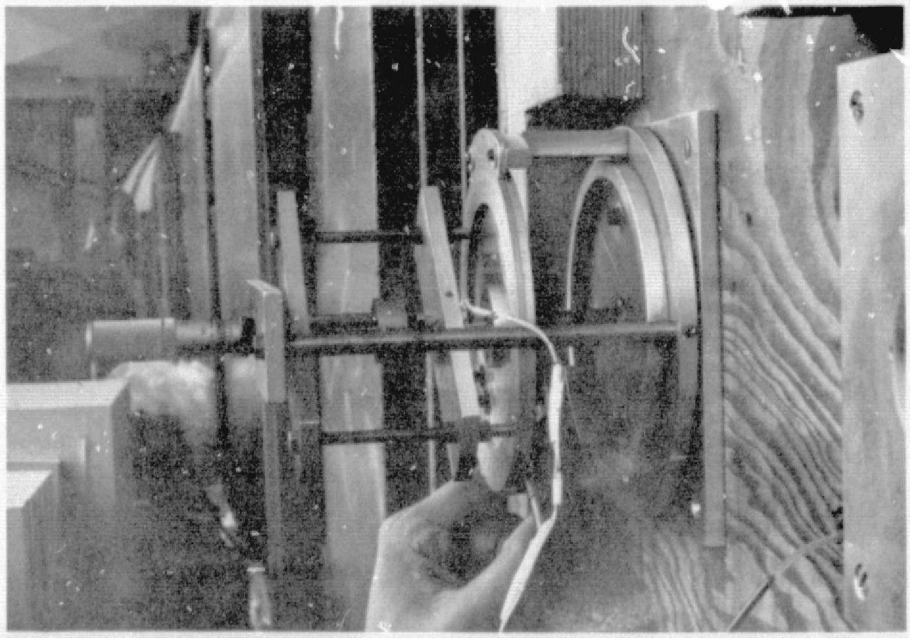

Traverse mechanism with the hot wire probe assembly secured

FIG. 4a: PHOTOGRAPHS OF THE TRAVERSE MECHANISM

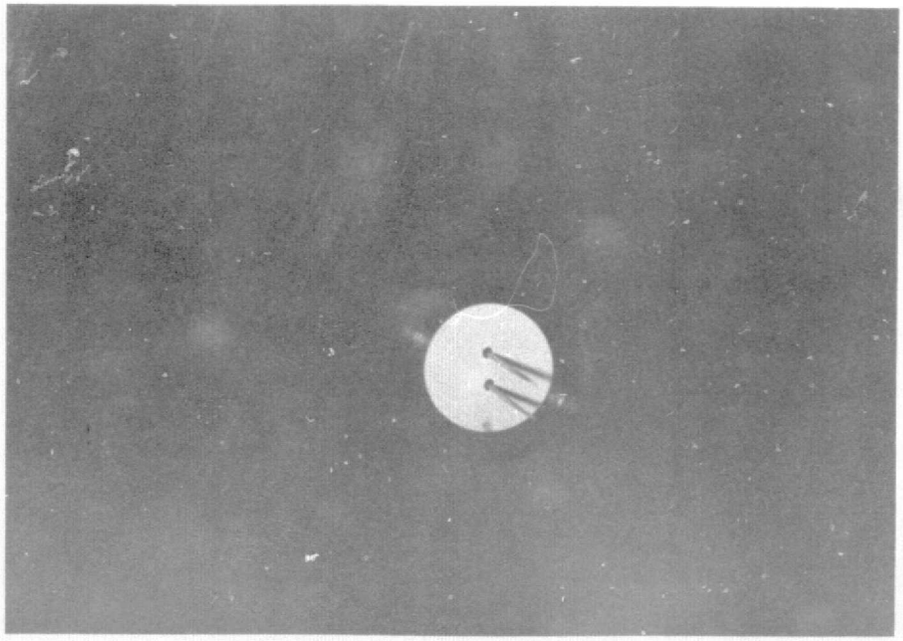

(Hot wire needles are protruding through holes in the boron nitride plug)

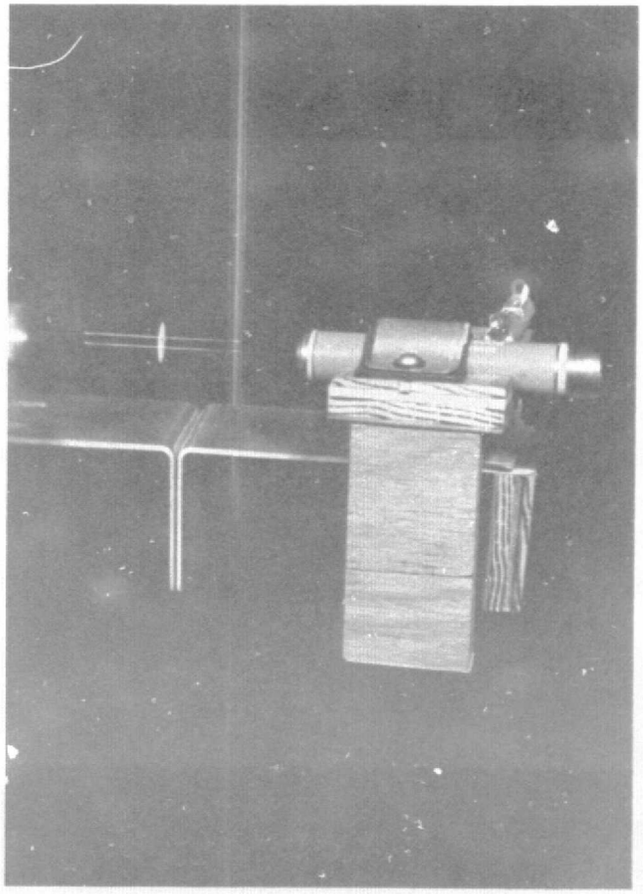

(Hot wire needles are reflected in the aluminum test wall)

FIG. 5: PHOTOGRAPH S OF THE HOT WIRE PROBE AND THE PROBE ALIGNMENT SIGHTING DEVICE MOUNTED ON THE TEST WALL FOR INITIAL ORIENTATION OF THE HOT WIRE

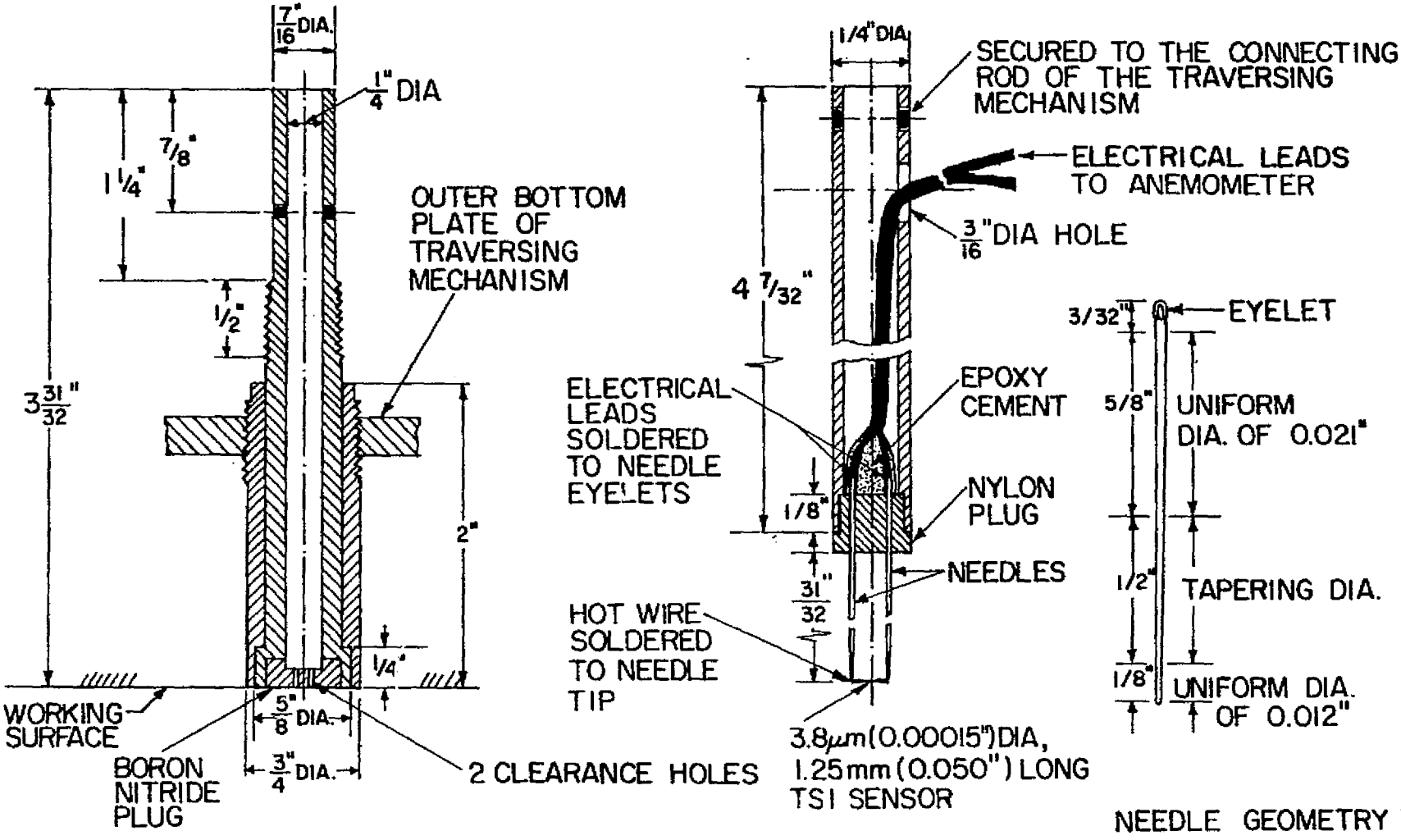

FIG. 6: SECTIONAL DRAWINGS OF HOT WIRE PROBE (FOR ASSEMBLY SEE FIGS. 4 AND 6A)

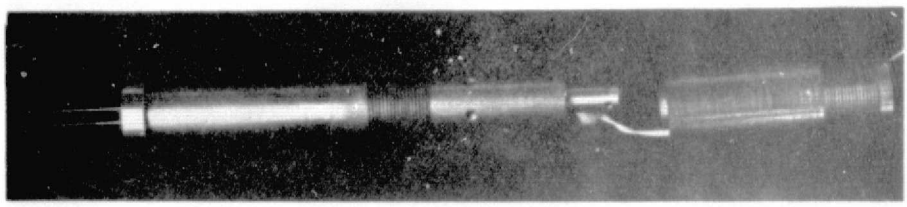

Photograph of the hot wire probe assembly

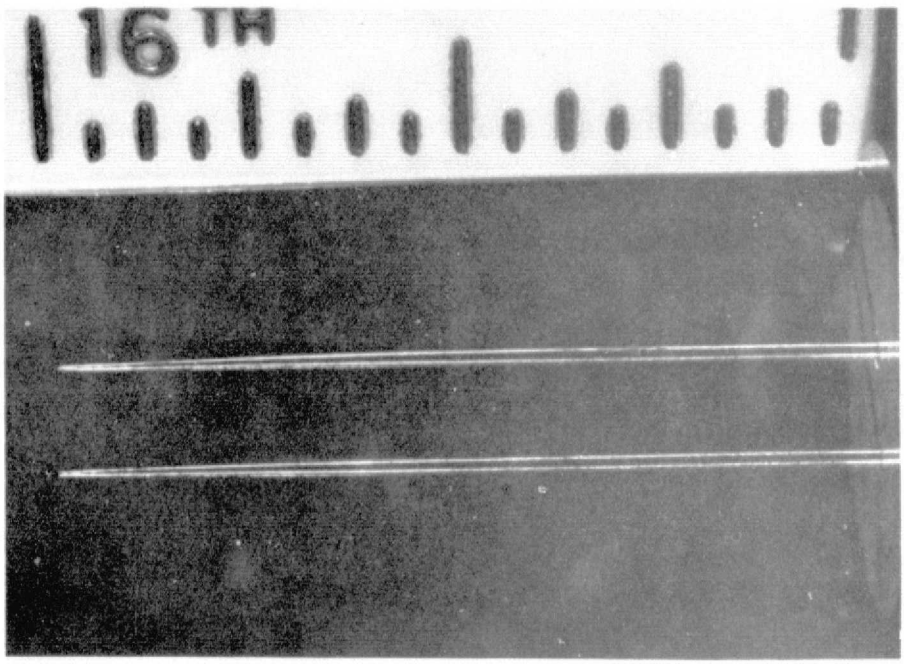

Photomacrograph (4.4 X) of the ground needles

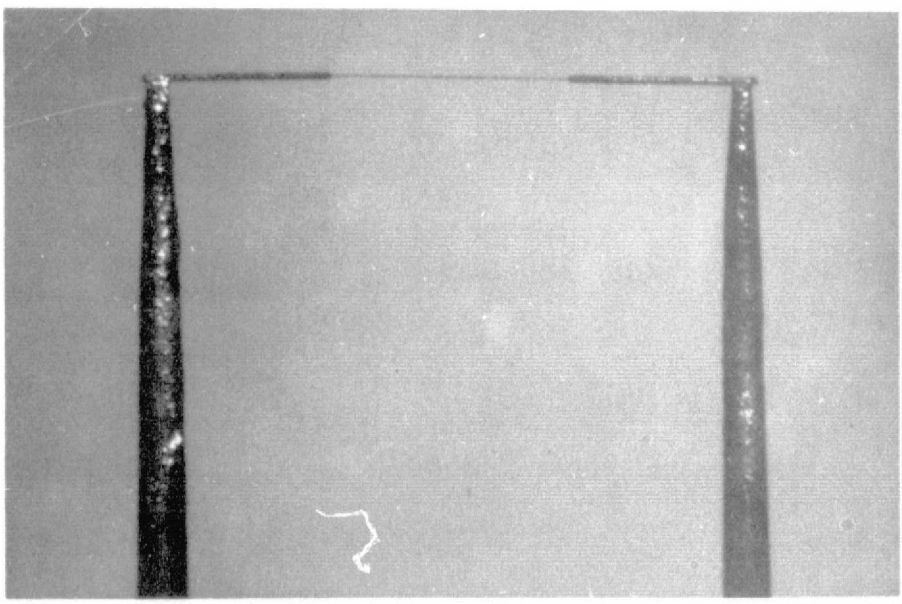

Photomacrograph (25.6 X) of the hot wire (3.8 μm dia tungsten wire) soldered to the needle tips (1/8" apart)

FIG. 6a: PHOTOGRAPH/PHOTOMACROGRAPHS OF HOT WIRE PROBE ASSEMBLY/HOT WIRE

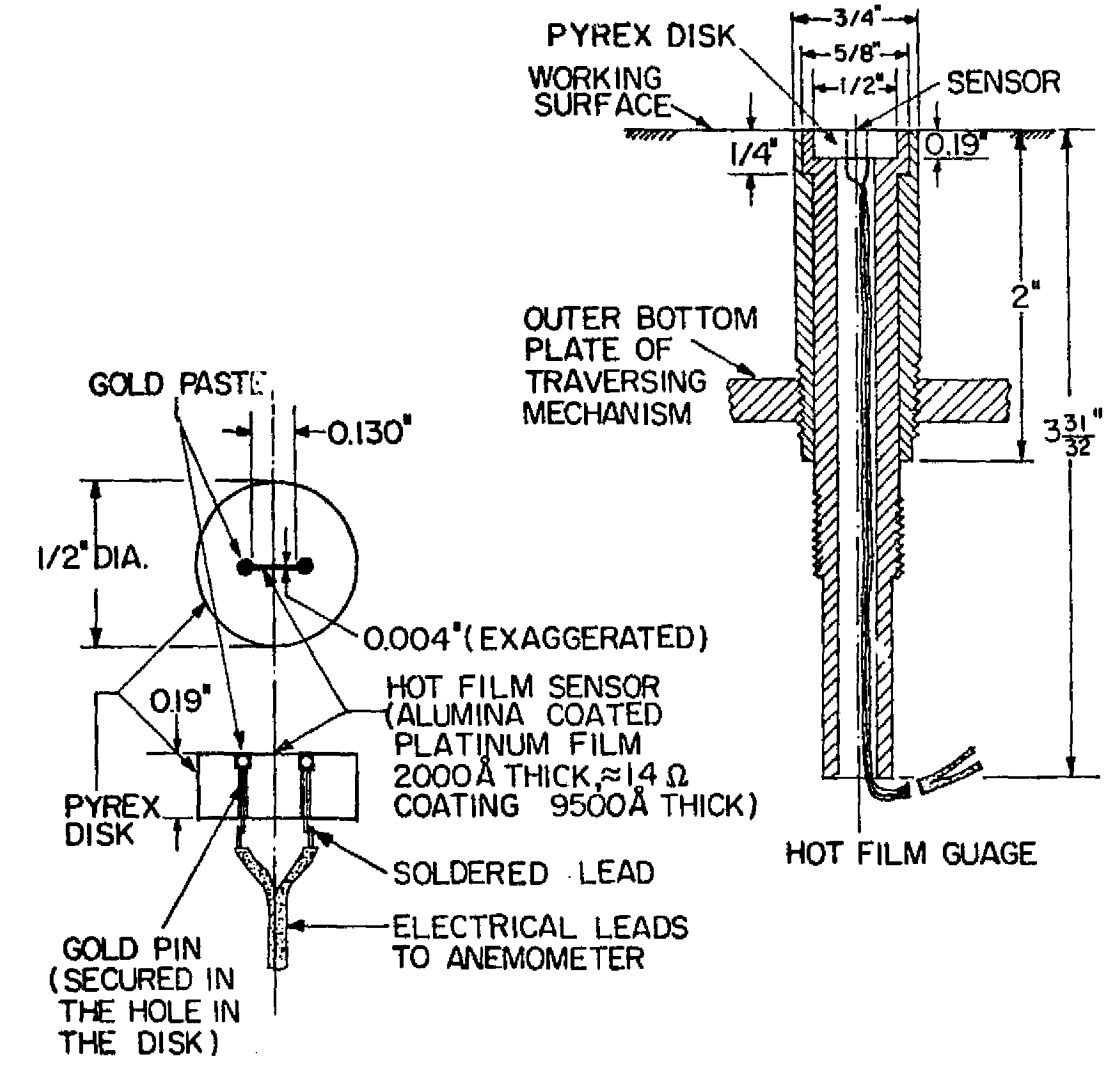

FIG. 7: FLUSH-MOUNTED HOT-FILM GAGE FOR WALL SHEAR STRESS STUDIES

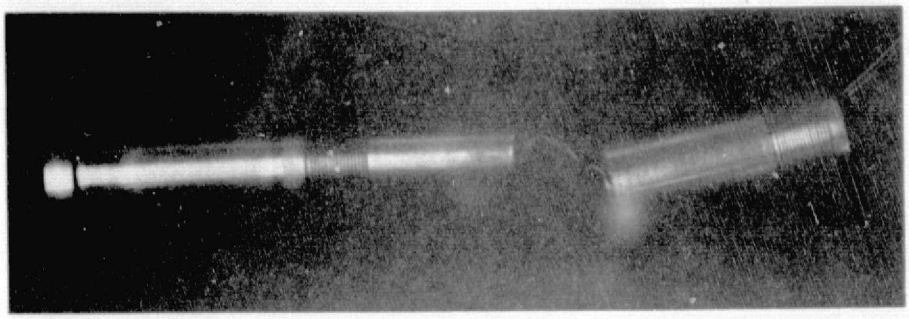

Photograph of the flush-mounted hot-film gage assembly

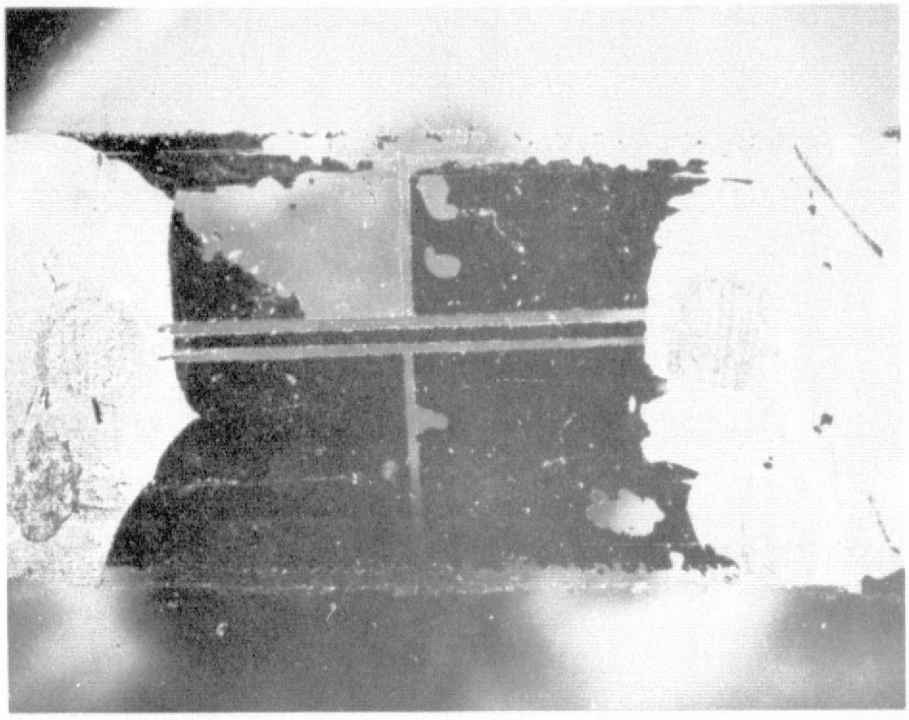

Photomacrograph (19.2 X) of the hot-film sensor (0.004" wide x 0.130" long x 2000°A thick platinum film)

FIG. 7a: PHOTOGRAPH/PHOTOMACROGRAPH OF HOT-FILM GAGE ASSEMBLY/HOT-FILM SENSOR

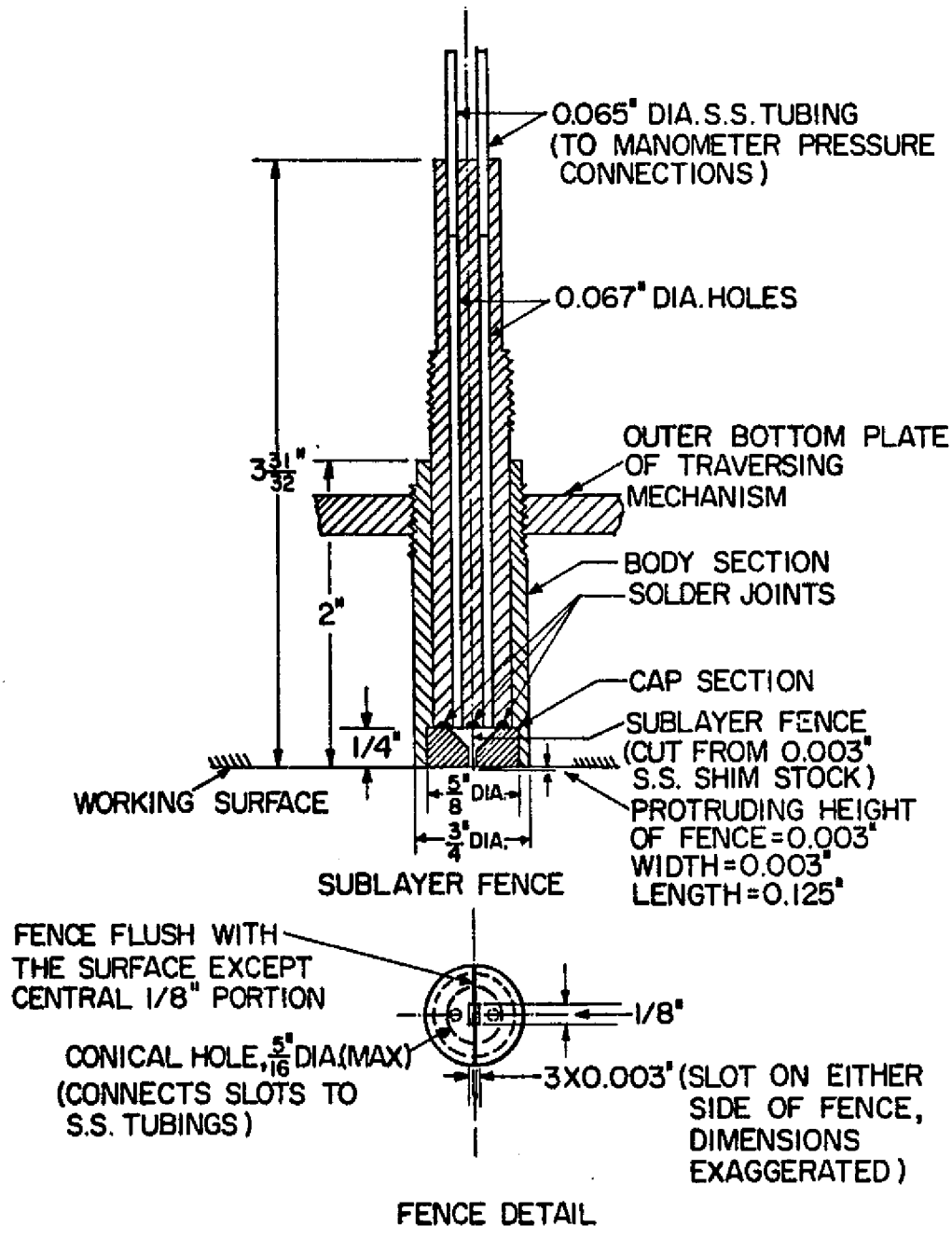

FIG. 8: SUBLAYER FENCE FOR WALL SHEAR STRESS STUDIES

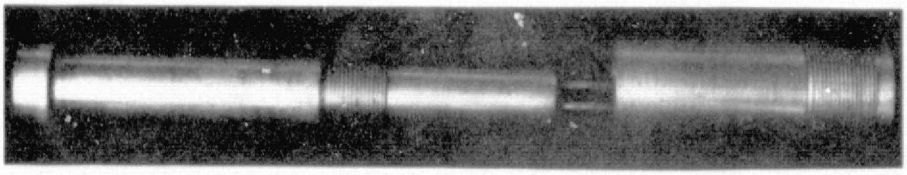

Photograph of the sublayer fence assembly

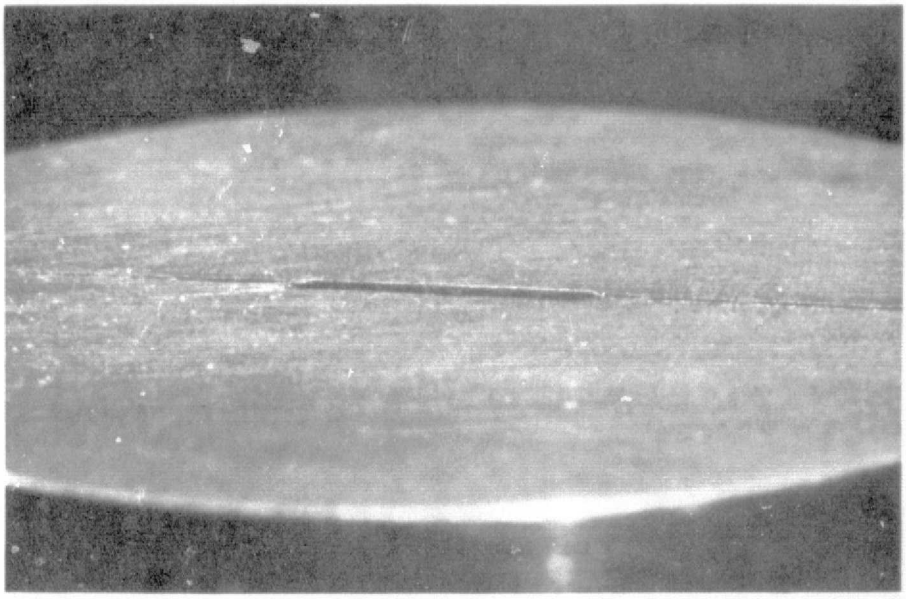

Photomacrograph (13.4 X) of the sublayer fence (fence height = 0.003")

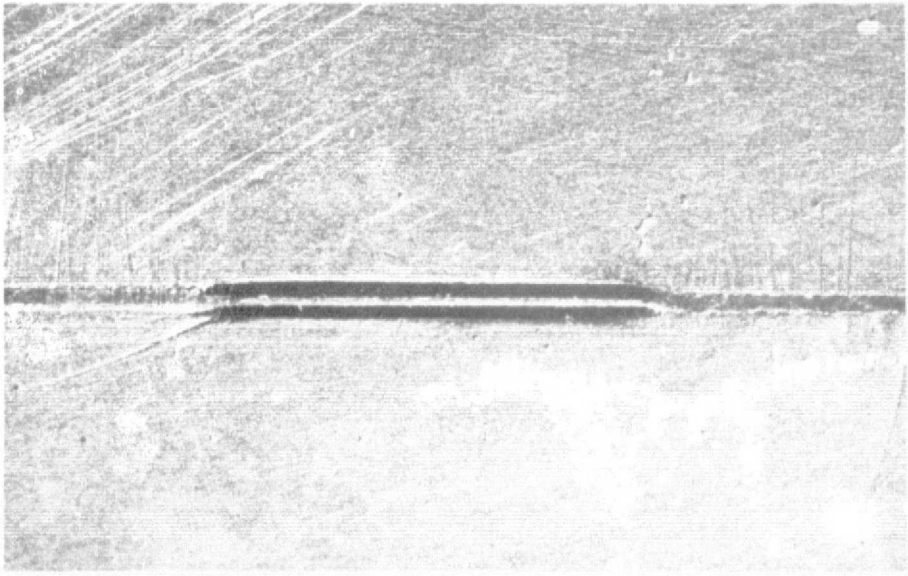

Photomacrograph (16 X) of the fence with 0.003" wide pressure slots on either side of it (fence is 0.003" wide x 0.125" long)

FIG 8a: PHOTOGRAPH/PHOTOMACROGRAPHS OF SUBLAYER FENCE ASSEMBLY/FENCE

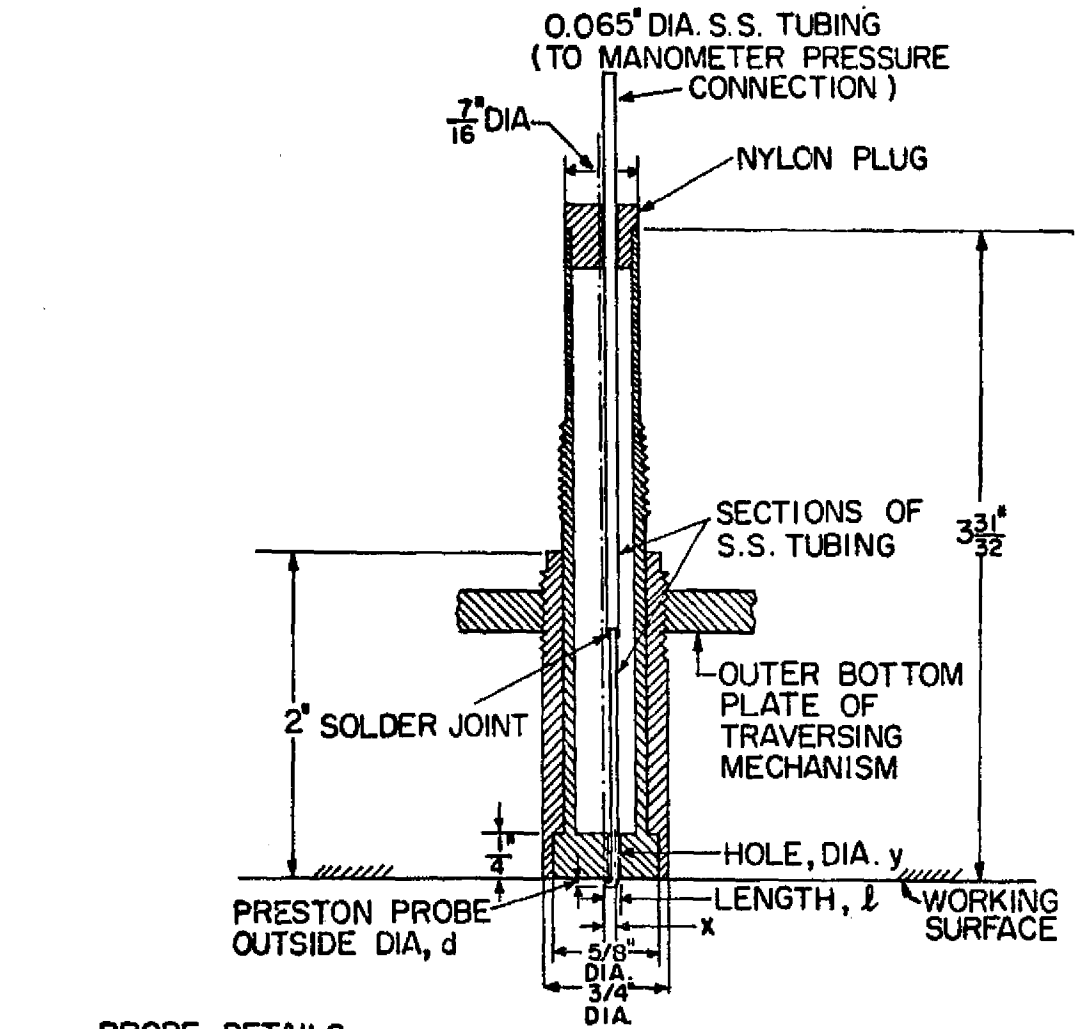

PROBE DETAILS

UNIT	#1	#2
d	0.032"	0.018"
ℓ	0.128"	0.126"
(ℓ/d)	4	7
x	0.112"	0.117"
y	0.046"	0.029"
SECTIONS OF S.S. TUBING USED	(i) 0.032" DIA 1.5" LONG (ii) 0.065" DIA 3.5" LONG	(i) 0.018" DIA 1.125" LONG (ii) 0.032" DIA 11/32" LONG (iii) 0.065" DIA 3 3/16" LONG

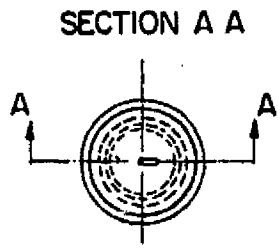

FIG. 9: PRESTON PROBES FOR WALL SHEAR STRESS STUDIES

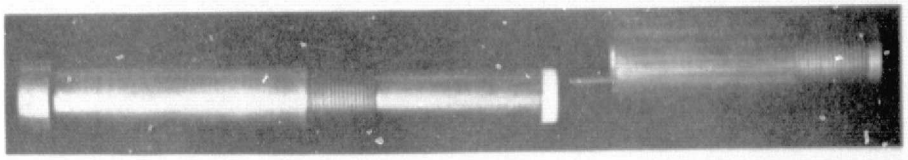

Photograph of the 0.032" dia Preston probe assembly

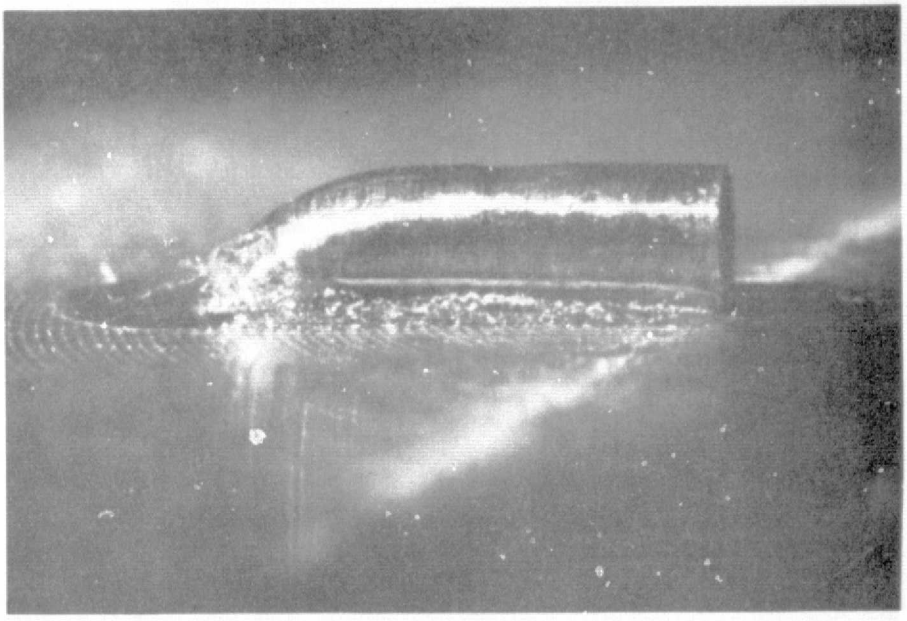

Photomacrograph (24 X) of the 0.032" dia Preston probe

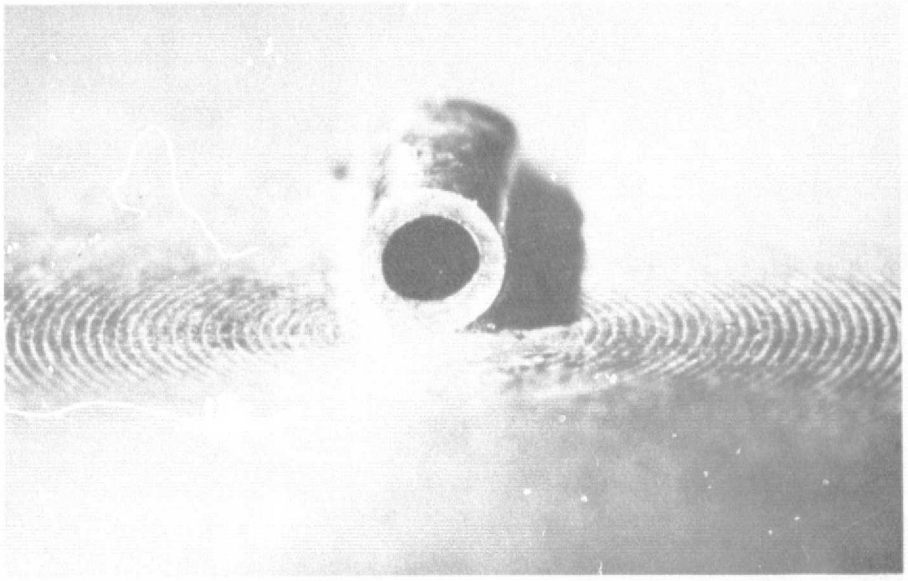

Photomacrograph (24 X) of the tip of the 0.032" dia Preston probe

FIG. 9a: PHOTOGRAPH/PHOTOMACROGRAPHS OF THE PRESTON PROBE ASSEMBLIES /PROBE TIPS

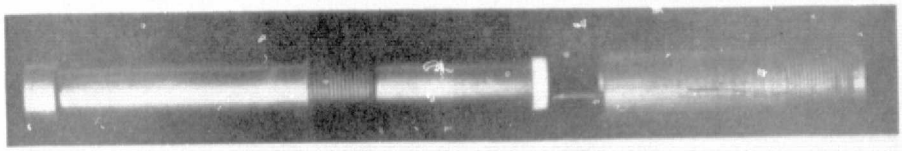

Photograph of the 0.018" dia Preston probe assembly

Photomacrograph (24 X) of the 0.018" dia Preston probe

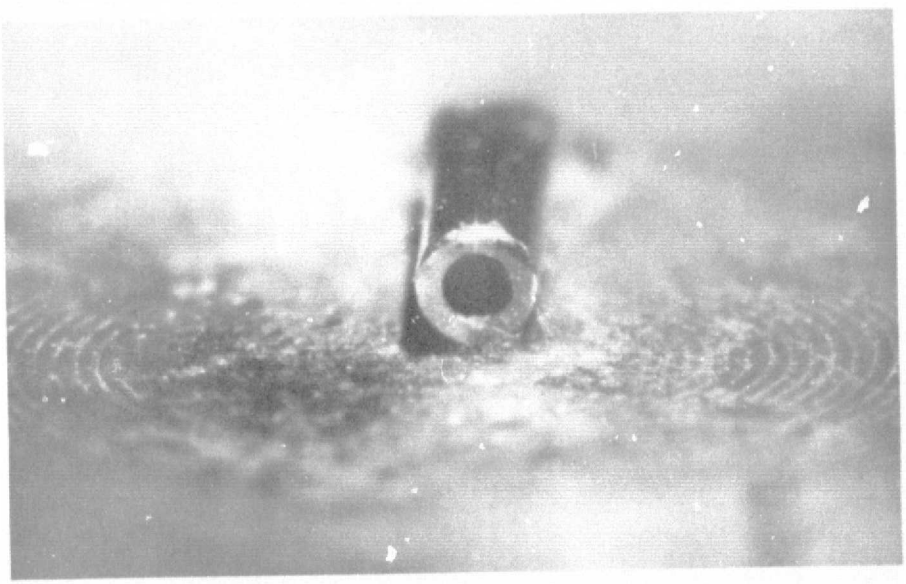

Photomacrograph (36.3 X) of the tip of the 0.018" dia Preston probe

FIG. 9a: CONCLUDED

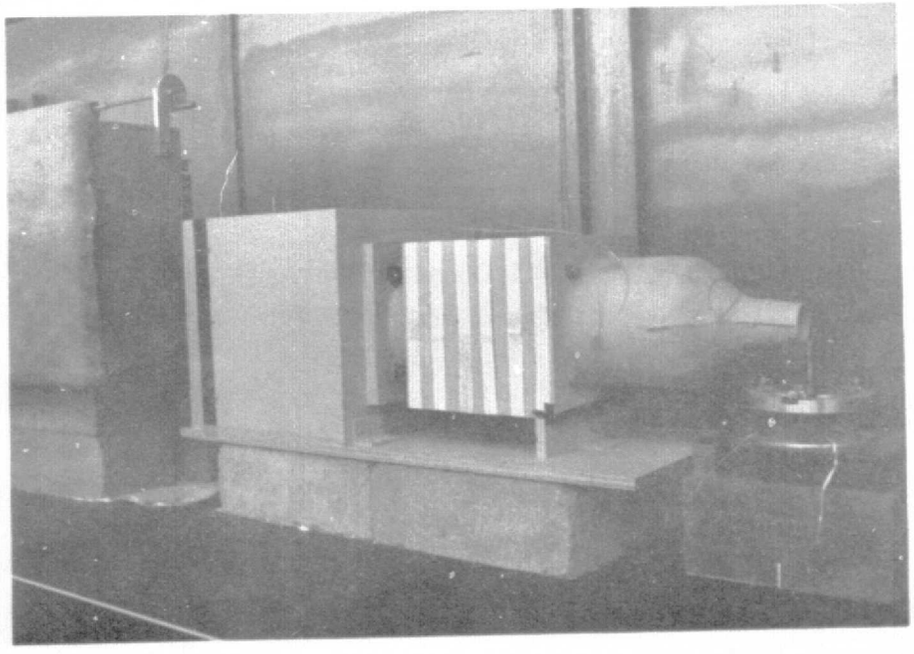

FIG. 10: PHOTOGRAPH OF THE FREE JET FACILITY WITH HOT WIRE MOUNTED FOR CALIBRATION

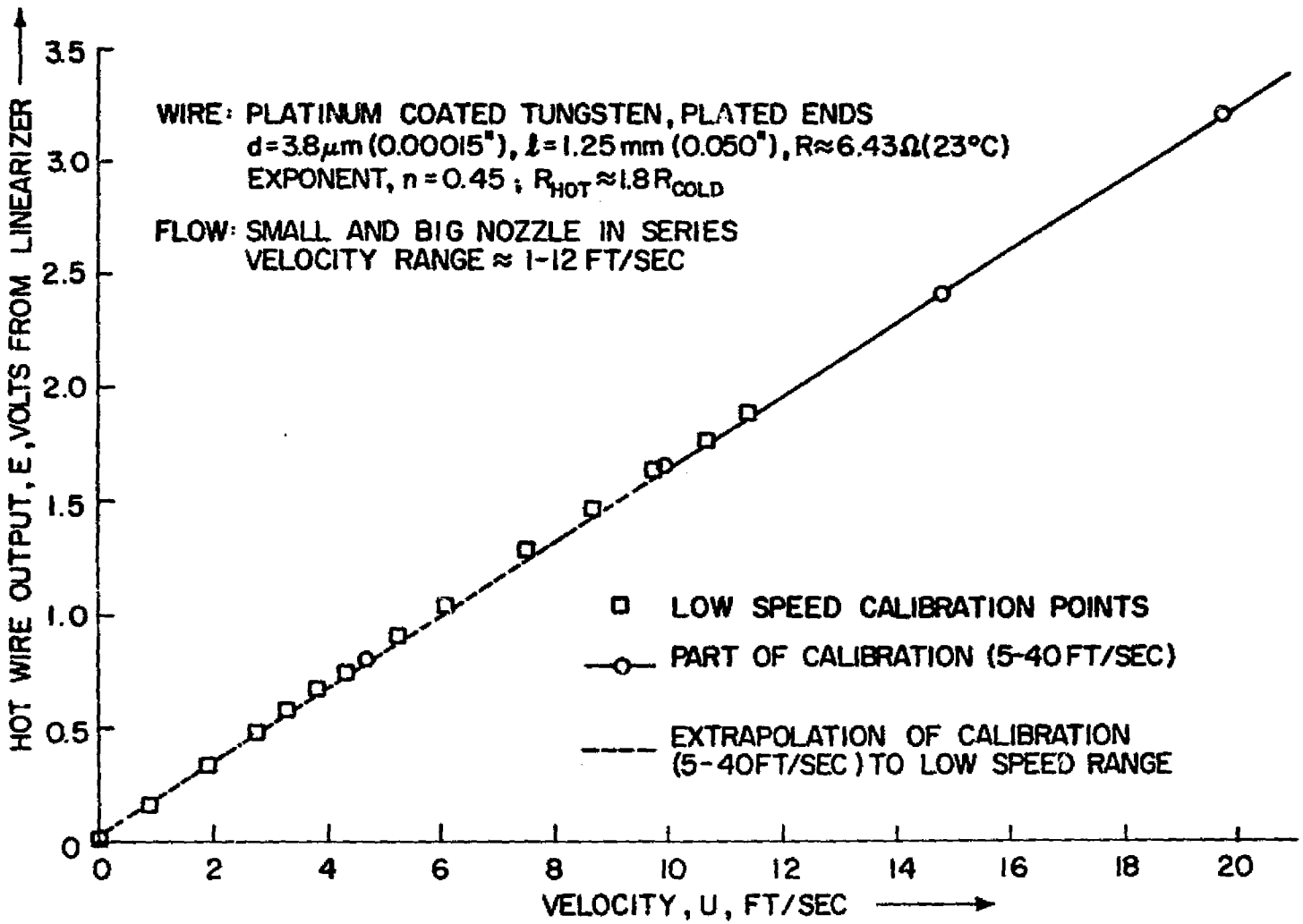

FIG. 11 : LOW SPEED CALIBRATION OF HOT WIRE IN THE FREE JET FACILITY (1-12 FT/SEC)

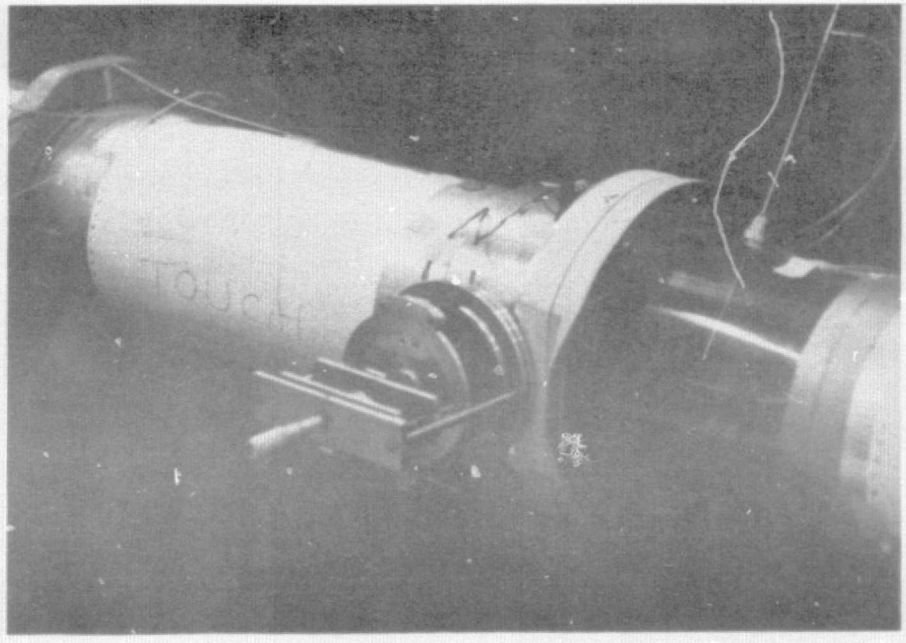

FIG. 12: PHOTOGRAPH OF A PORTION OF THE PIPE FLOW FACILITY SHOWING THE TRAVERSE MECHANISM MOUNTED AT THE TEST SECTION

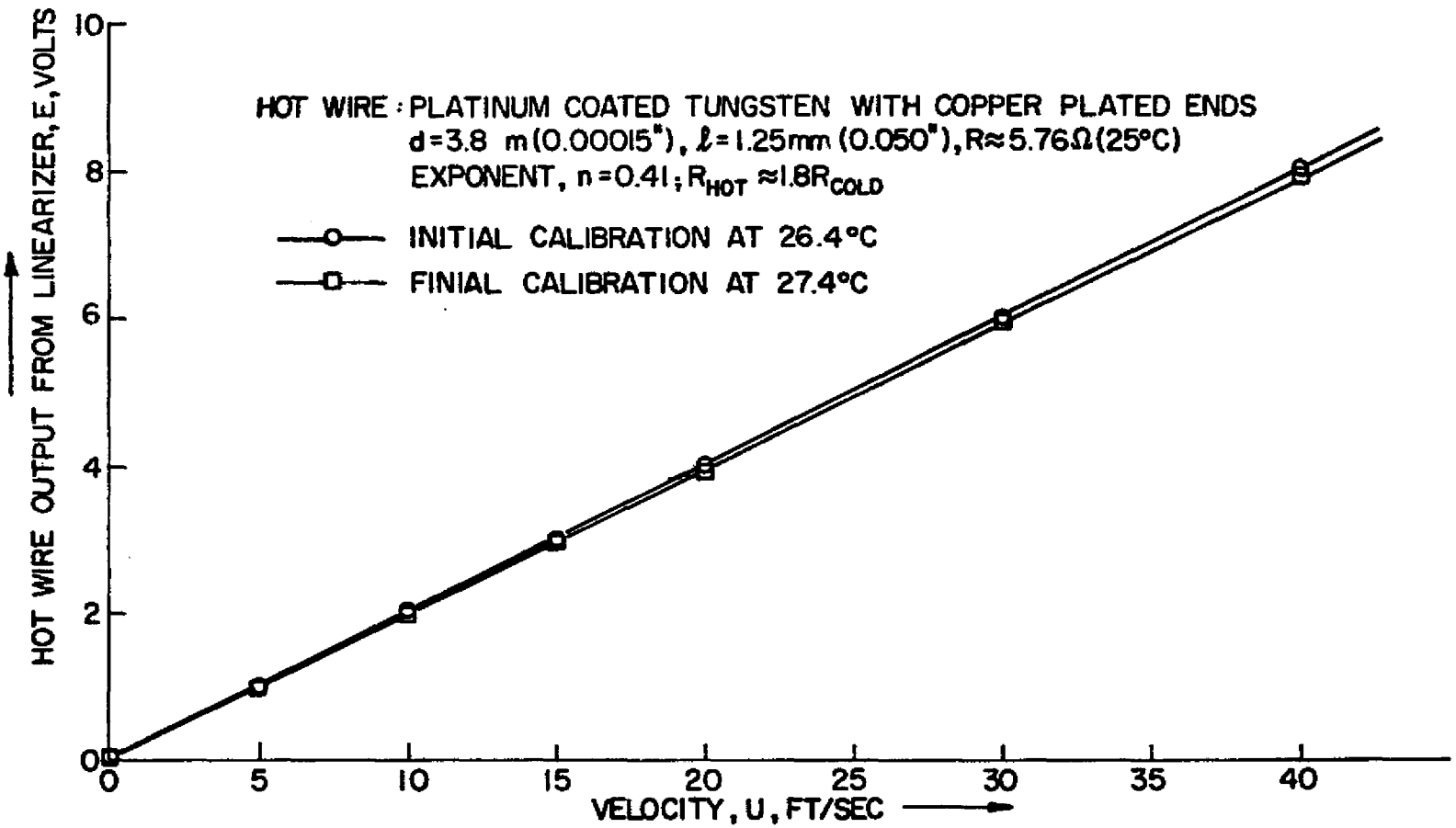

FIG. 13 : TYPICAL CALIBRATION CURVES FOR THE HOT WIRE PROBE WITH TSI 3.8 μm TUNGSTEN SENSOR (TIME ELASPED BETWEEN CALIBRATIONS DURING A 3-DIMENSIONAL BOUNDARY LAYER SURVEY = 11 HOURS)

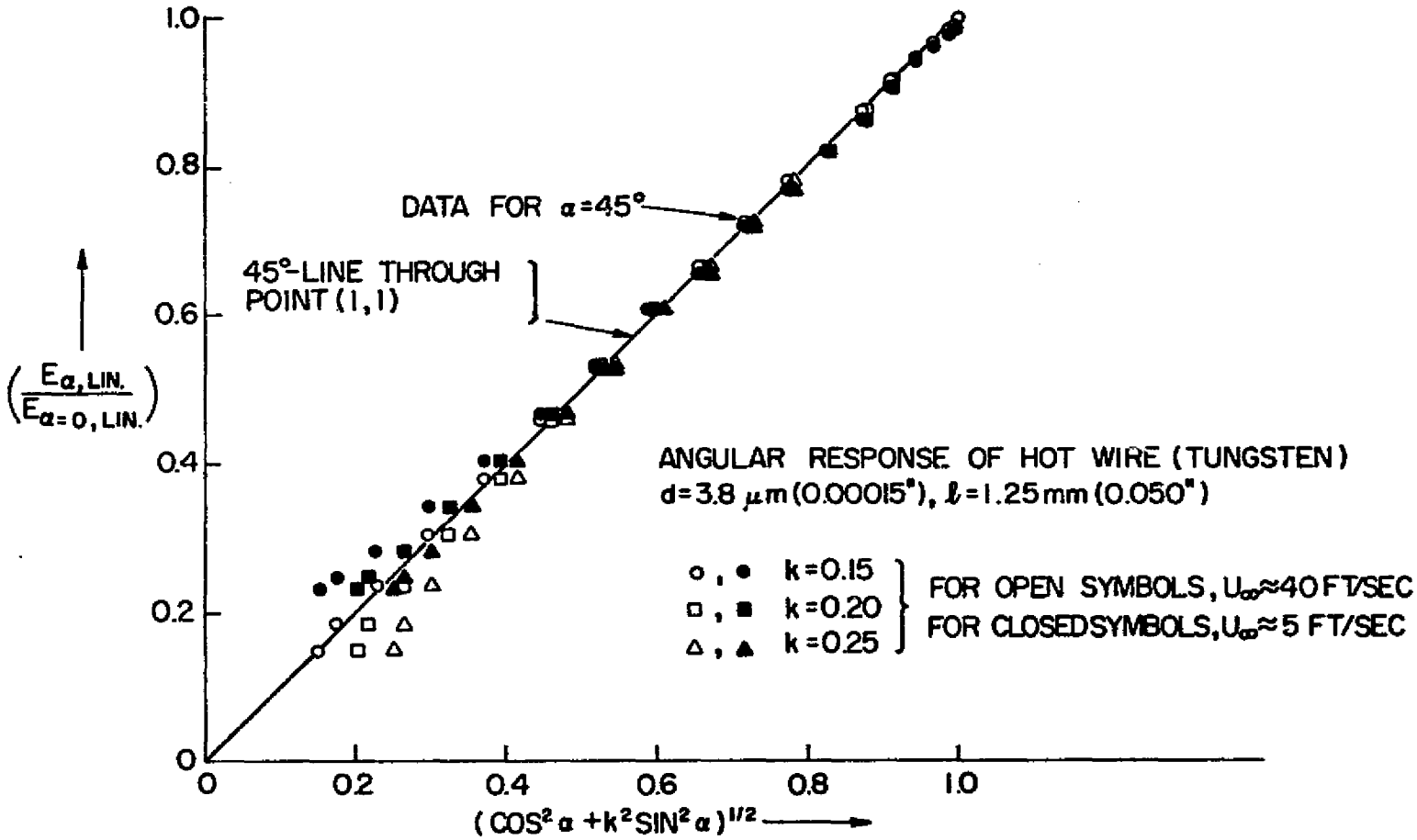

FIG. 14 : DETERMINATION OF K-FACTOR FOR HOW WIRE PROBE

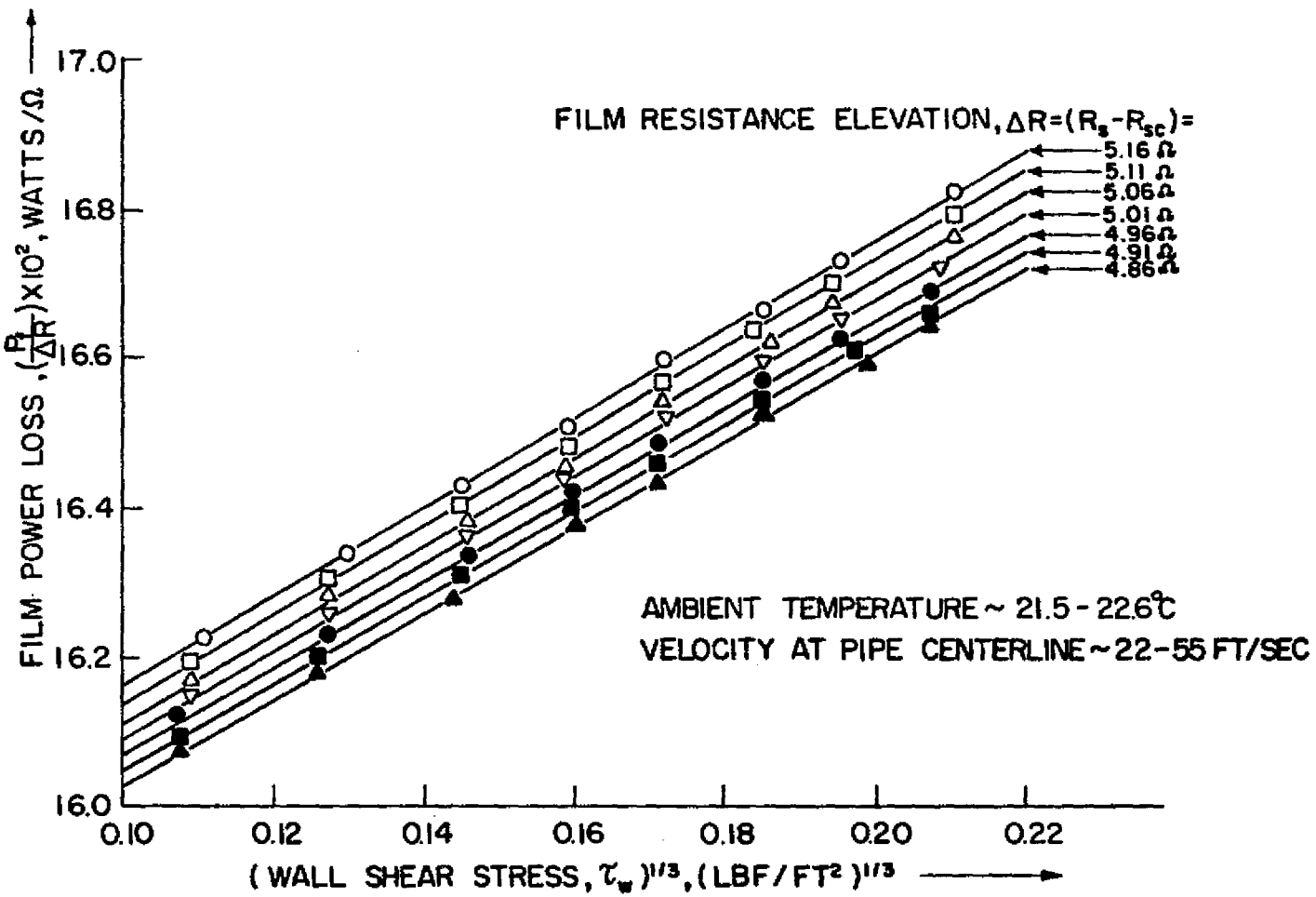

FIG. 15 : EXPERIMENTAL CALIBRATION CHARTS FOR FLUSH-MOUNTED HOT-FILM GAGE (CALIBRATION #1)

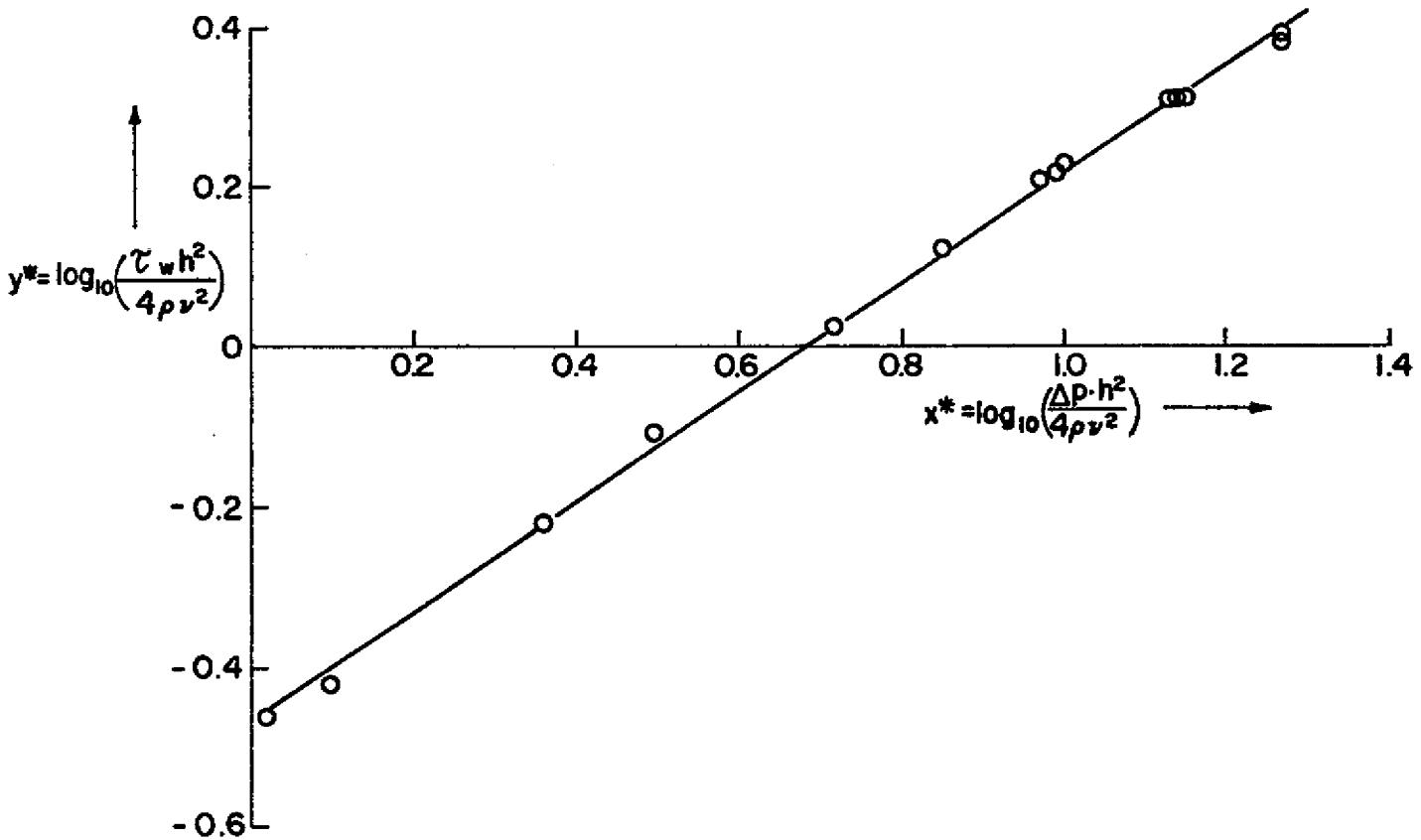

FIG. 16: EXPERIMENTAL CALIBRATION CURVE FOR SUBLAYER FENCE

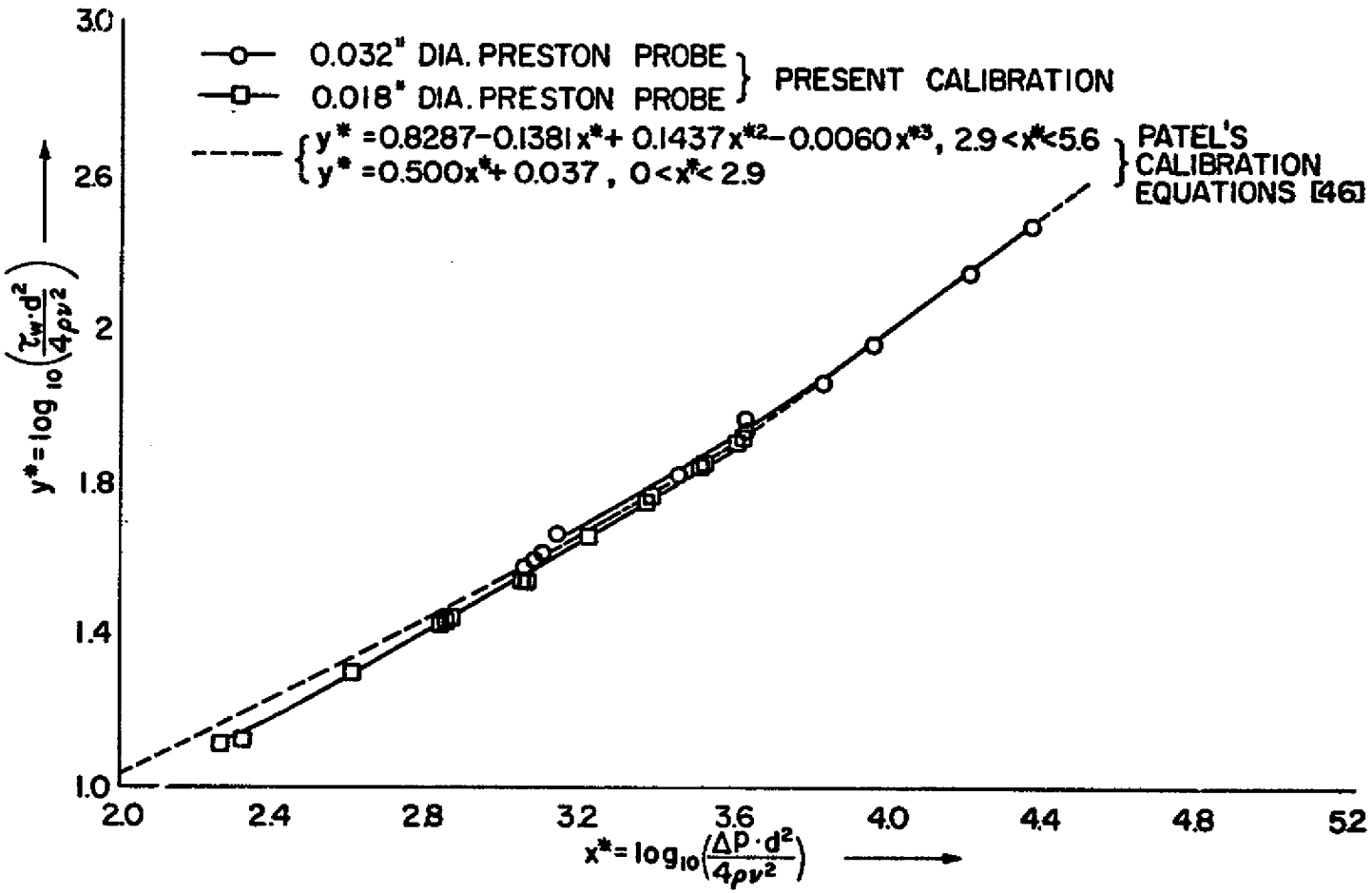

FIG. 17: EXPERIMENTAL CALIBRATION CURVES FOR PRESTON PROBES

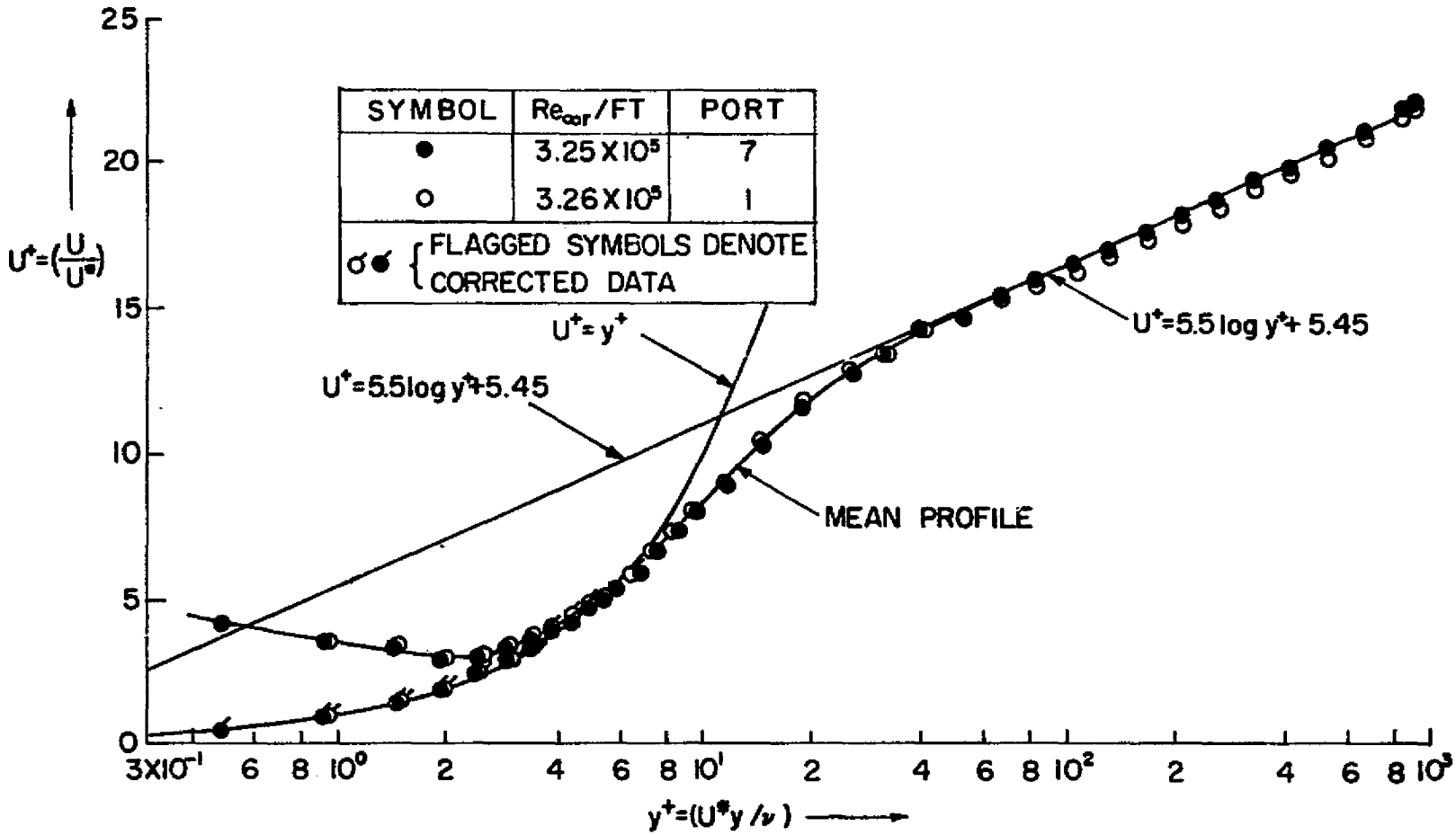

FIG. 18: TWO-DIMENSIONAL MEAN VELOCITY PROFILES IN WALL COORDINATES

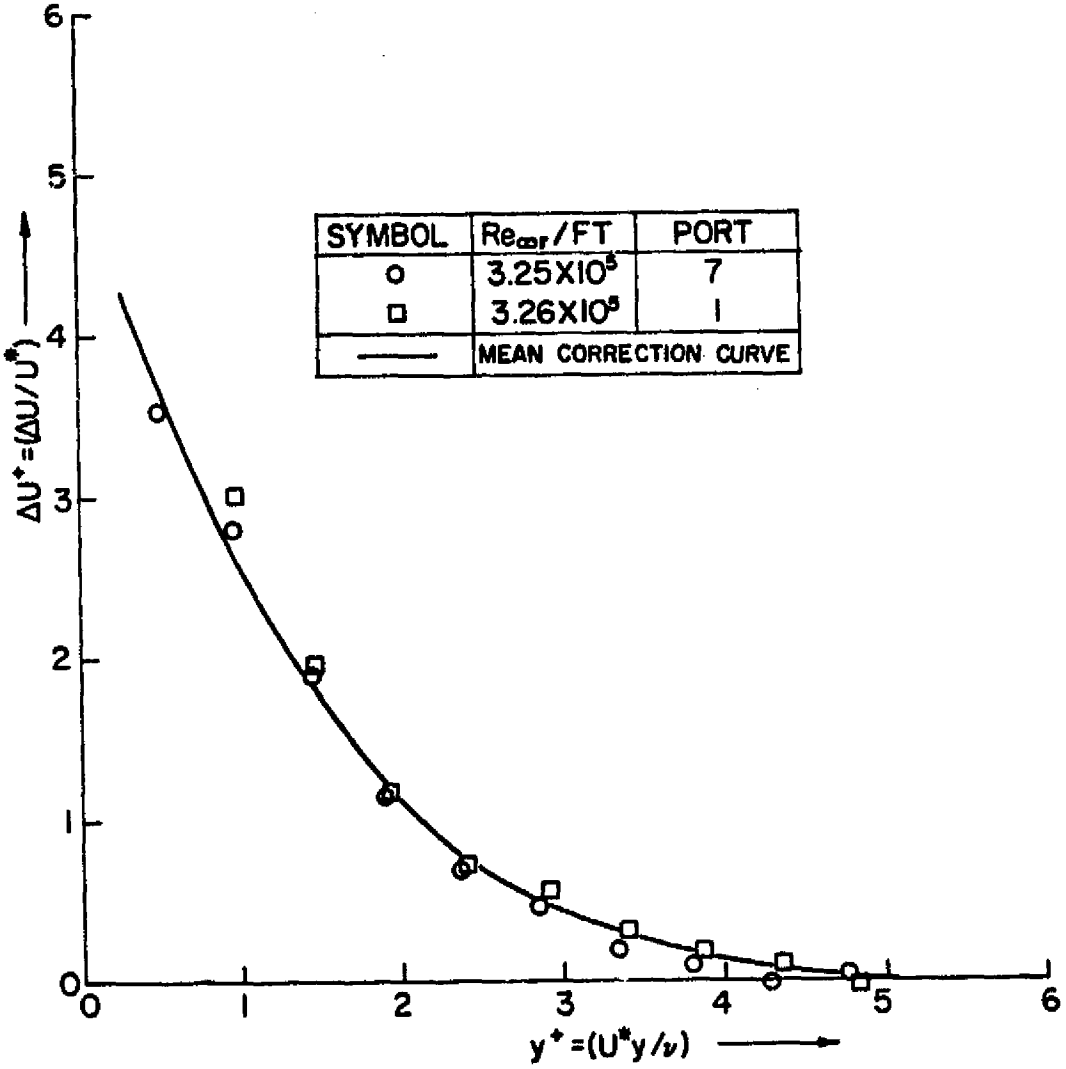

FIG. 19: DIMENSIONLESS DIFFERENCE BETWEEN APPARENT AND TRUE VELOCITY CLOSE TO THE WALL IN 2-DIMENSIONAL TURBULENT BOUNDARY LAYER (WALL PROXIMITY CORRECTION CURVE); NOMINAL $Re_{\infty r}$ = 3.25 x 10^5/foot

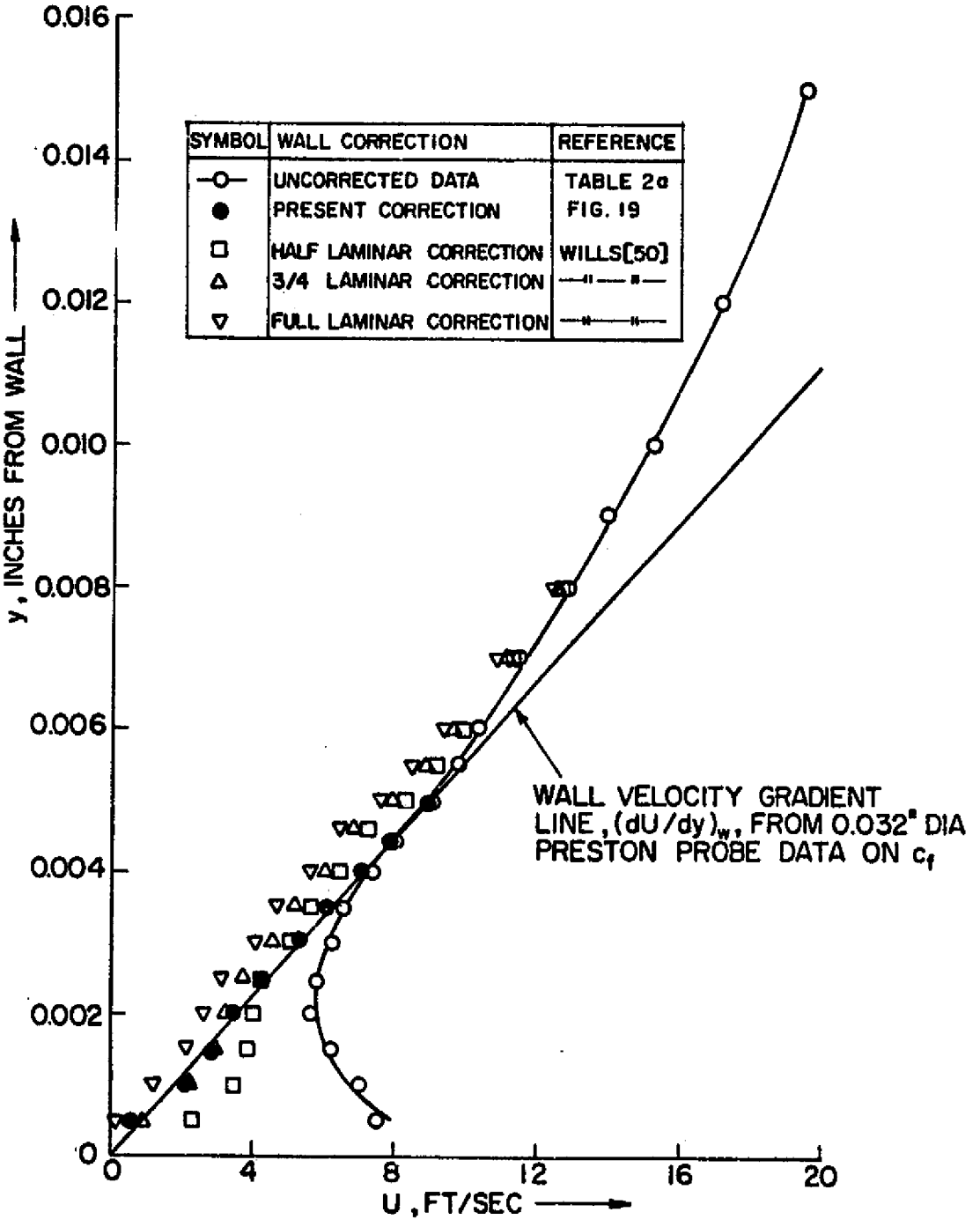

FIG. 20 : MEAN VELOCITY PROFILE CLOSE TO THE WALL (2-DIMENSIONAL BOUNDARY LAYER, PORT 7, $Re_{\infty r} = 3.25 \times 10^5$/foot)

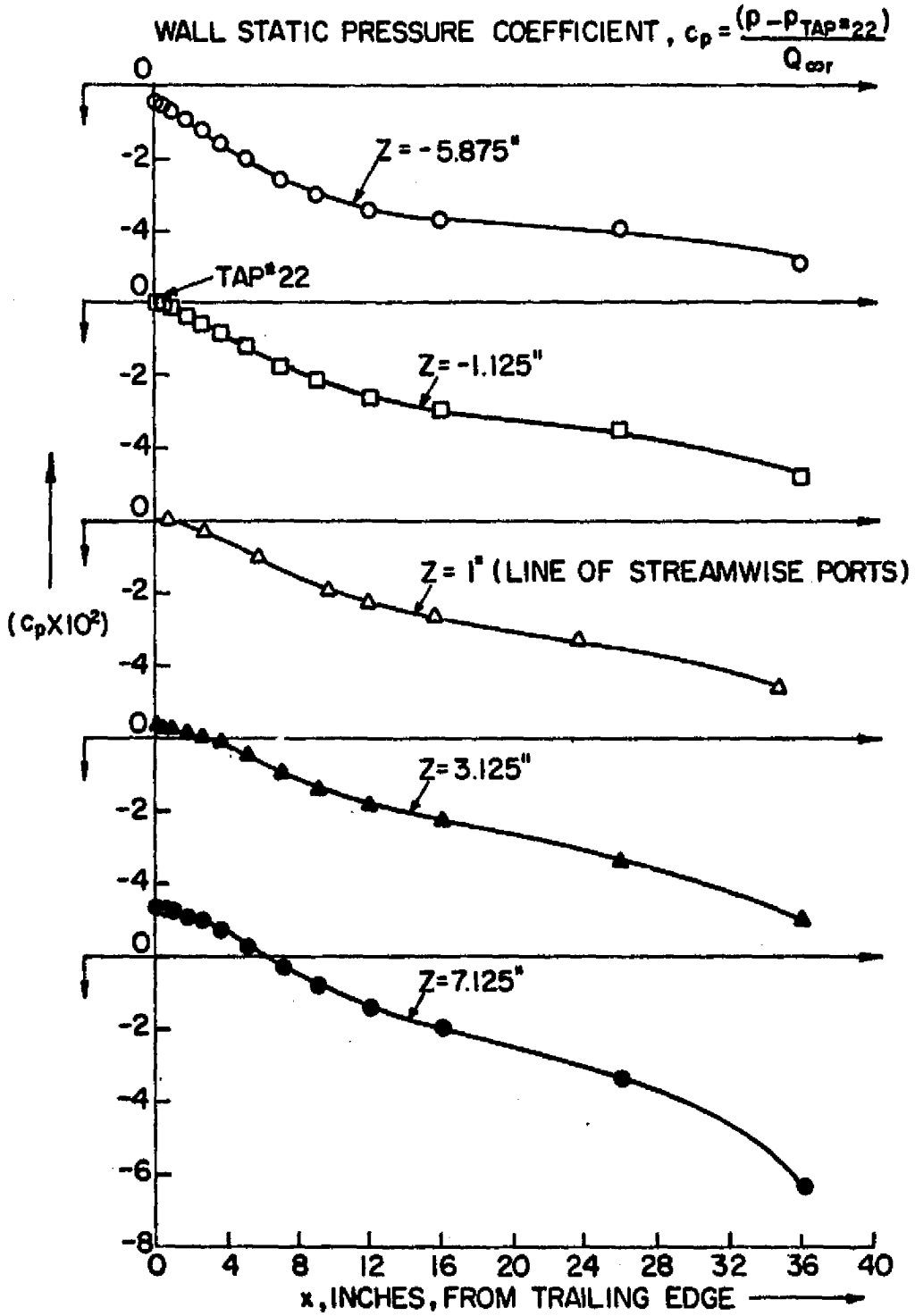

FIG 21: STREAMWISE WALL STATIC PRESSURE DISTRIBUTION IN THE RELAXING REGION ($Re_{\infty r}$: 3.25 x 10^5 to 3.29 x 10^5/foot)

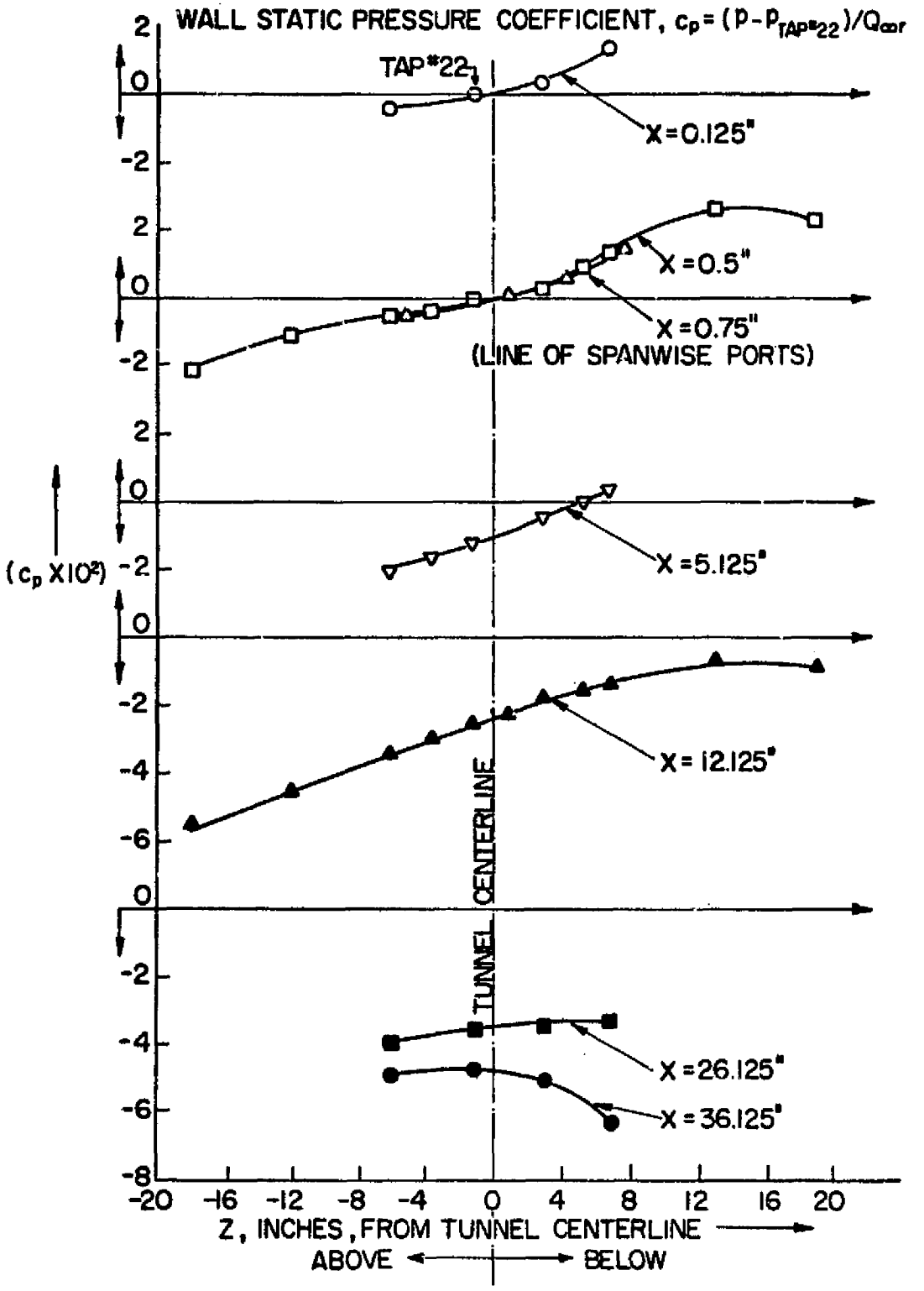

FIG 21a: SPANWISE WALL STATIC PRESSURE DISTRIBUTION IN THE RELAXING REGION ($R_{\infty r}$: 3.25 x 10^5 to 3.29 x 10^5/foot)

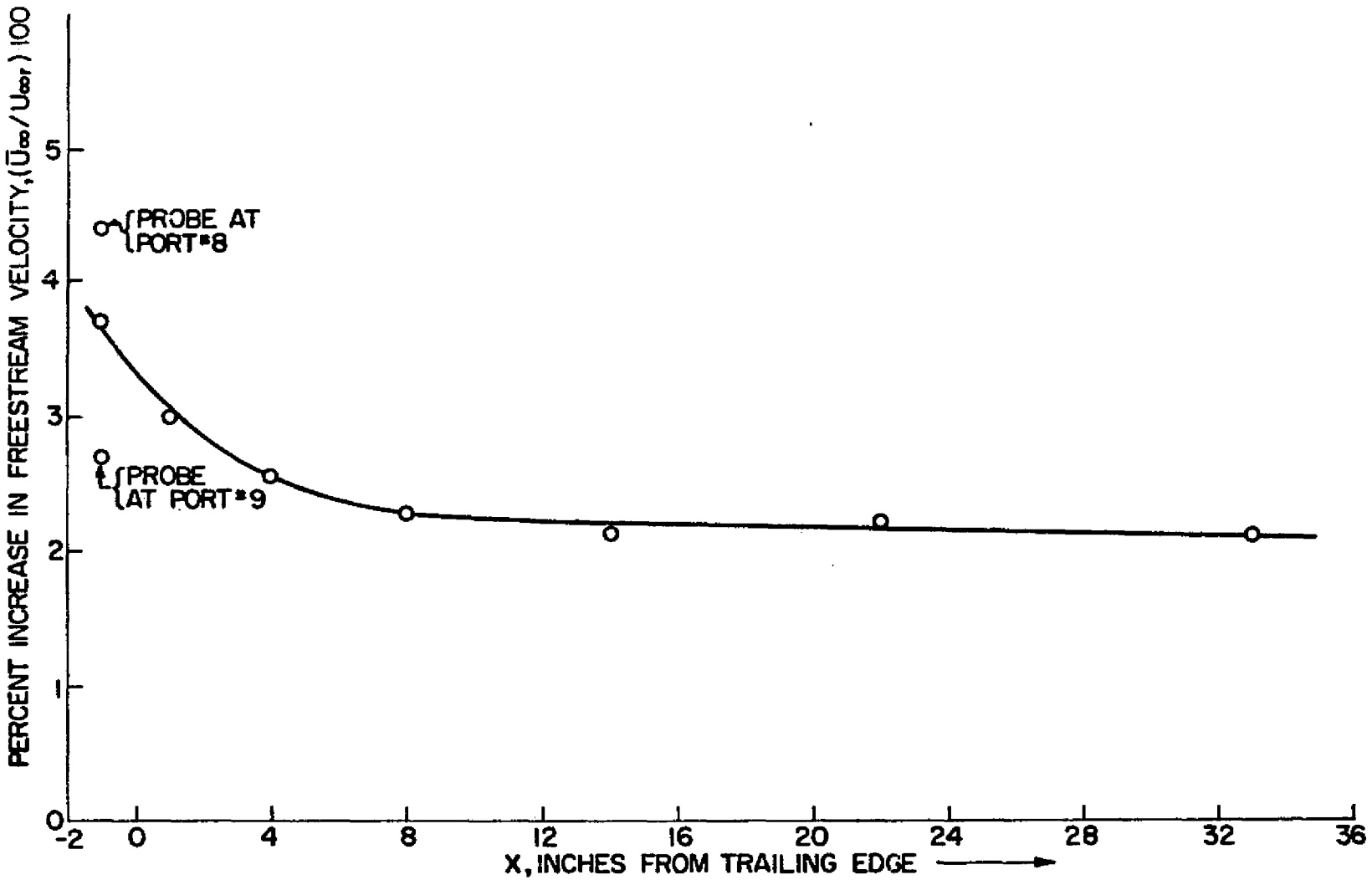

FIG. 22: VARIATION OF FREESTREAM VELOCITY IN THE RELAXING REGION; NOMINAL $Re_{\infty r}$ = 3.25 x 10^5/foot

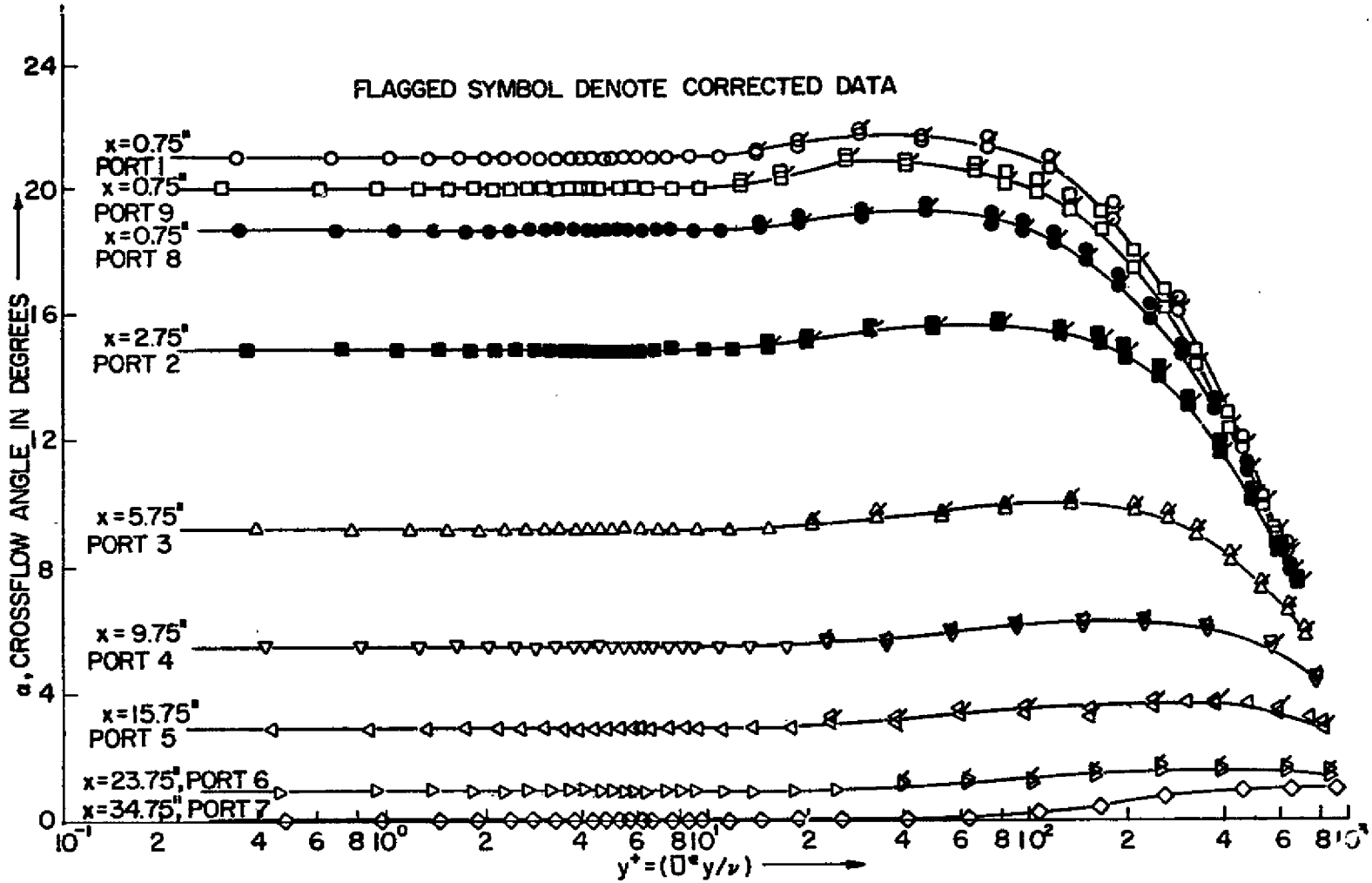

FIG. 23: MEAN DIRECTION PROFILES (CROSSFLOW ANGLES) REFERRED TO THE WALL COORDINATE Y^+; NOMINAL $Re_{\infty r} = 3.25 \times 10^5$/foot

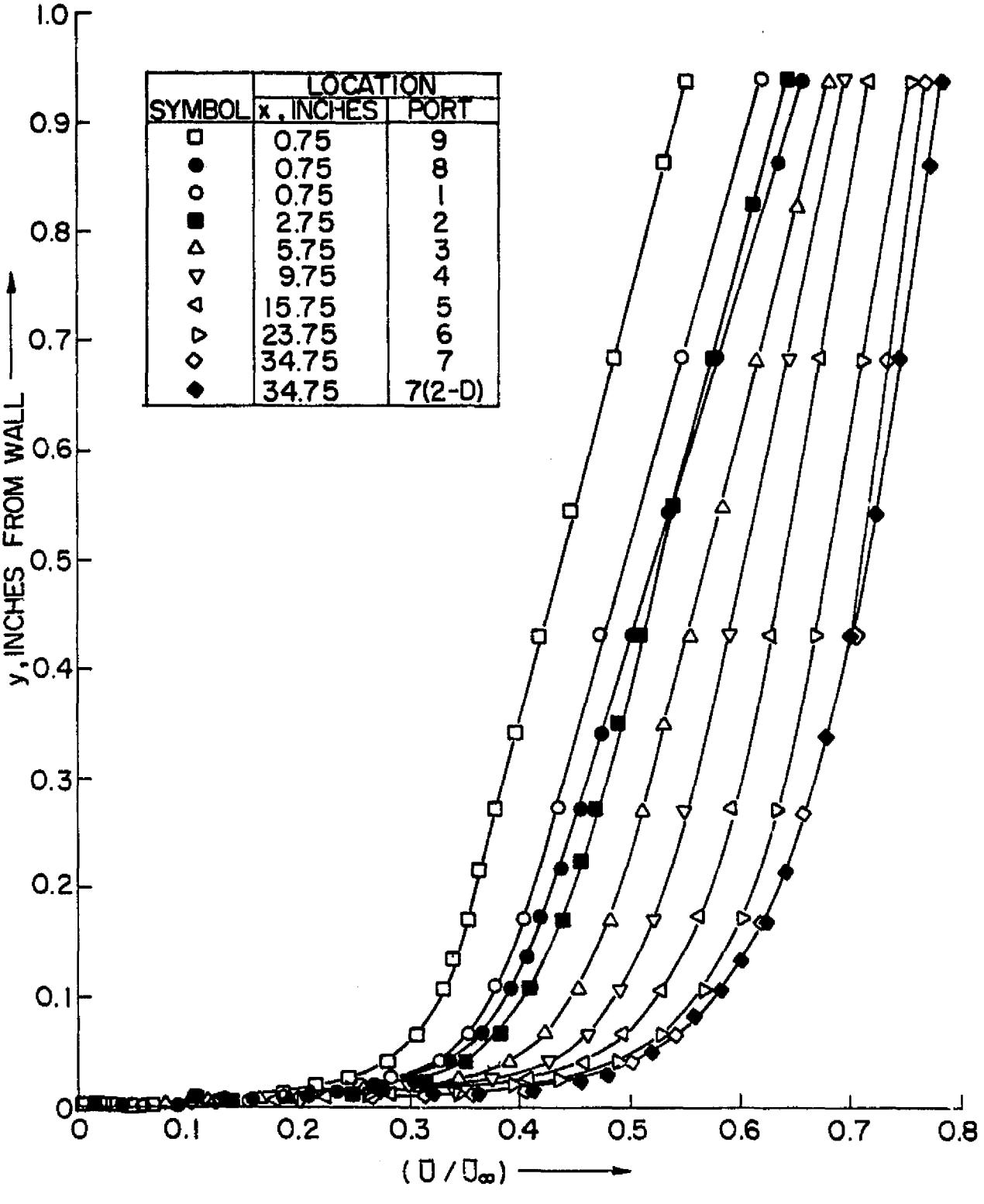

FIG. 24: RESULTANT MEAN VELOCITY PROFILES IN THE INNER LAYER OF THE RELAXING BOUNDARY LAYER; NOMINAL $Re_{\infty r}$ = 3.25 x 10^5/foot

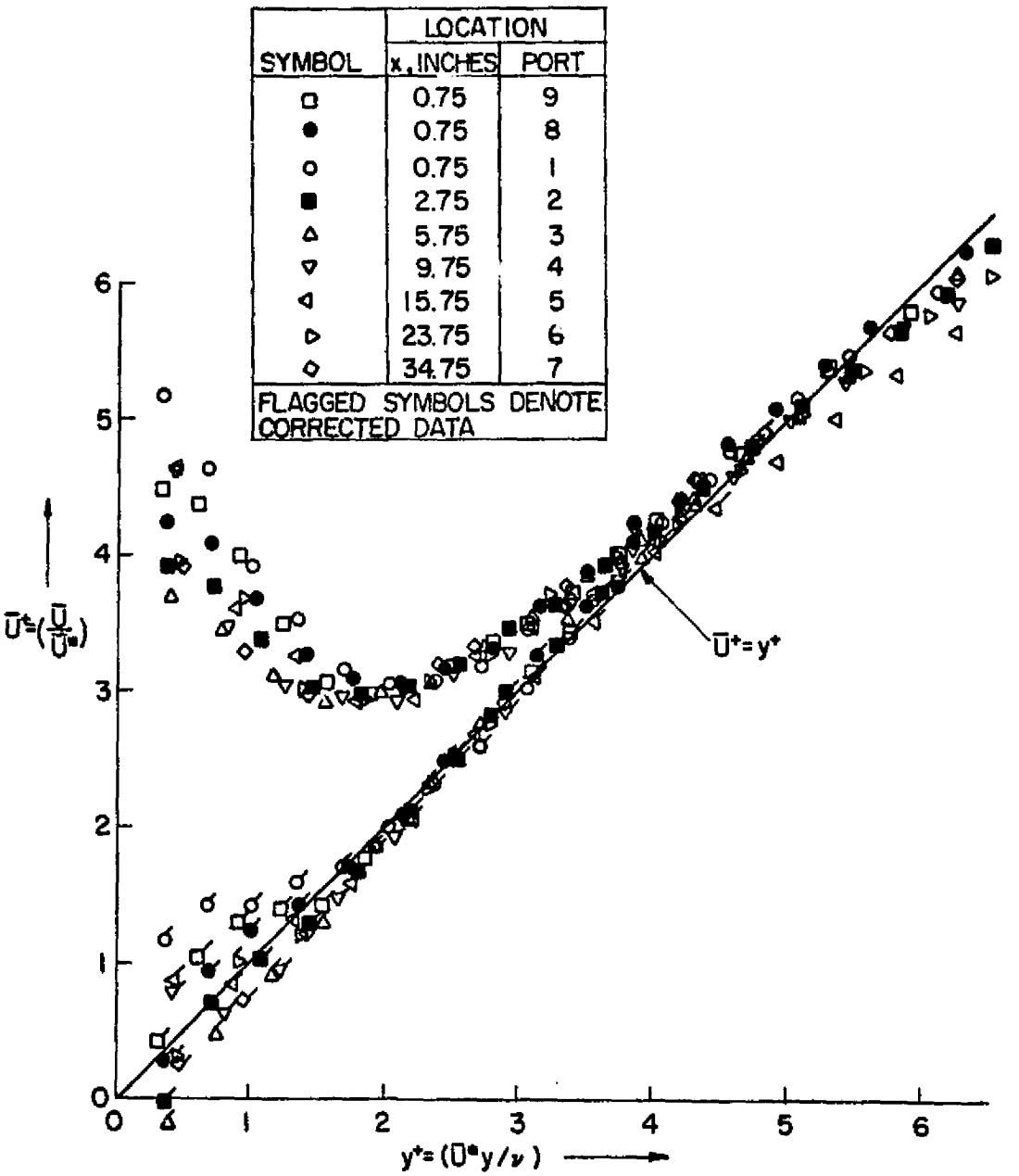

FIG. 25 : RESULTANT MEAN VELOCITY PROFILES CLOSE TO THE WALL IN THE WALL COORDINATES; NOMINAL $Re_{\infty r}$ = 3.25 x 10^5/foot

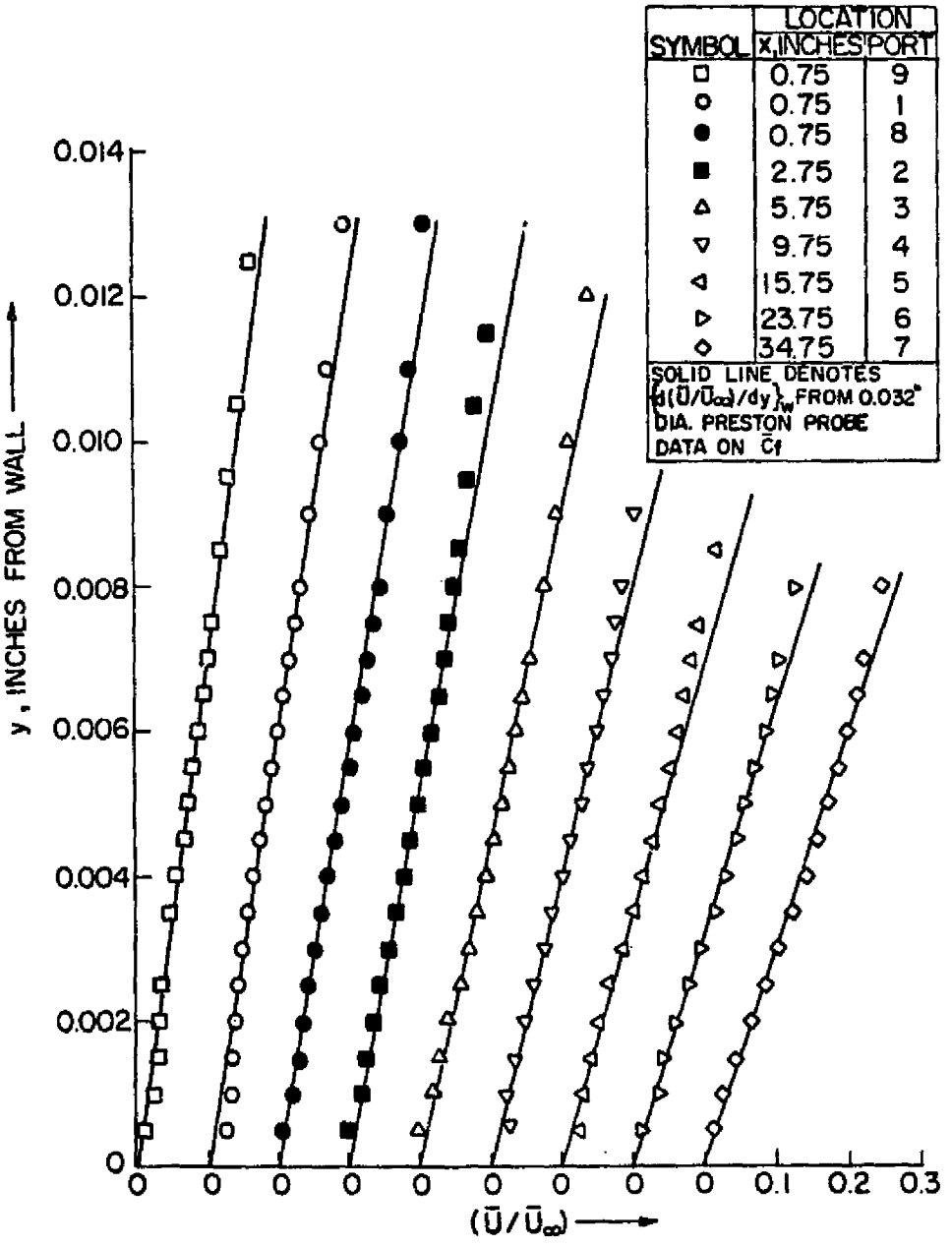

FIG. 26: CORRECTED MEAN VELOCITY PROFILES CLOSE TO THE WALL; NOMINAL $Re_{\infty r} = 3.25 \times 10^5$/foot

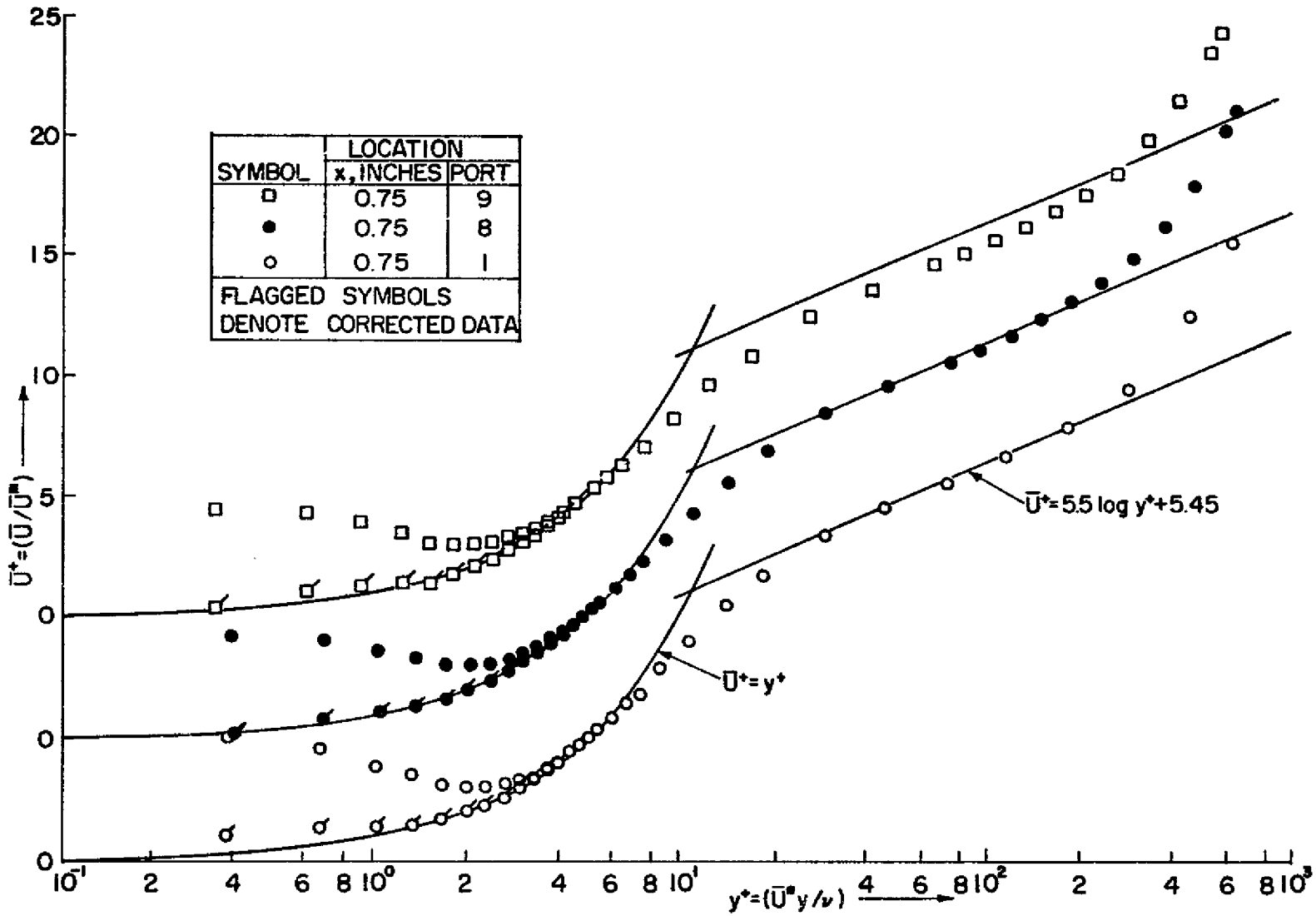

FIG. 27: LAW OF THE WALL PLOTS FOR THE RELAXING BOUNDARY LAYER (PORTS 1, 8 AND 9): NOMINAL $Re_{\infty r} = 3.25 \times 10^5$/foot

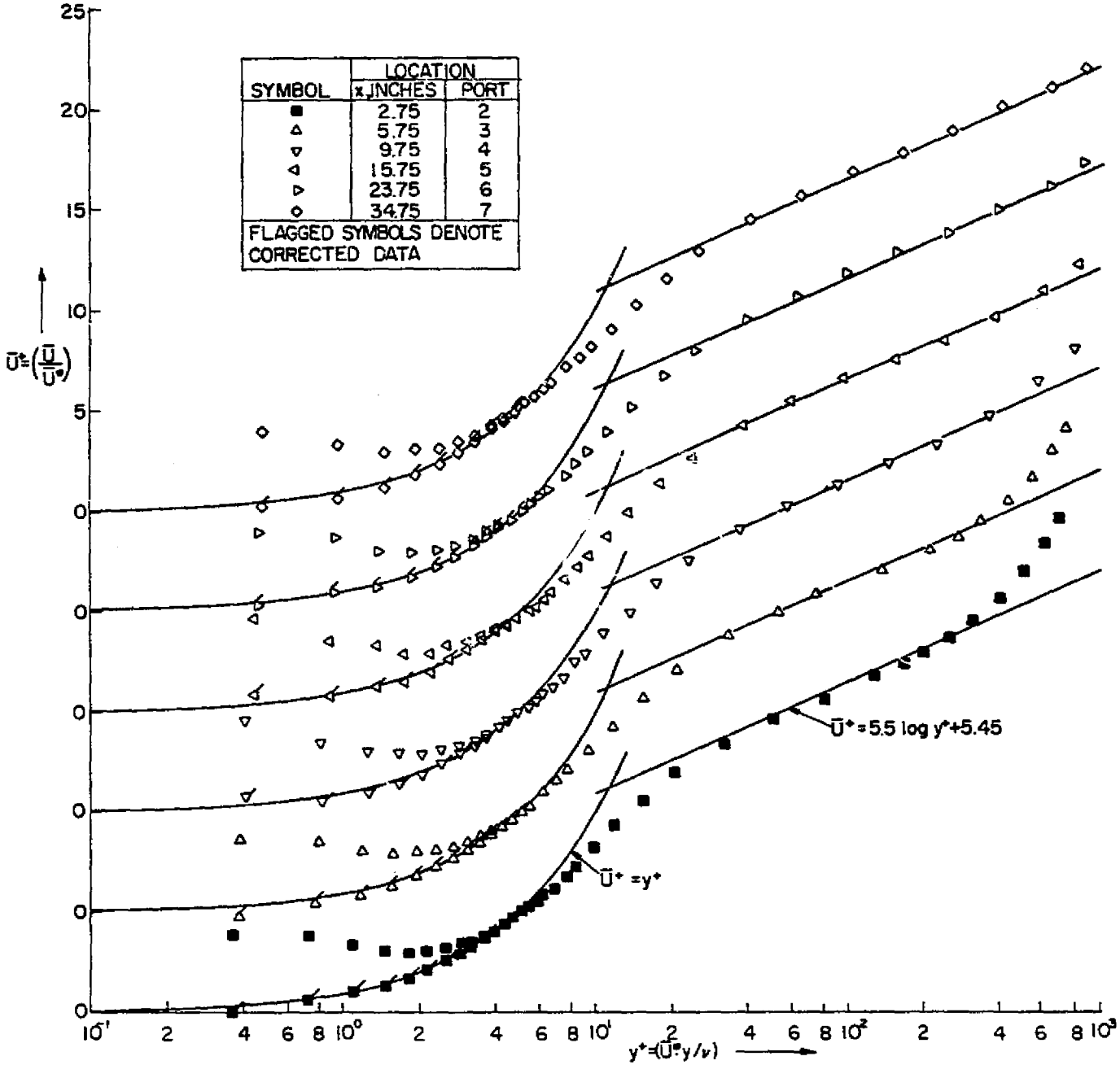

FIG. 27a: LAW OF THE WALL PLOTS FOR THE RELAXING BOUNDARY LAYER (PORTS 2-7): NOMINAL $Re_{\infty r}$ = 3.25 x 10^5/foot

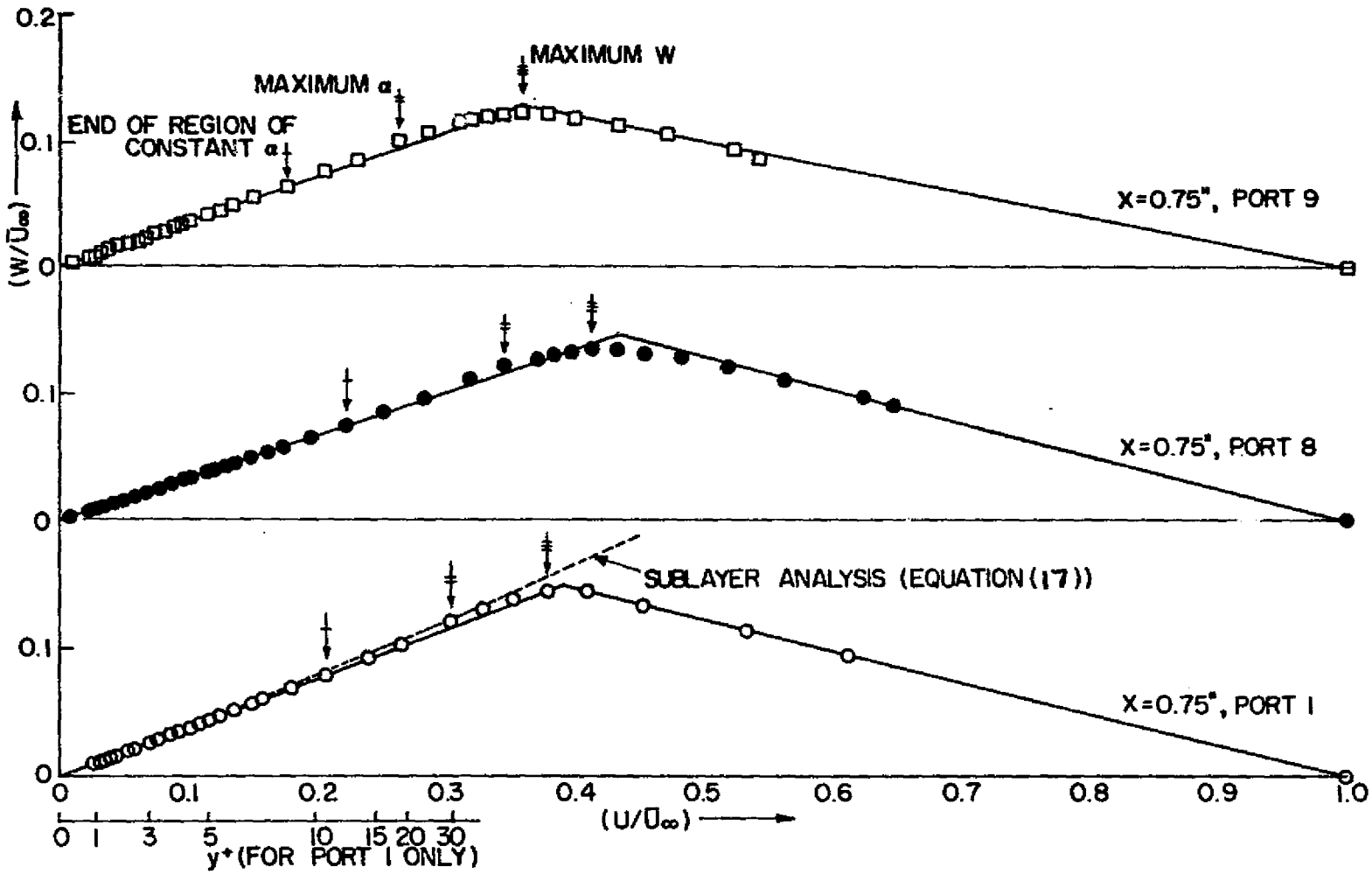

FIG. 28: POLAR PLOTS OF MEAN VELOCITY PROFILE (PORTS 1, 8 AND 9), NOMINAL $Re_{\infty r} = 3.25 \times 10^5$/foot

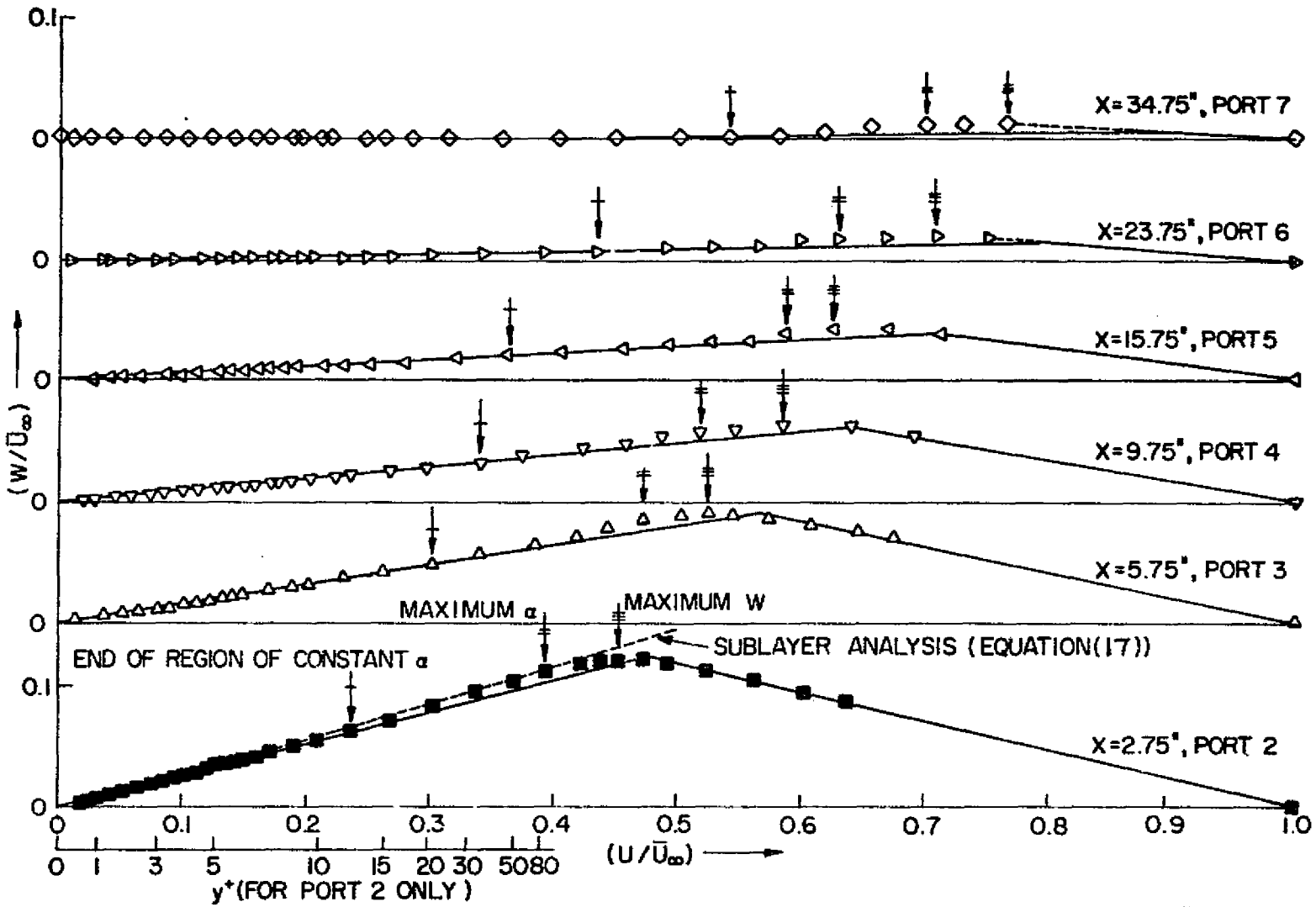

FIG. 28a : POLAR PLOTS OF MEAN VELOCITY PROFILE (PORTS 2-7); NOMINAL $Re_{\infty r}$ = 3.25 x 10^5/foot

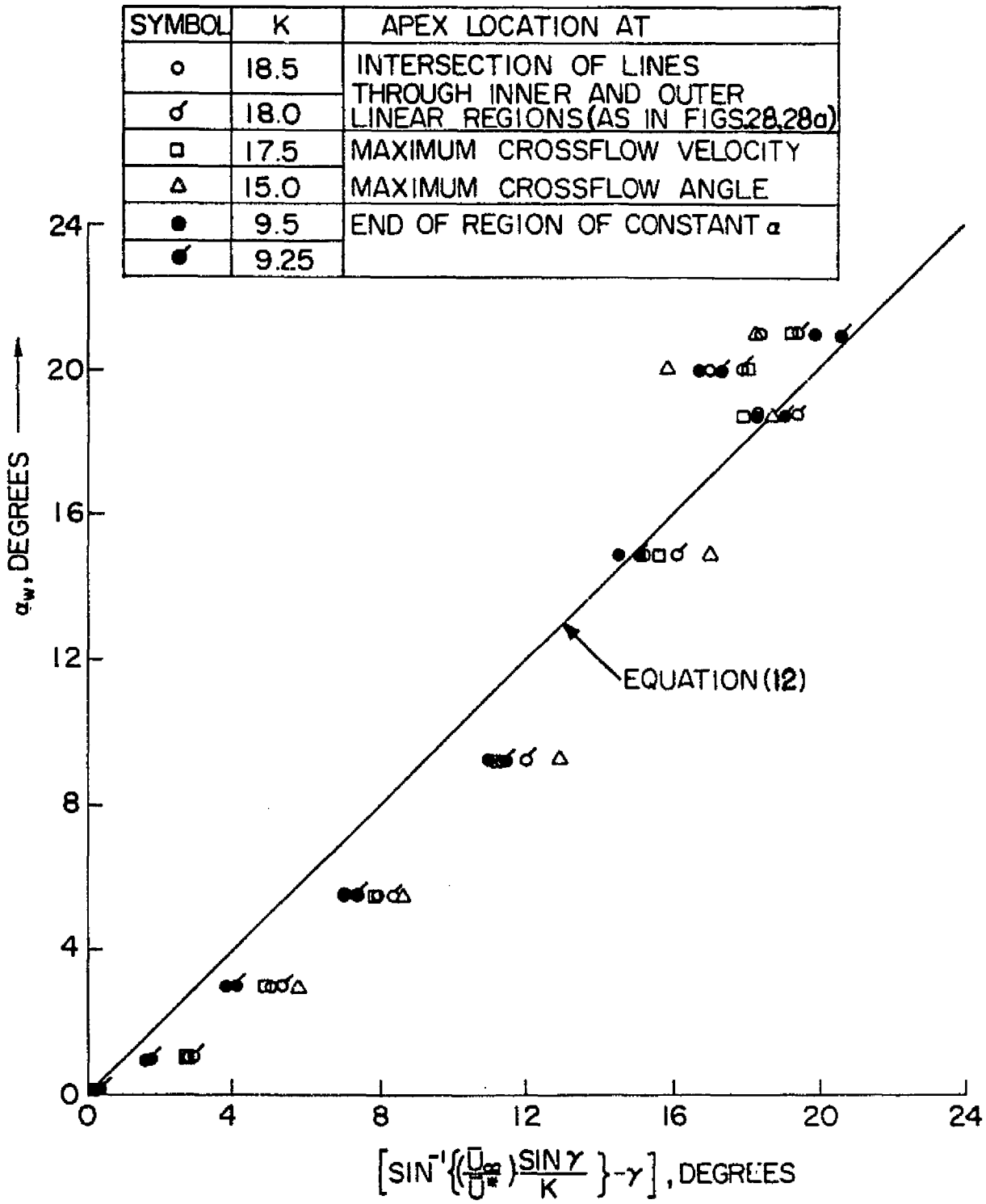

FIG. 29 : CORRELATION OF POLAR PLOT DATA IN TERMS OF WALL SHEAR STRESS VECTOR AND LOCAL FREESTREAM CONDITIONS; NOMINAL $Re_{\infty r} = 3.25 \times 10^5$ PER FOOT

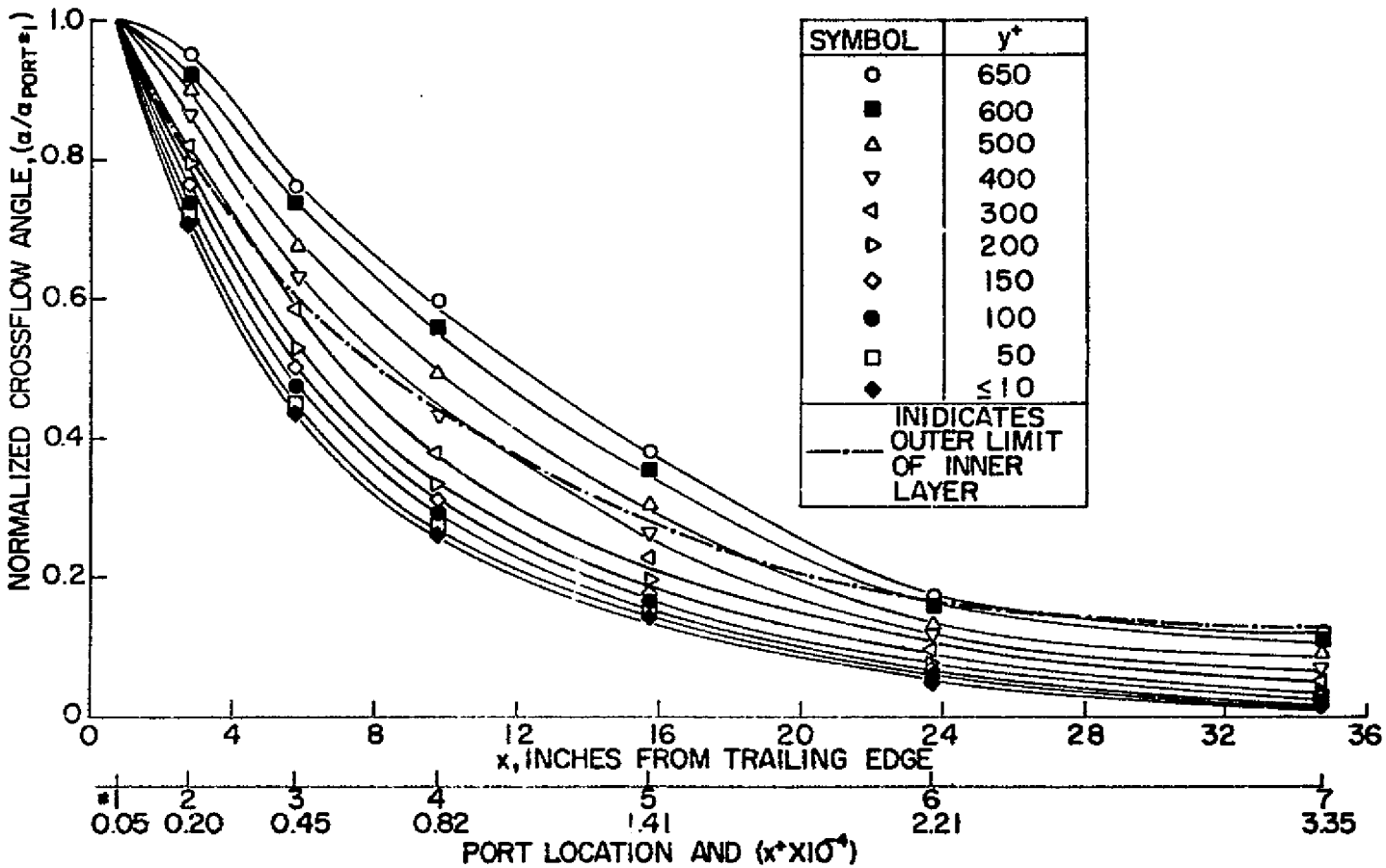

FIG. 30: STREAMWISE RELAXATION (DECAY) OF CROSSFLOW ANGLE IN THE INNER LAYER AT CONSTANT Y^+ VALUES; NOMINAL $Re_{\infty r} = 3.25 \times 10^5$/foot

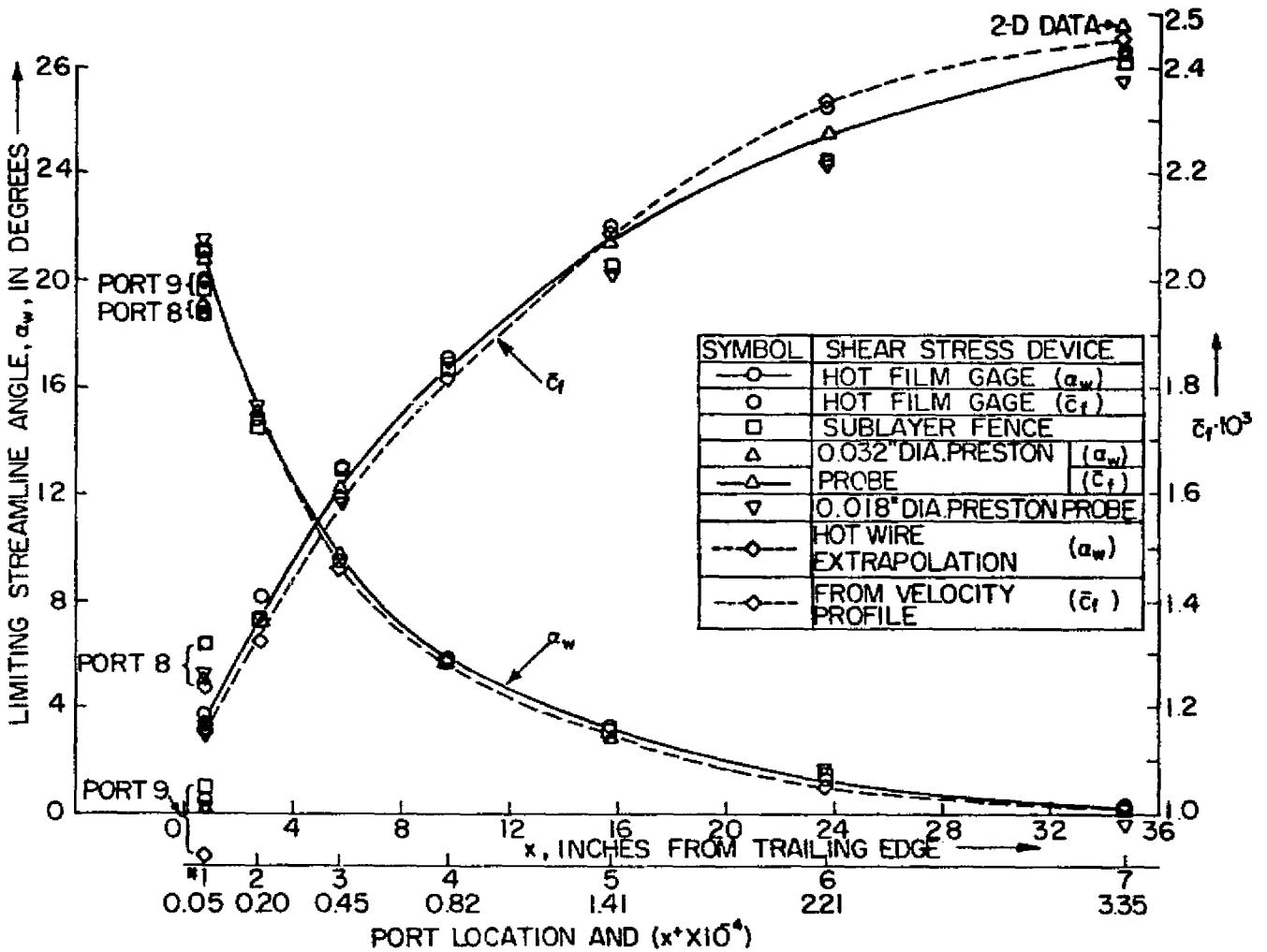

FIG. 31 : DISTRIBUTION OF LIMITING STREAMLINE ANGLE (WALL CROSSFLOW ANGLE) AND RESULTANT MEAN SKIN FRICTION COEFFICIENT IN THE RELAXING BOUNDARY LAYER; NOMINAL $Re_{\infty r}$ = 3.25 x 10^5/foot

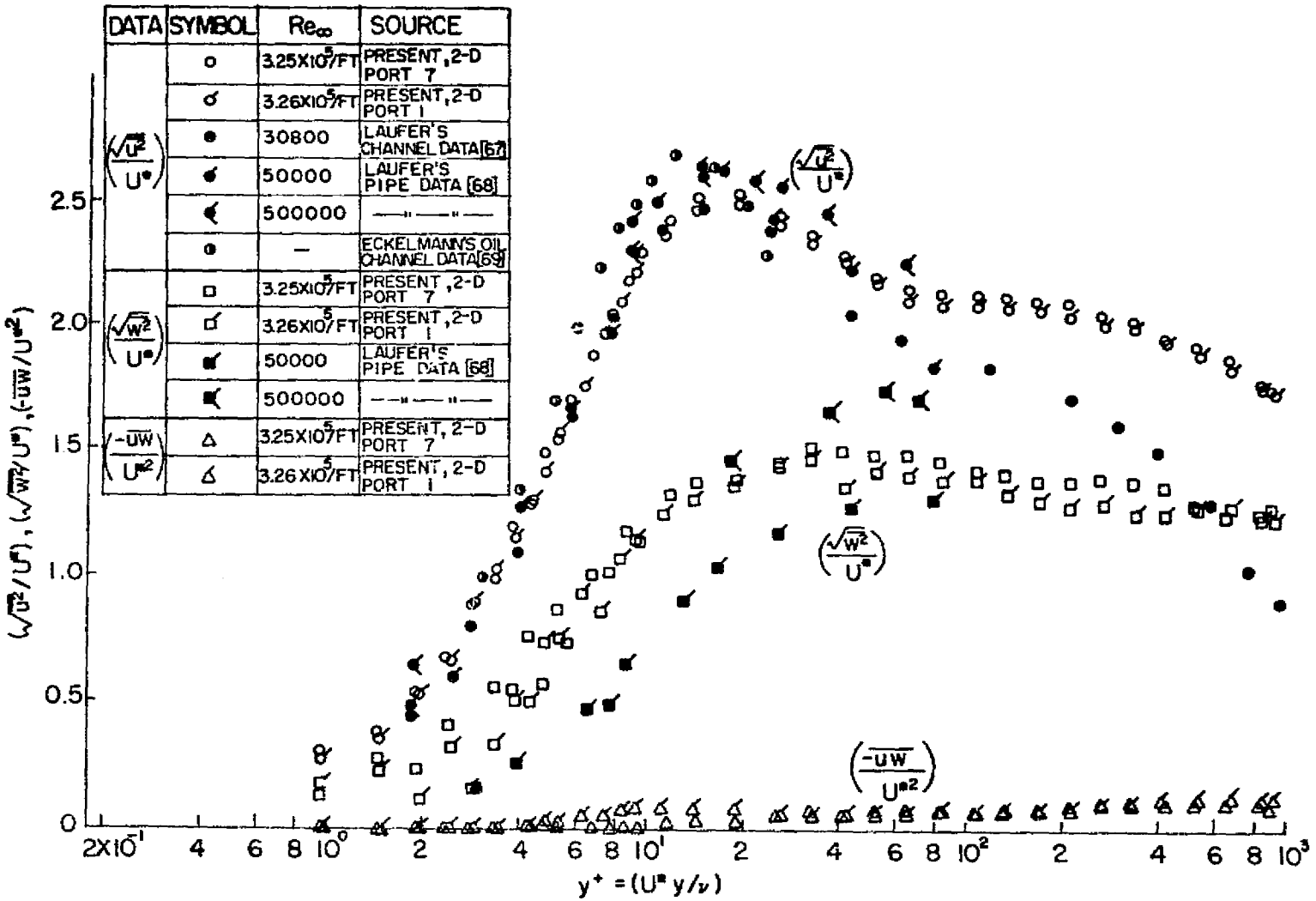

FIG. 32: HOT WIRE TURBULENCE DATA IN THE WALL COORDINATES (2-DIMENSIONAL BOUNDARY LAYER); NOMINAL $Re_{\infty r} = 3.25 \times 10^5$/foot

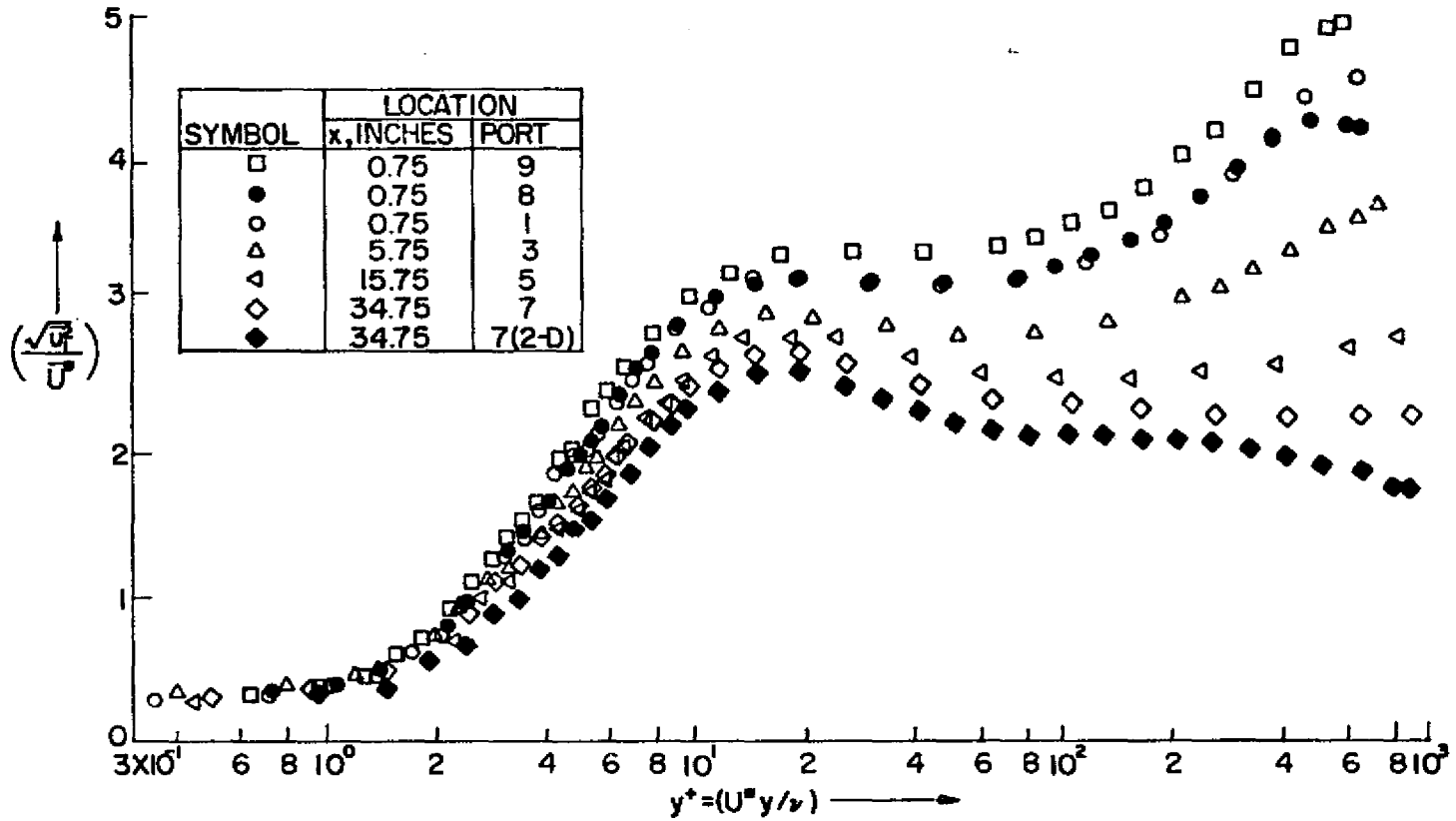

FIG. 33: LONGITUDINAL TURBULENCE DATA IN THE WALL COORDINATES; NOMINAL $Re_{\infty r}$ = 3.25 x 10^5/foot

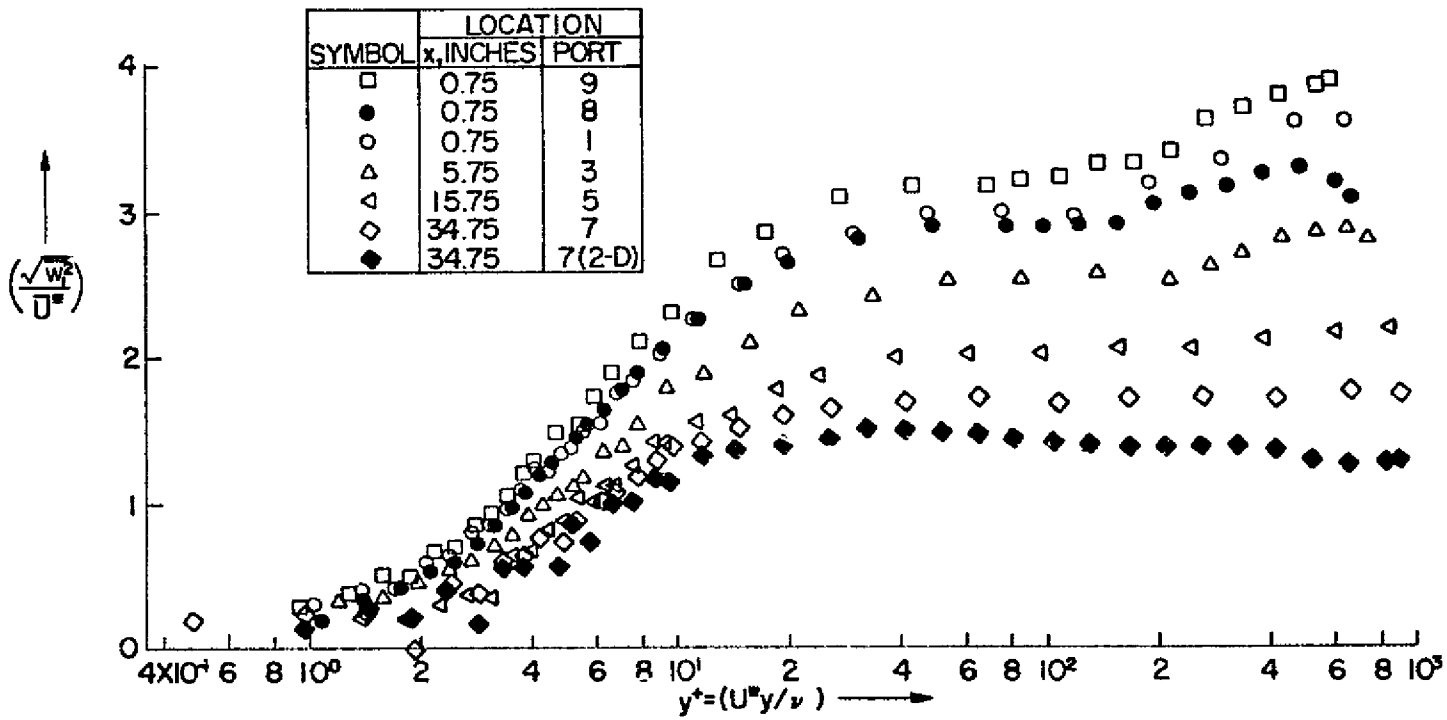

FIG. 33a: LATERAL TURBULENCE DATA IN THE WALL COORDINATES; NOMINAL $Re_{\infty r}$ = 3.25 x 10^5/foot

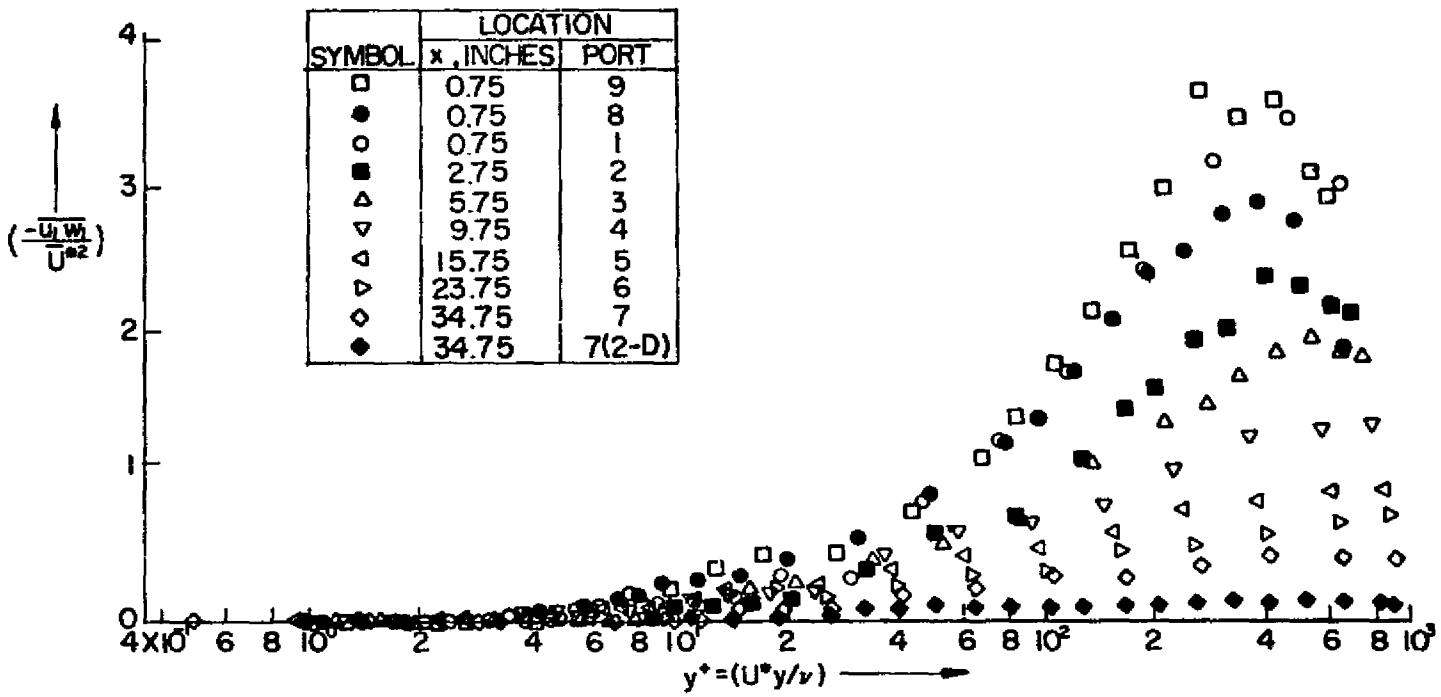

FIG. 33b: $-\overline{u_1 w_1}$ CORRELATION DATA IN THE WALL COORDINATES; NOMINAL $Re_{\infty r}$ = 3.25 x 10^5/foot

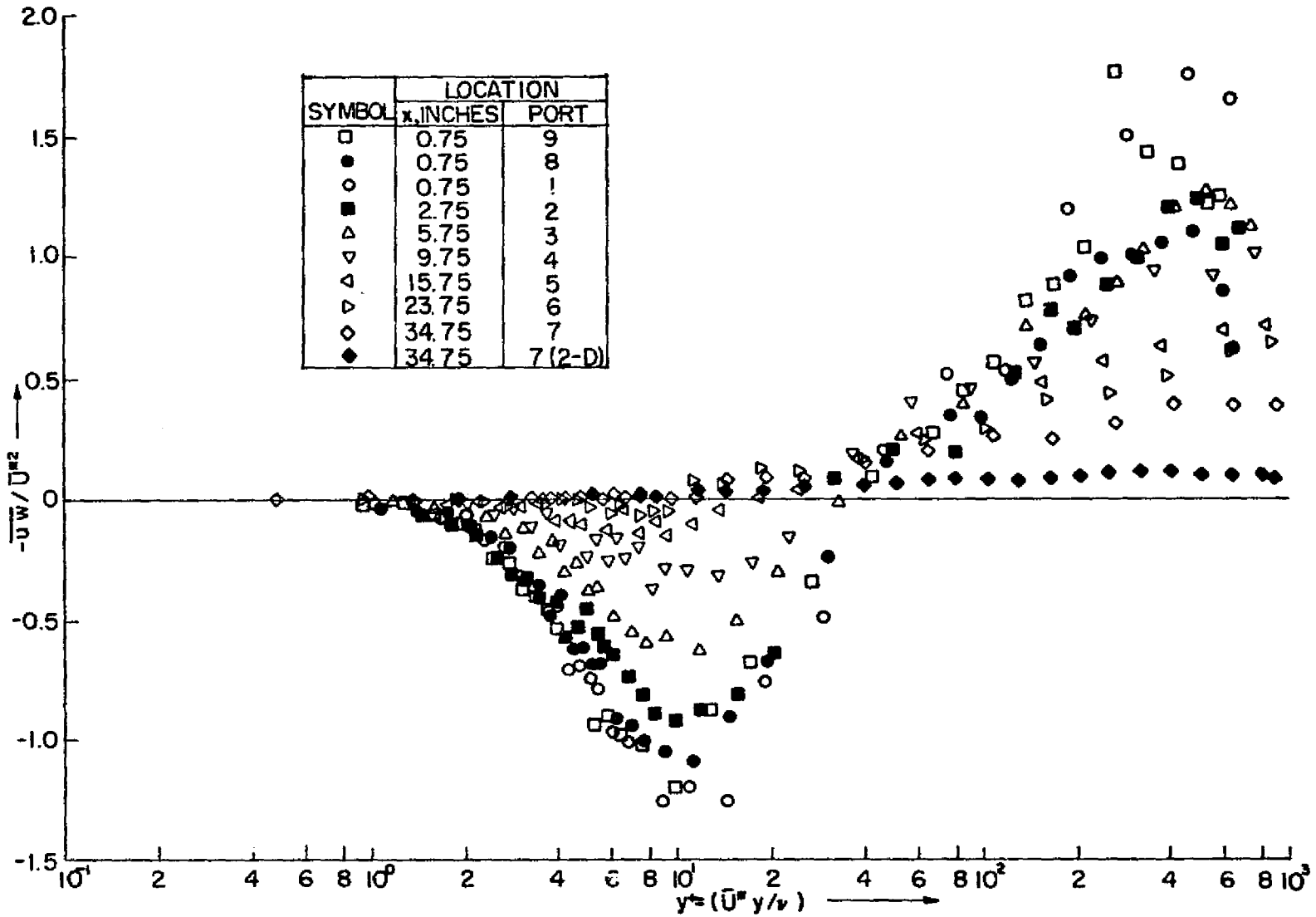

FIG. 34 : $-\overline{uw}$ CORRELATION DATA IN THE WALL COORDINATES; NOMINAL $Re_{\infty r}$ = 3.25 x 10^5/foot

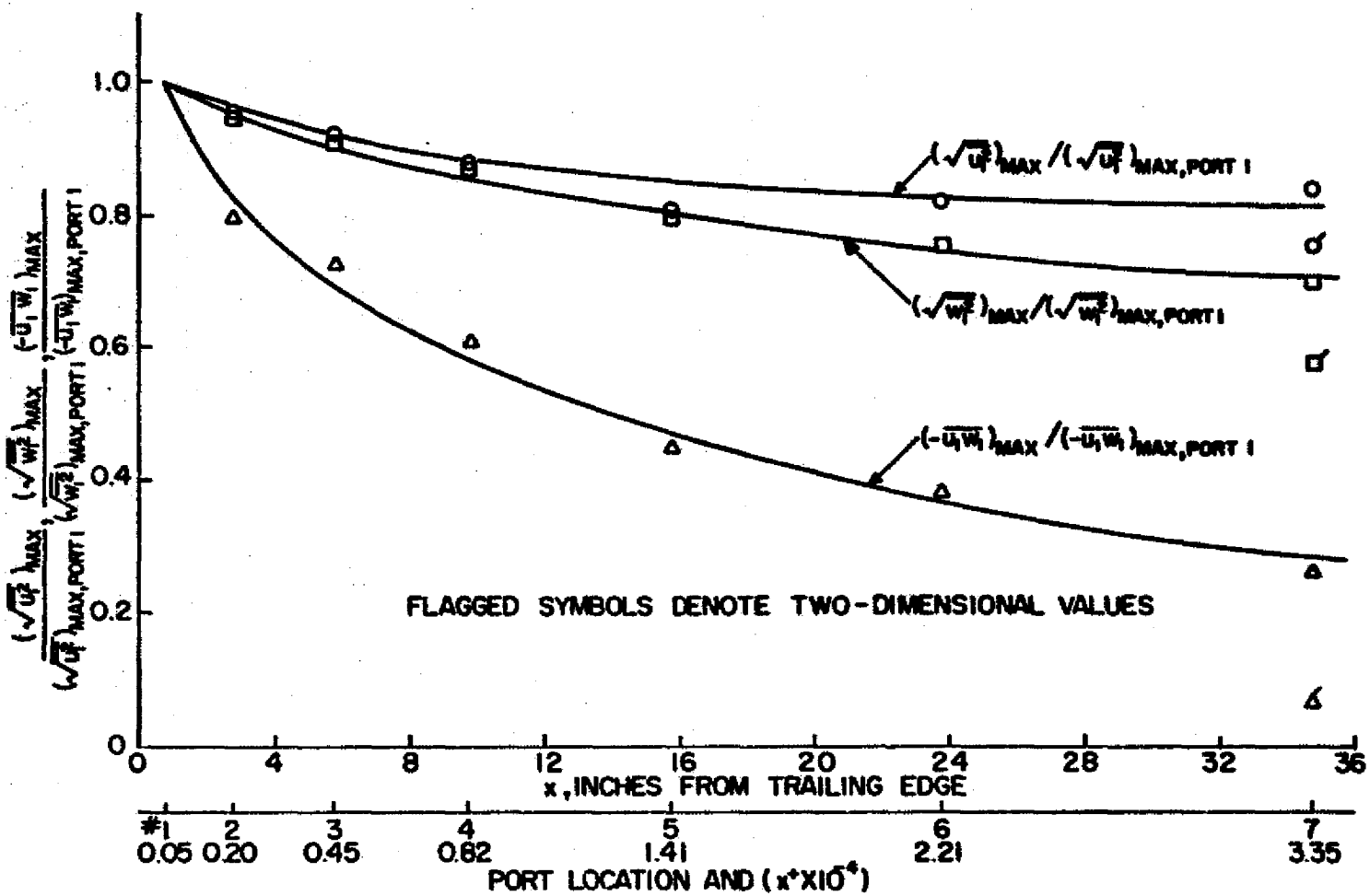

FIG. 35: STREAMWISE RELAXATION (DECAY) OF MAXIMUM TURBULENCE FLUCTUATIONS MEASURED DURING PARTIAL HOT WIRE SURVEYS; NOMINAL $Re_{\infty r}$ = 3.25 x 10^5/foot

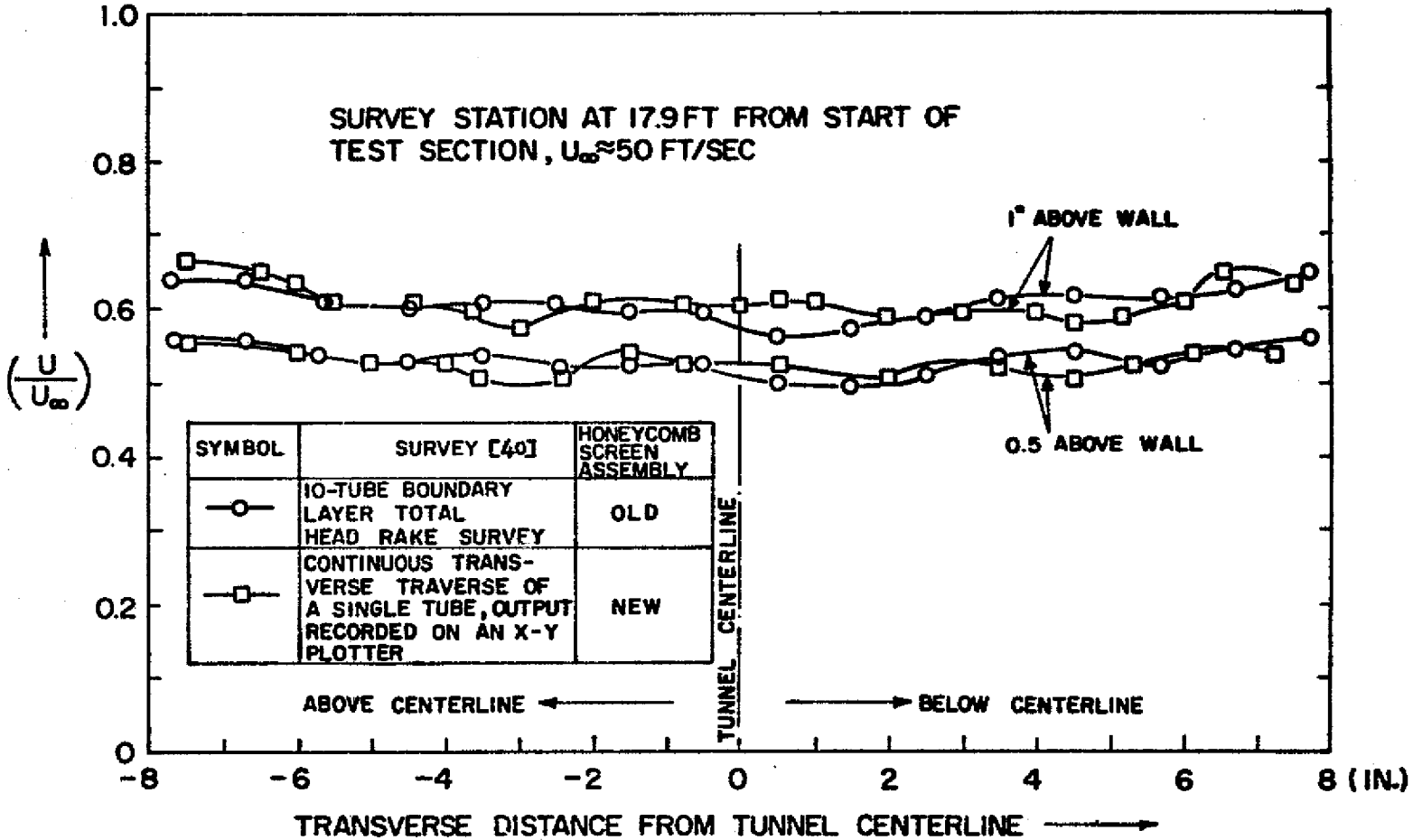

FIG A.1: TRANSVERSE VELOCITY DISTRIBUTION THROUGH BOUNDARY LAYER ON REAR SIDE WALL OF THE WIND TUNNEL